Ultrahigh-energy cosmic rays and stable *H* dibaryon

N. I. Kochelev*)

Bogoliubov Laboratory of Theoretical Physics, Joint Institute for Nuclear Research, 141980 Dubna, Moscow Region, Russia

(Submitted 9 September 1999)
Pis'ma Zh. Éksp. Teor. Fiz. **70**, No. 8, 483–486 (25 October 1999)

It is shown that an instanton-induced interaction between quarks produces a very deeply bound H dibaryon with mass below $2M_N$, viz., $M_H=1718\,\mathrm{MeV}$. Therefore the H dibaryon is predicted to be a stable particle. The reaction of photodisintegration of the H dibaryon to 2Λ in the course of its motion in the cosmic microwave background will result in a new possible cutoff in the cosmic-ray spectrum. This provides an explanation for the ultrahigh-energy cosmic ray events observed above the GZK cutoff as being the result of the strong interaction of high-energy H dibaryons from cosmic rays with nuclei in the Earth's atmosphere. © *1999 American Institute of Physics.* [S0021-3640(99)00120-6]

PACS numbers: 14.20.Pt, 13.85.Tp, 98.70.Sa, 98.70.Vc

The cosmic microwave background (CMB) gives the Greisen-Zatsepin-Kuzmin (GZK) cutoff on the possible energies of cosmic rays produced at extragalactic distances.[1] This cutoff is related to the threshold for pion production in proton(neutron)–CMB scattering. However, recently some number of cosmic ray events above the GZK cutoff has been found.[2] It turns out that this experimental result cannot be explained within the Standard Model (SM), and various explanations taking account of effects beyond the SM have been suggested (see review[3]).

In this letter we will argue for another possible explanation for ultrahigh-energy cosmic ray (UHECR) events within the SM.

The arguments are based on consideration of the influence of a complicated structure of the QCD vacuum on the masses of the hadron states. These effects are connected with the existence of instantons — strong fluctuations of the gluon fields in the QCD vacuum (see review[4]). The main idea is to show the possibility of a deeply bound $uuddss$ H-dibaryon state[5] in the instanton field.

This H dibaryon has vacuum quantum numbers $J^{PC}=0^{++}$, $T=0$, and therefore its interaction with the vacuum can be very strong. An explicit analysis shows that this strong interaction is related to the very specific wave function of the H dibaryon, which includes a large mixture of diquark configurations that interact strongly with instantons. In a sense, the dynamics of the H particle is similar to the dynamics of the π meson. In both cases the interaction with vacuum is very strong and leads to a large attraction

between quarks. As a result, we have a massless (in the chiral limit) π meson and the possibility of a small mass for the H dibaryon.

There have been many calculations of the H-dibaryon mass within different models (see the discussion in Ref. 6). Most of them predict the mass of the particle to be near $2M_\Lambda$, but only two of them took into account the instanton interaction between quarks.[7,8] In Ref. 7 a rather deeply bound H-dibaryon state was obtained, with a mass $M_H = 2090\,\mathrm{MeV}$. In the calculation some specific version of the bag model was used. In this version a very strong dependence of the confinement-force contribution to the hadron masses on the number of quarks inside the hadron was used. As a result, the mass of the H dibaryon was overestimated. In Ref. 8 it was argued that the three-body forces induced by instantons can lead to an unbound H dibaryon. We disagree with this conclusion. The estimate of Ref. 7 shows that only a tiny contribution of the three-quark interaction to the mass of H ($\Delta M_3 \approx 5\,\mathrm{MeV}$) is possible. This suppression is due to the very small probability of finding the three quarks simultaneously inside an instanton.

It is very important to take into account the instanton-induced interaction in diquark configurations inside a multiquark hadron state. Many years ago it was shown that even for ordinary baryons this interaction plays a fundamental role in the mass splitting between different hadron multiplets.[9,10] This is related to the instanton-induced strong attraction between quarks in the diquark configuration $q^2(\overline{3}^F, S=0, \overline{3}^C)$. In the dibaryon state, besides this configuration the mixture of diquarks $q^2(\overline{3}^F, S=1, 6^C)$ can also lead to a large decrease of the dibaryon mass. Furthermore, it was shown recently that the instanton-induced diquark configurations are also important in connection with the possibility of having a color superconductivity of the quark–gluon matter.[11]

Let us calculate the instanton contribution to the mass of the H dibaryon. The quark–quark t'Hooft interaction induced by instantons[12] has the following structure in flavor–color–spin space:

$$\mathcal{L}_{\mathrm{inst}} = \sum_{i>j} \mu_{ij} \left(1 + \frac{\lambda_i^a \lambda_j^a}{32} (1 + 3\boldsymbol{\sigma}_i \boldsymbol{\sigma}_j) \right), \tag{1}$$

where $i,j = u,d,s$, and the coefficients $\mu_{i,j}$ depend on the instanton density and quark masses. It was shown within the instanton-liquid model of the QCD vacuum that the strength of interaction (1) is enough to explain all of the spin–spin mass splittings between different hadronic states (see Ref. 4). Therefore one can consider the coefficients μ_{ij} as parameters determined by the spin–spin mass splitting between baryon states. Within the constituent quark model with an instanton-induced interaction, which describes the masses of the ground states of the octet and decuplet of baryons with an accuracy of a few MeV,[10] the formula for the hadron mass is

$$M_{\mathrm{hadron}} = N_U U + N_S S + \Delta M_{\mathrm{inst}}, \tag{2}$$

where N_U and N_S are the numbers of light and strange quarks in the hadron, U and S are their constituent masses, and ΔM_{inst} is the contribution of instantons. By using the wave function of the baryons, one can show that for the baryon decuplet the instanton contribution is zero and for the baryon octet it is[9]

$$\Delta M_N = -3\alpha/2, \quad \Delta M_\Lambda = -(\alpha + \beta/2), \quad \Delta M_\Sigma = \Delta_\Xi = -3\beta/2, \tag{3}$$

where

$$\alpha = 3\mu_{u,d}R_{00}, \quad \beta = 3\mu_{u(d),s}R_{00}, \tag{4}$$

and R_{00} is the radial matrix element of interaction (1). The best values of the parameters, which provide a very good description of the baryon masses, are[10]

$$U = 412.9 \text{ MeV}, \quad S = 557.5 \text{ MeV}, \quad \alpha = 200.5 \text{ MeV}, \quad \beta = 132.7 \text{ MeV}. \tag{5}$$

To calculate the instanton contribution to the H-dibaryon mass, one must know the decomposition of the H wave function

$$q^6 = \sum_j C_j q_j^4 \times q_j^2 . \tag{6}$$

In this case the matrix element of the two-particle operator R_2 for the q^6 state is

$$\langle q^6|R_2|q^6\rangle = 15\sum_j C_j^2 \langle q^2|R_2|q^2\rangle. \tag{7}$$

The decomposition has been obtained in Ref. 7, and in the basis $SU_3^F \times SU_2^S \times SU_3^C$ it is given by the formula

$$|H(0^F,0^S,0^C)\rangle = \sqrt{\frac{1}{10}} q^4 \times q^2(6^F,0,6^C) + \sqrt{\frac{3}{10}}[q^4 \times q^2(\overline{3}^F,0,\overline{3}^C) + q^4 \times q^2(\overline{3}^F,1,6^C) + q^4 \times q^2(6^F,1,\overline{3}^C)]. \tag{8}$$

By using (8) and the well-known matrix elements of the $\lambda_1\lambda_2$, $\vec{\sigma}_1\vec{\sigma}_2$ operators for the different diquark states in (8), one can easily calculate the instanton contribution to the mass of the H dibaryon:

$$\Delta M_H = -9(\alpha + 2\beta)/4. \tag{9}$$

With the parameter values (5) the mass of the H dibaryon is

$$M_H = 1718 \text{ MeV}. \tag{10}$$

This mass is below $2M_N = 1876$ MeV, and therefore the H dibaryon should be a *stable particle*.

The experimental status of the H dibaryon is uncertain.[13,14] For example, one of the best results on the H-dibaryon properties is only an upper limit for the H production cross section, obtained by the BNL E836 Collabobation[14] in the mass interval $M_H = 1850-2180$ MeV, which lies above our prediction (10).

The unique properties of the H particle should lead not only to some anomalies in the cross sections with strange particles (see the discussion in Ref. 14) but also to fundamental cosmological consequences. One of these consequences is a natural explanation for the observed UHECR above the GZK cutoff, in terms of the H-particle component in cosmic rays. The H dibaryon has no electric charge and its spin is zero. That means that the magnetic moment of H is also zero. Therefore this particle should has a rather small cross section for interactions with the cosmic microwave background. The H dibaryon is a deeply bound state of two Λ. Therefore a significant part of its interaction cross section with the CMB can originate from the reaction of photodisintegration to 2Λ. The threshold for this reaction for a mass $M_H = 1718$ MeV is approximately 7

$\times 10^{20}$ eV. This threshold is above the GZK cutoff and is not inconsistent with the available experimental data.[2] Therefore the existence of a stable H dibaryon may explain the UHECR. All that is needed is some source of ultrahigh-energy cosmic H dibaryons. One possible source of these cosmic H dibaryons could be their production by accelerated protons in radio galaxies beyond the GZK radius. Another, much more interesting source of high-energy cosmic H dibaryons is the phase transition from nuclear to H-dibaryon matter inside a neutron star. In this case a very large mass difference between two neutrons and an H dibaryon could lead to explosion of the neutron star and the production of ultrahigh-energy cosmic H dibaryons.

In summary, a stable H dibaryon is predicted. Its stability derives from a strong attraction between quarks due to interaction with the QCD vacuum. It is shown that ultrahigh-energy cosmic H dibaryons give an explanation for the observed deviation from the GZK prediction.

The author is grateful to A. E. Dorokhov, S. B. Gerasimov, R. Jaffe, A. De Roeck, T. Morii, and V. Vento for helpful discussions. My special thanks go to I. I. Tkachev, because a discussion with him about problems related to UHECR led me to the idea of this paper. This paper was started during my visit to CERN. I am grateful to the Theory Division of CERN for warm hospitality. This work was partially supported by the Heisenberg–Landau program.

*)e-mail: kochelev@thsun1.jinr.ru

---

[1] K. Greisen, Phys. Rev. Lett. **16**, 748 (1966); G. T. Zatsepin and V. A. Kuzmin, JETP Lett. **4**, 78 (1966).
[2] N. N. Efimov *et al.*, *Proceedings of the International Symposium on Astrophysical Aspects of the Most Energetic Cosmic Rays*, edited by M. Nagano and F. Takahara, World Scientific, Singapore (1991), p. 20; T. A. Egorov *et al.*, *Proceedings of the Tokyo Workshop on Techniques for the Study of Extremely High Energy Cosmic Rays*, edited by M. Nagano, ICRR, Univ. of Tokyo (1993); B. N. Afanasiev, *Proceedings of the International Symposium on Extremely High Energy Cosmic Rays; Astrophysics and Future Observations*, edited by M. Nagano ICRR, Univ. of Tokyo (1996); M. A. Lawrence, R. J. O. Reid, and A. A. Watson, J. Phys. G Nucl. Part. Phys. **17**, 733 (1991); D. J. Bird *et al.*, Phys. Rev. Lett. **71**, 3401 (1993); Astrophys. J. **424**, 491 (1994); **441** 144 (1995); N. Hayashida *et al.*, Phys. Rev. Lett. **73**, 3491 (1994); for recent reviews see P. Bhattacharjee and G. Sigl, http://xxx.lanl.gov/abs/astro-ph/9811011; V. Berezinsky, http://xxx.lanl.gov/abs/astro-ph/9811268.
[3] V. A. Kuzmin and I. I. Tkachev, http://xxx.lanl.gov/abs/hep-ph/9903542.
[4] T. Schäfer and E. V. Shuryak, Rev. Mod. Phys. **70**, 1323 (1998).
[5] R. L. Jaffe, Phys. Rev. Lett. **38**, 195 (1977); **38**, 1617 (E) (1977).
[6] S. V. Bashinsky and R. L. Jaffe, Nucl. Phys. A **625**, 167 (1997).
[7] A. E. Dorokhov and N. I. Kochelev, JINR preprint, E2-86-847 (1986); A. E. Dorokhov, N. I. Kochelev and Yu. A. Zubov, Fiz. Élem. Chastits. At. Yadra **23**, 1192 (1992) [Sov. J. Part. Nucl. **23**, 522 (1992)].
[8] S. Takeuchi and M. Oka, Phys. Rev. Lett. **66**, 1271 (1991).
[9] N. I. Kochelev, Yad. Fiz. **41**, 456 (1985) [Sov. J. Nucl. Phys. **41** 291 (1985)]; A. E. Dorokhov and N. I. Kochelev, JINR preprint, E2-86-355 (1986); Yad. Fiz. **52**, 214 (1990) [Sov. J. Nucl. Phys. **52**, 135 (1990)].
[10] E. V. Shuryak and J. L. Rosner, Phys. Lett. B **218**, 72 (1989).
[11] M. Alford, K. Rajagopal, and F. Wilczek, Phys. Lett. B **422**, 427 (1998); R. Rapp, T. Schäfer, E. V. Shuryak, and M. Velkovsky, Phys. Rev. Lett. **81**, 53 (1998).
[12] G.'t Hooft, Phys. Rev. D **14**, 3432 (1976).
[13] B. A. Shahbazian, T. A. Volokhovskay, V. N. Emelyanenko, and A. S. Martynov, Phys. Lett. B **316**, 593 (1993); S. Ahmad *et al.*, Nucl. Phys. A **590** 477c (1995); J. Belz *et al.*, Phys. Rev. D **53**, R3487 (1996).
[14] R. L. Stotzer *et al.*, Phys. Rev. Lett. **78**, 274 (1997).

Published in English in the original Russian journal. Edited by Steve Torstveit.

Generation of 10^{15}–10^{17} eV photons by ultrahigh-energy cosmic rays in the Galactic magnetic field

S. L. Dubovsky*) and P. G. Tinyakov†)
Institute for Nuclear Research of the Russian Academy of Sciences, 117312 Moscow, Russia

(Submitted 18 June 1999; resubmitted 17 September 1999)
Pis'ma Zh. Éksp. Teor. Fiz. **70**, No. 8, 487–492 (25 October 1999)

It is shown that the expected dip in the diffuse photon spectrum above the threshold of e^+e^- pair production, i.e., at energies $10^{15}-10^{17}$ eV, may be absent due to the synchrotron radiation by the electron component of the extragalactic ultrahigh-energy cosmic rays (UHE CRs) in the Galactic magnetic field. The mechanism we propose requires small ($<2\times10^{-12}$ G) extragalactic magnetic fields and a large photon fraction in the UHE CRs. For a typical photon flux expected in top-down scenarios of UHE CRs, the predicted flux in the region of the dip is close to the existing experimental limit. The sensitivity of our mechanism to the extragalactic magnetic field may be used to improve existing bounds on the latter by two orders of magnitude. © *1999 American Institute of Physics.* [S0021-3640(99)00220-0]

PACS numbers: 98.70.Sa, 95.30.Cq, 98.35.Eg, 98.62.En

1. INTRODUCTION

The spectrum of diffuse photons is expected to have a dip of more than two orders of magnitude at energies $10^{15}-10^{17}$ eV.[1] This dip is similar in nature to the well-known Greisen–Zatsepin–Kuzmin (GZK) cutoff[2] and is caused by electron pair production on the cosmic microwave background, $\gamma\gamma_b\to e^+e^-$. The cross section of the latter process reaches its maximum of $0.3\sigma_T\sim0.2$ barn near the threshold at 3×10^{14} eV and decreases at higher energies (see, e.g., Ref. 3). The attenuation length of photons in the region of the dip is of order 100 kpc, so the dip in the spectrum is a universal feature of models in which high-energy photons have extragalactic origin. Indeed, the existence of the dip is confirmed by simulations in various models of ultrahigh-energy cosmic rays (UHE CRs); for a review see, e.g., Refs. 3 and 4. For instance, in the region of the dip the top-down models typically give the photon flux[1)] of order 10^{-3} eV·cm^{-2}·s^{-1}·sr^{-1}, while at ultrahigh energies, $E\gtrsim10^{20}$ eV, the predicted flux is more than two orders of magnitude larger and reaches a value of a few times 10^{-1} eV·cm^{-2}s^{-1}sr^{-1}.

The spectrum of diffuse photons at energies above $\sim10^{11}$ eV is known rather poorly. Detection of the photons at the lower and upper boundaries of the dip were reported by the Tien-Shan air shower array and Yakutsk experiment. They claimed that a γ-ray intensity is at the level ~100 eV·cm^{-2}·s^{-1}·sr^{-1} at $E\geqslant4\times10^{14}$ eV,[5] and 1 eV·cm^{-2}·s^{-1}·sr^{-1} at $E\geqslant10^{17}$ eV.[6] In the region of the dip the bounds have been

obtained by EAS-TOP[7] and CASA-MIA.[8] At $E\sim 10^{16}$ eV the bound is of order ~ 0.5 $\mathrm{eV\cdot cm^{-2}\cdot s^{-1}\cdot sr^{-1}}$, about two orders of magnitude higher than has been predicted by top-down models. At ultrahigh energies the photon flux can be as large as ~ 1 $\mathrm{eV\cdot cm^{-2}\cdot s^{-1}\cdot sr^{-1}}$ if the observed UHE CR events are interpreted as photons (recent results from AGASA[9] suggest this possibility[10]).

While experimentally the existence of the dip in the photon spectrum is an open question, theoretically the case is not closed either. Calculations of the spectrum cited above do not take into account the possibility that high-energy photons can be generated in our Galaxy by UHE electrons via synchrotron radiation in the Galactic magnetic field. As we argue below, taking synchrotron emission into account may substantially alter the photon spectrum at $E\sim 10^{15}-10^{17}$ eV, filling the dip and bringing the expected photon flux close to the existing experimental limit.

The synchrotron mechanism requires a large flux of UHE electrons to hit the Galactic magnetic field. It has been recently pointed out[11] that this condition is naturally satisfied in the halo models of UHE CRs (these models attribute UHE CRs to decays of heavy relic particles clustered in the Galactic halo[12]). Due to the fragmentation process, the decay products of the superheavy particles contain a large fraction of UHE electrons.

In this paper we show that the UHE electrons necessary for the synchrotron mechanism to work can be of extragalactic origin, provided that the extragalactic magnetic fields are small. We will see that, in fact, a large flux of UHE electrons is inherent in top-down models of UHE CR, so that the generation of high-energy photons by the synchrotron mechanism is a generic prediction of top-down scenarios and is not specific to halo models of UHE CRs.

The key observation is that UHE photons propagate in the extragalactic space via a cascade process, being converted to electrons and back with a small energy loss. As a result, the flux of UHE photons is necessarily accompanied by the flux of UHE electrons. At energies of order $10^{22}-10^{23}$ eV and in the absence of extragalactic magnetic fields, the electron flux is at least as large, or even much larger, than the photon flux.[2)] While the UHE photons reach the Earth and contribute to the observable flux of UHE CRs, the UHE electrons emit synchrotron radiation in the Galactic magnetic field and transfer their energy to high-energy photons. As we will see below, the energy of the photons produced lies in the region of the dip, and their flux is similar to that of UHE electrons (and, thus, of UHE photons). Hence, in the absence of extragalactic magnetic fields, a flux of UHE photons at the level of ~ 1 $\mathrm{eV\cdot cm^{-2}\cdot s^{-1}\cdot sr^{-1}}$ implies a flux of synchrotron photons at the same level, which fills the dip in the photon spectrum. Since a large flux of UHE photons is one of the signatures of the top-down mechanisms of UHE CRs, in the absence of extragalactic magnetic fields these models generically predict no dip in the spectrum of diffuse photons.

The mechanism we propose is sensitive to magnetic fields at distances up to 50 Mpc from our Galaxy. If no dip in the photon spectrum is observed and halo models are ruled out, the extragalactic magnetic field at these distances must be smaller than 2×10^{-12} G. This is two orders of magnitude better than the existing bounds.[13] Conversely, if a dip is found and, at the same time, the UHE CRs have a large photon fraction, the extragalactic magnetic field must be larger than 2×10^{-12} G.

This paper is organized as follows. In Sec. 2 we estimate the flux of UHE electrons

given the flux of UHE photons and zero extragalactic magnetic field. In Sec. 3 we calculate the spectrum of synchrotron radiation in the Galactic magnetic field for injected electrons of given energy. In Sec. 4 we estimate the effect of extragalactic magnetic fields. Section 5 contains our conclusions.

2. THE FLUX OF UHE ELECTRONS

Our aim in this section is to show that in the energy range $10^{22}-10^{23}$ eV the flux of UHE photons is necessarily accompanied by a comparable or larger flux of UHE electrons, provided that there are no extragalactic magnetic fields. The argument is based on the observation that at these energies, photon propagation is a cascade process (see, e.g., Ref. 4), i.e., a propagating photon is converted to an electron and back with small energy loss. As this process is random, one should expect a certain ratio of photons and electrons far from the source.

The main reactions driving the cascade are e^+e^- pair production (PP) on the radio background, $\gamma\gamma_b\to e^+e^-$, double pair production (DPP), $\gamma\gamma_b\to e^+e^-e^+e^-$, and the inverse Compton scattering (ICS), $e\gamma_b\to e\gamma$ Ref. 3. Since double pair production dominates in the energy range of interest, one should expect to find more electrons than photons.

A simple estimate can be obtained if one neglects secondary particles and energy losses. In this (rather crude) approximation, PP and DPP lead to the conversion of photons to electrons at rates a_{PP} and a_{DPP}, respectively, while ICS converts electrons back to photons at a rate b. The set of equations which describes the propagation of photons and electrons reads

$$dn_\gamma/dR=-an_\gamma+bn_e, \quad dn_e/dR=an_\gamma-bn_e, \tag{1}$$

where R is the distance from the source, $n_\gamma(R)$ and $n_e(R)$ are the photon and electron fractions at the distance R, respectively, and $a\equiv a_{PP}+a_{DPP}$. The solution to this system is

$$n_e/n_\gamma=[ae^{R(a+b)}-C]/[be^{R(a+b)}+C],$$

where C is an integration constant whose value is determined by the ratio n_e/n_γ at $R=0$. Far from the source the value of this constant is irrelevant.

The observed fluxes $F_{e,\gamma}$ are given by integrals over the space of $n_{e,\gamma}$ multiplied by the particle injection rate. To estimate F_e/F_γ we note that the integrals are dominated by large distances, where the ratio n_e/n_γ is constant, $n_e/n_\gamma\sim a/b$. Therefore,

$$F_e/F_\gamma\sim a/b. \tag{2}$$

Both a and b depend on energy. At $E\sim10^{22}$ eV one has $a\sim2\times10^{-2}$ Mpc^{-1}, $b\sim8\times10^{-3}$ Mpc^{-1} (Ref. 3), and thus

$$F_e/F_\gamma\sim2 \quad \text{at} \quad E=10^{22}\ \text{eV}. \tag{3}$$

At higher energies the rate a is dominated by DPP process and tends to a constant, $a\to8\times10^{-3}$ Mpc^{-1}, while the rate b rapidly falls off.[3] At $E\sim10^{23}$ eV, Eq. (2) gives

$$F_e/F_\gamma\sim10 \quad \text{at} \quad E=10^{23}\ \text{eV}. \tag{4}$$

In a more accurate estimate one should take into account the energy losses by the leading particles and possible energy sharing in the leading e^+e^- pair in DPP. In this approximation the result depends on the energy distribution of initial particles and on the energy dependence of the rates a_{PP}, a_{DPP}, and b. We have performed such estimate by dividing the energy interval $10^{21}-10^{24}$ eV into 10 energy bands and solving numerically the system of 20 coupled equations analogous to Eqs. (1). We have found that the corrections to Eqs. (3) and (4) are small and do not alter our conclusions, unless the extragalactic magnetic field is nonzero (the latter case is considered in Sec. 4).

3. SYNCHROTRON RADIATION IN THE GALACTIC MAGNETIC FIELD

Consider now the synchrotron radiation of UHE electrons in the Galactic magnetic field. An ultrarelativistic particle of energy E moving in a magnetic field B emits radiation at the characteristic frequency[14]

$$\omega_c=\frac{3\sqrt{\alpha}B}{2m_e^3}E^2=6.7\times 10^{14}\left(\frac{E}{10^{20}\,\mathrm{eV}}\right)^2\left(\frac{B}{10^{-6}\,\mathrm{G}}\right)\,\mathrm{eV}. \tag{5}$$

The width of the frequency band is roughly $\delta\omega\sim\omega_c$. As a result of this process, the particle loses energy at the rate

$$dE/dx=-2\alpha^2B^2E^2/3m^4. \tag{6}$$

Both equations are written for the case of particle momentum normal to the direction of the magnetic field. Generalization to other cases is straightforward.

Equation (5) implies that in the Galactic magnetic field, $B\sim 10^{-6}$ G, electrons with energy $E\sim 10^{20}$ eV radiate at the characteristic frequency $\omega_c\sim 10^{15}$ eV. This process is the source of high-energy photons in the Galactic halo models of UHE CRs.[11] Since the Galactic magnetic field far from the Galactic center is smaller, the extragalactic electrons which we consider in this paper must have higher energy in order to produce synchrotron radiation in the same frequency range.

For the quantitative analysis of the synchrotron emission by the extragalactic electrons consider an UHE electron moving in a varying magnetic field $B(x)$ perpendicular to its velocity. Integration of Eq. (6) gives

$$\frac{1}{E(x)}-\frac{1}{E_0}=\frac{2\alpha^2}{3m_e^4}\int_{-\infty}^{x}B^2(x)dx, \tag{7}$$

where E_0 is the initial energy of the electron.

For definiteness, let us take an exponentially decaying magnetic field,

$$B(x)=B_0\exp(x/x_0) \tag{8}$$

(note that we consider a particle propagating from $x=-\infty$). This behavior is expected in some recent Galactic magnetic field models[15] for the field in the direction normal to the Galactic disk. The scale x_0 is of the order of 4 kpc. Making use of Eqs. (7) and (8), one finds the relation between E and B at a given point of the particle trajectory,

$$(1/E)-(1/E_0)=\alpha^2x_0B^2/3m_e^4.$$

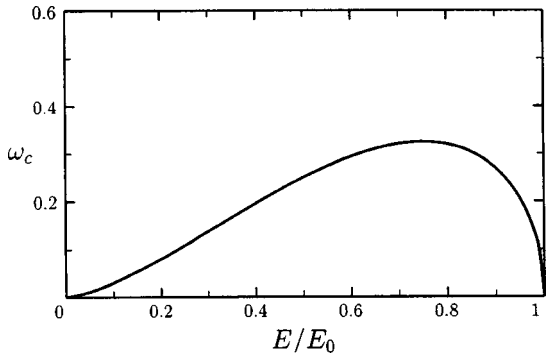

FIG. 1. The dependence of ω_c (arbitrary units) on particle energy for the exponential model of the Galactic magnetic field.

This equation, together with Eq. (5), determines the dominant radiation frequency as a function of particle energy,

$$\omega_c(E)=\frac{9E_0^{3/2}}{2m_e\sqrt{3\alpha x_0}}f(E/E_0), \quad \text{where} \quad f(y)=y^{3/2}\sqrt{1-y}.$$

This function is shown in Fig. 1, from which we see that most of the electron energy is emitted at frequencies close to

$$\omega_{\max}=\omega_c(3E_0/4)=\frac{27E_0^{3/2}}{32m_e\sqrt{\alpha x_0}}=0.8\times 10^{15}\left(\frac{E_0}{10^{22}\,\text{eV}}\right)^{3/2}\left(\frac{x_0}{4\ \text{kpc}}\right)^{-1/2}\text{eV}. \tag{9}$$

According to Eqs. (5) and (9), at $E=10^{22}$ eV the electron loses most of its energy in the region where the magnetic field is $\sim 10^{-10}$ G, i.e., at a distance of ~ 36 kpc from the Galactic disk for $B_0\sim 10^{-6}$ G.

In the case where the magnetic field is not perpendicular to the particle velocity, the spectrum of synchrotron photons is softer. The same is true for a magnetic field which falls off more slowly than in Eq. (8), as is usually assumed for the Galactic magnetic field in the direction parallel to the Galactic plane. Thus one should expect an angular dependence of the photon spectrum with the more energetic photons coming from the direction normal to the Galactic plane and a softer spectrum from the directions in the Galactic plane. The above estimates indicate that this effect is small, and its detailed study at this point seems premature.

Finally, let us estimate the flux of synchrotron photons, assuming a flux of UHE photons which is typical for top-down scenarios, viz., a few times 10^{-1} eV$\cdot$cm$^{-2}\cdot$s$^{-1}\cdot$sr^{-1} at energies $\sim 10^{22}-10^{23}$ eV. Equation (3) implies that, outside the Galactic magnetic field, there is at least as large a flux of UHE electrons which transfer their energy to high-energy photons in the Galactic magnetic field. Since the synchrotron spectrum has $\delta\omega\sim\omega$, energy conservation implies that the flux of synchrotron photons is approximately the same as the flux of UHE electrons, which is larger by a factor of F_e/F_γ than the flux of UHE photons.

4. EFFECT OF EXTRAGALACTIC MAGNETIC FIELD

As was shown above, in the absence of extragalactic magnetic fields the observed flux of $10^{15}-10^{17}$ eV photons is proportional to the flux of UHE photons and the ratio F_e/F_γ at energies above $E \gtrsim 10^{22}$ eV. The presence of a large enough extragalactic magnetic field can significantly decrease this ratio. Indeed, if the $\gamma \to e$ conversion length, $a^{-1}=(a_{PP}+a_{DPP})^{-1}$, is large compared to the energy loss length of the electron due to synchrotron radiation in the extragalactic magnetic field, the flux of UHE electrons should be much smaller than the flux of UHE photons.

Let us estimate the value of the extragalactic magnetic field at which the ratio $F_e/F_\gamma \sim 1$ at $E \gtrsim 10^{22}$ eV. For this purpose note that the solution to Eq. (6) in a constant magnetic field B can be written in the form

$$l=(3m^4/2\alpha^2B^2E)[1-(E/E_0)], \tag{10}$$

where l is the distance traveled by the electron as its energy decreases from E_0 to E. Equation (10) implies that electrons with energy E can only come from distances smaller than

$$l_E=3m^4/2\alpha^2B^2E \sim 50(2\times 10^{-12}\mathrm{G}/B)^2(10^{22}\mathrm{eV}/E)\mathrm{Mpc}\ . \tag{11}$$

Taking into account that the length a^{-1} of $e \to \gamma$ conversion is of the order of 50 Mpc at $E=10^{22}$ eV (Ref. 3), one finds that the extragalactic magnetic field must be smaller than 2×10^{-12} G at distances $\leqslant 50$ Mpc from our Galaxy in order for the ratio F_e/F_γ to be comparable to or larger than one. If the magnetic field at distances of order 50 Mpc is much larger than 2×10^{-12} G (for a discussion of present limits on the extragalactic magnetic field see, e.g., Ref. 16), the ratio F_e/F_γ is much smaller than one, and the flux of UHE electrons is not sufficient to fill the dip in the photon spectrum by synchrotron mechanism.

It is worth noting that the mechanism we propose is not sensitive to magnetic fields at distances larger than ~ 50 Mpc, because this distance is sufficient for the generation of a large electron fraction $F_e/F_\gamma \sim 1$. The effect of distant magnetic fields is merely to decrease the UHE photon flux, which is not important for our argument since we normalize the UHE photon flux to the observed flux of UHE CRs.

5. CONCLUSIONS

When the synchrotron radiation in the Galactic magnetic field is properly taken into account, the top-down models, under certain conditions, generically predict a flux of $10^{15}-10^{17}$ eV photons, which is close to the current experimental limits. Thus, it is important to improve the sensitivity of the experiments in the energy range $10^{15}-10^{17}$ eV. The detection of a diffuse photon flux at a level of $\sim 10^{-1}$ eV$\cdot$cm$^{-2}\cdot$s$^{-1}\cdot$sr^{-1} would strongly suggest that the UHE CRs are produced by a top-down mechanism. Moreover, this would imply that either the mechanism based on the halo model[11] or the one proposed here works. The two possibilities can be distinguished by measuring the angular anisotropy of the UHE CRs[17] and of the high-energy photons produced.[11] On the contrary, if the photon flux in the region of the dip is smaller than $\sim 10^{-3}$ eV$\cdot$cm$^{-2}\cdot$s$^{-1}\cdot$sr^{-1} and, at the same time, the UHE CRs have a large photon fraction, the extragalactic magnetic field must be larger than 2×10^{-12} G.

The authors are indebted to D. S. Gorbunov, O. E. Kalashev, M. V. Libanov, V. A. Rubakov, and D. V. Semikoz for helpful discussions and comments. The work of S. D. is supported in part by Russian Fund for Fundamental Research under Grant 99-02-18410, INTAS Grant 96-0457 within the research program of the International Center for Fundamental Physics in Moscow, and an ISSEP fellowship.

*)e-mail: sergd@ms2.inr.ac.ru
†)e-mail: peter@ms2.inr.ac.ru

1)Here and below we mean the energy flux $F(E)$, which is expressed in terms of the differential spectrum $j(E)$ by means of the relation $F(E)=E^2j(E)$ and is measured in units of $\mathrm{eV}\cdot\mathrm{cm}^{-2}\cdot\mathrm{s}^{-1}\cdot\mathrm{sr}^{-1}$.

2)In the presence of the extragalactic magnetic field the electrons rapidly lose energy via synchrotron radiation, and the argument may not work (see Sec. 4 for details).

[1] R. J. Could and G. Schreder, Phys. Rev. Lett. **16**, 252 (1966); J. P. Jelley, Phys. Rev. Lett. **16**, 479 (1966).
[2] K. Greisen, Phys. Rev. Lett. **16**, 748 (1966); G. T. Zatsepin and V. A. Kuzmin, JETP Lett. **4**, 78 (1966).
[3] S. Lee, Phys. Rev. D **58**, 043004 (1998).
[4] P. Bhattacharjee and G. Sigl, ''Origin and propagation of extremely high energy cosmic rays,'' http://xxx.lanl.gov/abs/astro-ph/9811011.
[5] S. I. Nikolsky, I. N. Stamenov, and S. Z. Ushev, J. Phys. G **13**, 883 (1987).
[6] A. V. Glushkov, L. G. Dedenko, N. N. Efimov *et al.*, *Proceedings of the 19th International Conference, La Jolla*, edited by F. C. Jones, J. Adams, and G. M. Mason, National Technical Information Service, Springfield, Virginia (1985), Vol. 2, p. 186.
[7] M. Aglietta, B. Alessandro, P. Antonioli *et al.*, Astropart. Phys. **6**, 71 (1996).
[8] M. C. Chantel, C. E. Covault, J. W. Cronin *et al.*, Phys. Rev. Lett. **79**, 1805 (1997).
[9] M. Takeda, N. Hayashida, K. Honda *et al.*, Phys. Rev. Lett. **81**, 1163 (1998); http://xxx.lanl.gov/abs/astro-ph/9807193.
[10] M. Teshima, Talk presented at 10th International School ''Particles and Cosmology,'' Baksan, 1999.
[11] P. Blasi, ''Gamma rays from superheavy relic particles in the halo,'' http://xxx.lanl.gov/abs/astro-ph/9901390.
[12] V. A. Kuzmin and V. A. Rubakov, Yad. Fiz. **61**, 1122 (1988) [Phys. At. Nucl. **61**, 1028 (1998); V. Berezinsky, M. Kachelriess, and A. Vilenkin, Phys. Rev. Lett. **79**, 4302 (1997).
[13] P. P. Kronberg, Rep. Prog. Phys. **47**, 325 (1994).
[14] L. D. Landau and E. M. Lifshits, *The Classical Theory of Fields*, 4th ed., Pergamon Press, Oxford (1975) [Russian original, 6th ed., Nauka, Moscow (1973)].
[15] T. Stanev, Astrophys. J. **479**, 290 (1997).
[16] D. Ryu, H. Kang, and P. L. Biermann, Astron. Astrophys. **335**, 19 (1998), http://xxx.lanl.gov/abs/astro-ph/9803275; T. A. Enßlin, P. L. Biermann, P. P. Kronberg, and X. P. Wu, Astrophys. J. **477**, 560 (1997); http://xxx.lanl.gov/abs/astro-ph/9609190.
[17] S. L. Dubovsky and P. G. Tinyakov, JETP Lett. **68**, 107 (1998).

Published in English in the original Russian journal. Edited by Steve Torstveit.

Energy and angular distributions of photoelectrons in multiphoton ionization

V. S. Popov
Institute of Theoretical and Experimental Physics, 117218 Moscow, Russia

(Submitted 21 September 1999)
Pis'ma Zh. Éksp. Teor. Fiz. **70**, No. 8, 493–497 (25 October 1999)

The energy and angular distributions of photoelectrons in the photoionization of an atom or ion by powerful laser radiation are calculated. The results obtained are valid for all values of the Keldysh parameter γ. Linear and circular polarizations of the light are considered. © *1999 American Institute of Physics.* [S0021-3640(99)00320-5]

PACS numbers: 32.80.Rm

The theoretical investigation of the ionization of atoms and ions by high-power laser radiation was initiated in the 1960s.[1–4] The results of subsequent investigations in this field are reviewed in Refs. 5 and 6.[1)] The character of the ionization process depends on the adiabaticity parameter γ introduced by Keldysh:[1] Tunneling ionization occurs for $\gamma \ll 1$, and multiphoton ionization occurs for $\gamma \gg 1$.

Formulas for the ionization probability (including the pre-exponential factor) that are valid for arbitrary values of γ are obtained in Refs. 3 and 4. Our objective in the present letter is to investigate the energy and angular distributions of the photoelectrons and their variation with increasing parameter γ for linear and circular polarizations of the radiation. On account of progress in laser technology, these quantities have now become an object of experimental investigations (see, for example, the review in Ref. 6 and the literature cited therein).

For linear polarization the momentum spectrum of photoelectrons has the form[2)]

$$w(\mathbf{p}) = w(0)\exp\left\{ -\frac{1}{\omega}[c_1(\gamma)p_\parallel^2 + c_2(\gamma)p_\perp^2] \right\}, \tag{1}$$

where $c_1 = \sinh^{-1}\gamma - \gamma(1+\gamma^2)^{-1/2}$, $c_2 = \sinh^{-1}\gamma$, $\gamma = \omega/\omega_t = \omega\kappa/F$, ω and F are the frequency of the laser radiation and the electric field intensity, ω_t is the tunneling frequency of an electron in a field F, $E_i = \kappa^2/2$ is the ionization potential, and $\mathbf{p} = (p_\parallel, p_\perp)$ is the momentum of an electron after emerging from under the barrier.

Formula (1) requires almost no discussion. For $\gamma \ll 1$ (adiabatic case — i.e., the frequency ω is low and the field intensity F is high)

$$w(\mathbf{p}) = w(0)\exp\left\{ -\frac{\kappa p^2}{F}\left(\frac{1}{3}\gamma^2 + \theta^2\right)\right\}, \tag{1'}$$

where θ is the angle between the direction of emergence of an electron and the axis of

linear polarization of the radiation. The angular distribution of electrons has a sharp peak in the direction of the field, $\theta_{\text{eff}} \lesssim \gamma$. In the opposite case $\gamma \gg 1$ (rapidly varying field)

$$w(\mathbf{p}) = w(0)\exp\left\{-\frac{p^2}{\omega}(\ln 2\gamma - \cos^2\theta)\right\}. \tag{1''}$$

For intermediate transverse and longitudinal (with respect to the field **F**) electron momenta we obtain

$$\langle p_\perp^2\rangle^{1/2}/\langle p_\parallel^2\rangle^{1/2} = \left(1 - \frac{\gamma}{\sqrt{1+\gamma^2}\sinh^{-1}\gamma}\right)^{1/2} = \begin{cases} 0.577\gamma, & \gamma \ll 1, \\ 1-(2\ln\gamma)^{-1}, & \gamma \gg 1. \end{cases} \tag{2}$$

For circular polarization the probability of n-photon ionization of an atomic s level is[4]

$$w_n = \kappa^2 C_\kappa^2 R(t,\gamma)\exp\{-4\nu_c\,\varphi(t,\gamma)\}, \tag{3}$$

where

$$\varphi(t,\gamma) = \frac{\tanh^{-1}u - u}{1+t}, \quad u = \sqrt{\frac{t^2+\gamma^2}{1+\gamma^2}} \tag{3'}$$

(we have introduced in place of n the auxiliary variable $t = (2\nu_c/n) - 1$, such that $-1 < t < 1$), $\nu_c = K_0(1+\gamma^{-2})$ is the photoionization threshold, $K_0 = \kappa^2/2\omega$ is the multiphoton parameter ($K_0 \gg 1$), and C_κ is the asymptotic coefficient of the atomic wave function at infinity[3)] (the pre-exponential factor R is also calculated in Ref. 4, but we shall not require it here).

The function $\varphi(t,\gamma)$ has a minimum at the point $t = t_0(\gamma)$ corresponding to maximum ionization probability and determined from the equation $t = 1 - u/\tanh^{-1}u$. In addition, this point corresponds to the number of absorbed photons $n_0(\gamma) = 2\nu_c/(1+t_0)$. Near the maximum, the distribution over n, i.e., the electron energy spectrum, is Gaussian:[4]

$$w_n = w_{\max}\cdot\exp\{-c_3(n-n_0)^2/n_0\} = w_{\max}\cdot\exp\{-(E_n - E_{\max})^2/2\Delta^2\}, \tag{4}$$

where

$$c_3(\gamma) = \frac{\gamma^2(1+t_0^2)+2t_0^2}{(1-t_0)^2\sqrt{(1+\gamma^2)(t_0^2+\gamma^2)}} = \begin{cases} \gamma\left(1+\dfrac{1}{3}\gamma^2\right), & \gamma \ll 1 \\ 2(\ln\gamma)^2, & \gamma \gg 1, \end{cases} \tag{4'}$$

$$\Delta = [\omega E_i(1+\gamma^{-2})/(1+t_0)c_3(\gamma)]^{1/2}, \tag{4''}$$

$\Delta \sim \gamma^{-3/2}\sqrt{\omega E_i}$ for $\gamma \ll 1$, and $\Delta = \sqrt{\omega E_i}/2\ln\gamma$ for $\gamma \gg 1$. The most probable energy of the photoelectrons emerging from under the barrier is

$$E_{\max} = (n_0 - \nu_c)\omega = \frac{F^2}{2\omega^2}(1+\gamma^2)\frac{1-t_0}{1+t_0} = \begin{cases} \gamma^{-2}E_i, & \gamma \ll 1 \\ E_i/2\ln\gamma, & \gamma \gg 1. \end{cases} \tag{5}$$

A numerical calculation using the formulas presented above gives the curves in Figs. 1 and 2. The most probable number n_0 of absorbed photons for $\gamma \ll 1$ is two times greater

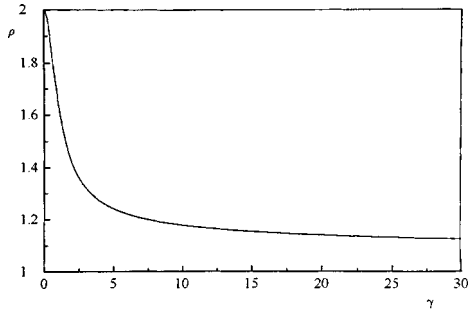

FIG. 1. Circular polarization. Ratio $\rho = n_0/\nu_c$ as a function of the Keldysh parameter γ. Here n_0 is the most probable and ν_c is the minimum number of absorbed photons.

than the photoionization threshold ν_c, approaching it, though quite slowly, for $\gamma \gg 1$ (Fig. 1). The coefficient c_3 in Eq. (4) increases monotonically with γ (Fig. 2). For $\gamma \gg 1$

$$w_n = w_{\max} \cdot \exp\left\{ -\frac{2(\ln\gamma)^2}{K_0}(n-n_0)^2 \right\}, \quad n_0 = \left(1 + \frac{1}{2\ln\gamma} \right) K_0 . \tag{6}$$

Since

$$\frac{\Delta n}{\nu_c} \sim \begin{cases} \omega/\sqrt{\kappa F} \sim \sqrt{\gamma/K_0}, & \gamma \ll 1 \\ (\sqrt{K_0}\ln\gamma)^{-1}, & \gamma \gg 1, \end{cases} \tag{7}$$

the distribution over n has the form of a comparatively narrow peak[3,4] (in units of ν_c or n_0). We note that for $\gamma \ll 1$ the distribution w_n (4) is much wider than the Poisson distribution and, conversely, for $\gamma \gg 1$ it is narrower ($\Delta n = \sqrt{n_0}$ for $\gamma \approx 0.47$).

The distribution of photoelectrons over the angle ψ between the emergence direction of the photoelectrons and the plane of polarization of the laser radiation is also of interest. It is determined by Eq. (64) in Ref. 4, into which the values $n = n_0$ and the momentum $p_0 = \sqrt{2\omega(n_0 - \nu_c)}$, corresponding to the maximum ionization probability, must be substituted:

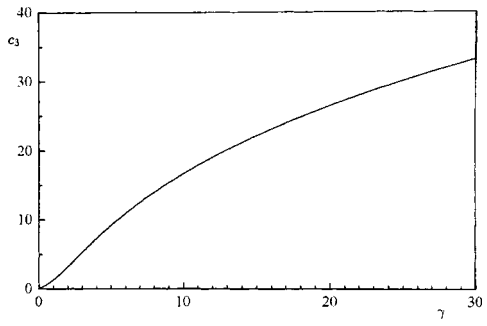

FIG. 2. The coefficient $c_3(\gamma)$ as a function of γ.

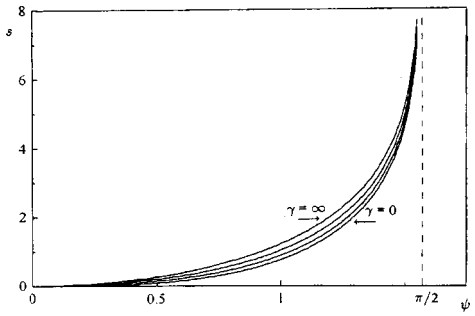

FIG. 3. $s(\psi,\gamma)$ from Eq. (9), determining the angular distributions of the photoelectrons. The curves (bottom to top) correspond to $\gamma=0$, 0.5, 1, and ∞.

$$w(\psi)\propto[J_{n_0}(n_0\xi)]^2, \quad \xi=\sqrt{\frac{1-t_0^2}{1+\gamma^2}}\cos\psi, \tag{8}$$

where $J_{n_0}(z)$ is a Bessel function. Using Langer's asymptotic expression[11] for the Bessel function for $n_0\gg 1$, we find

$$w(\psi)=u_0\eta^{-1}\exp\{-n_0\, s(\psi,\gamma)\}w(0), \tag{9}$$

where

$$s=2[\tanh^{-1}\eta-\eta-(\tanh^{-1}u_0-u_0)], \quad \eta=\sqrt{1-\xi^2}, \tag{9'}$$

and the variable η ranges from u_0 (for $\psi=0$) to 1 (for $\psi=\pi/2$). The width of the angular distribution is

$$\Delta\psi\sim\begin{cases}\omega/\sqrt{F\kappa}\sim\sqrt{\gamma/K_0}, & \gamma\ll 1\\ K_0^{-1/2}, & \gamma\gg 1.\end{cases} \tag{10}$$

As Fig. 3 shows, the function $s(\psi,\gamma)$ varies little with increasing parameter γ (this was difficult to predict beforehand). For this reason, the variation of $w(\psi)$ from the adiabatic region to the case $\gamma\gtrsim 1$ is determined mainly by the variation of $n_0(\gamma)$.

Expression (9) simplifies in the adiabatic region $\gamma\ll 1$:

$$w(\psi)=(1+\chi^2)^{-1/2}\exp\left\{-\frac{2\kappa^3}{3F}[(1+\chi^2)^{3/2}-1]\right\}, \tag{11}$$

where $\chi=\psi/\gamma$. For very small angles we obtain a Gaussian distribution:

$$w(\psi)\approx\exp\left(-\frac{F\kappa}{\omega^2}\psi^2\right), \quad \psi\ll\gamma\ll 1, \tag{11'}$$

which agrees with Refs. 6, 12, and 13. However, the number of photoelectrons then decreases more rapidly:

$$w(\psi)\approx\gamma\psi^{-1}\exp\left(-\frac{2F^2}{3\omega^3}\psi^3\right), \quad \gamma\lesssim\psi\ll 1, \tag{11''}$$

and most of the photoelectrons always emerge near the plane of polarization of the light.

As $\psi \to 0$ (and for any value of γ), we have $s = u_0 \psi^2 + O(\psi^4)$, where u_0 is determined in Eq. (3′) with $t = t_0(\gamma)$. For this reason, for small angles

$$w(\psi) = \text{const} \cdot \exp\left\{ -c_4(\gamma) \frac{F\kappa}{\omega^2} \psi^2 \right\}, \tag{12}$$

$c_4 = \sqrt{(1+\gamma^{-2})(t_0^2+\gamma^2)}/(1+t_0)$. If $\gamma \ll 1$, then $c_4 = 1$, and expression (12) goes over to expression (11′). At the same time, for $\gamma \gg 1$ the coefficient $c_4 = \gamma/2$ and $w(\psi) \approx \exp(-K_0 \psi^2)$. A comparison with expression (11′) shows that as γ increases, the angular distribution broadens substantially, but even for $\gamma \gg 1$ it remains quite narrow ($\Delta\psi \sim K_0^{-1/2} \ll 1$). In the two limiting cases we have

$$s(\psi, \gamma) = \begin{cases} 2[\tanh^{-1}(\sin\psi) - \sin\psi], & \gamma \to 0 \\ -2 \ln\cos\psi, & \gamma \to \infty, \end{cases} \tag{13}$$

which determines the limiting curves in Fig. 3.

In summary, we have analyzed the form of the energy and angular distributions of photoelectrons in the entire range of the Keldysh parameter, $0 < \gamma < \infty$, for linear and circular polarizations of the light. The general case of elliptic polarization can be examined on the basis of the formulas in Ref. 14, but the expressions obtained are quite complicated and require a separate discussion.

In closing, we note that a generalization of Eq. (1) for the electron momentum spectrum with an arbitrary dependence of the electric field $F(t)$ can be obtained for linear polarization. The only assumption is that $F(t)$ is an analytic function of t, and the ''imaginary time'' method[14] is used.

I am deeply grateful to V. D. Mur for helpful suggestions in the course of this work, to V. S. Imshennik, A. I. Nikishov, L. B. Okun', and V. I. Ritus for discussing some questions associated with this work and for moral support, and to V. A. Gan' and M. N. Markina for assisting in the numerical calculations and for setting up the manuscript.

This work was supported in part by the Russian Fund for Fundamental Research under Grant 98-02-17007.

[1)] Unfortunately, it must be said that the contributions of Refs. 3, 4, and 7, the importance of which remains undiminished to this day, is treated extremely unobjectively in Refs. 5 and 6. See Ref. 8 for details.
[2)] See Eq. (53) in Ref. 4. We employ atomic units, $\hbar = m = e = 1$.
[3)] These coefficients are often encountered in quantum mechanics and atomic and nuclear physics. Tables of their numerical values for the s states of neutral atoms and certain ions can be found in Ref. 9.
[4)] This result is contained in a somewhat different form in Ref. 10, where expansions in the limiting cases of small and large γ are also presented.

[1] L. V. Keldysh, Zh. Éksp. Teor. Fiz. **47**, 1945 (1964) [Sov. Phys. JETP **20**, 1307 (1964)].
[2] A. Gold and H. B. Bebb, Phys. Rev. Lett. **14**, 60 (1065).
[3] A. I. Nikishov and V. I. Ritus, Zh. Éksp. Teor. Fiz. **50**, 255 (1966) [Sov. Phys. JETP **23**, 168 (1966)].
[4] A. M. Perelomov, V. S. Popov, and M. V. Terent'ev, Zh. Éksp. Teor. Fiz. **50**, 1393 (1966) [Sov. Phys. JETP **23**, 1924 (1966)].
[5] N. B. Delone and V. P. Krainov, *Multiphoton Processes in Atoms* (Springer, Berlin, 1994).
[6] N. V. Delone and V. P. Kraĭnov, Usp. Fiz. Nauk **16**, 531 (1998).

[7] A. M. Perelomov and V. S. Popov, Zh. Éksp. Teor. Fiz. **52**, 514 (1967) [Sov. Phys. JETP **25**, 336 (1967)].
[8] V. S. Popov, Usp. Fiz. Nauk **19**, 819 (1999).
[9] V. S. Popov, B. M. Karnakov, and V. D. Mur, Phys. Lett. A **229**, 306 (1997); Zh. Éksp. Teor. Fiz. **113**, 1579 (1998) [JETP **86**, 860 (1998)].
[10] A. I. Nikishov, Tr. Fiz. Inst. Akad. Nauk SSSR **111**, 152 (1979).
[11] R. E. Langer, Trans. Am. Math. Soc. **33**, 23 (1931); *ibid*. **34**, 447 (1932).
[12] P. B. Corkum, N. H. Burnett, and F. Brunel, Phys. Rev. Lett. **62**, 1259 (1989).
[13] N. B. Delone and V. P. Krainov, J. Opt. Soc. Am. B **8**, 1207 (1991).
[14] A. M. Perelomov, V. S. Popov, and M. V. Terent'ev, Zh. Éksp. Teor. Fiz. **51**, 309 (1966) [Sov. Phys. JETP **24**, 207 (1967)].

Translated by M. E. Alferieff

Light-induced conversion of nuclear spin modifications of molecules

A. M. Shalagin*) and L. V. Il'ichev
Institute of Automation and Electrometry, Siberian Branch of the Russian Academy of Sciences, 630090 Novosibirsk, Russia

(Submitted 27 August 1999)
Pis'ma Zh. Éksp. Teor. Fiz. **70**, No. 8, 498–503 (25 October 1999)

We report a new effect in which one nuclear spin modification of molecules is converted into another in a resonance laser radiation field. The effect is based on selective (with respect to modifications) optical excitation and the difference of the conversion rates of spin modifications for excited and unexcited molecules. The effect is expected to be very substantial and should occur for all molecules capable of absorbing the radiation of existing lasers. © *1999 American Institute of Physics.* [S0021-3640(99)00420-X]

PACS numbers: 33.80.−b, 33.25.+k

A recent paper[1] on which the present authors collaborated predicts enrichment of the spin modifications of molecules under selective laser excitation of one of the modifications. It was assumed that the effect occurs in molecules for which the principal mechanism of conversion of spin modifications is an intramolecular interaction that mixes the spin states of the nuclei. In Ref. 1 it is shown that for a suitable choice of the frequency of the exciting radiation the enrichment effect could be extremely large (the relative concentration of the spin modifications can change by orders of magnitude). At the same time, the requirements imposed in Ref. 1 on the frequency of laser radiation turned out to be quite stringent. Specifically, for CH_3F molecules, which otherwise are suitable for exhibiting the effect, the capabilities of the CO_2 laser and other known sources are inadequate for discriminating the required frequency. The laser lines of a CO_2 laser which are efficiently absorbed by CH_3F molecules do not meet the requirements of Ref. 1. Thus the implementation of the idea of Ref. 1 turned out to be a difficult problem because of the difficulties of matching suitable excitation sources to the experimental object.

It turns out that the vexing restrictions of Ref. 1 on the radiation frequency can be lifted with almost no loss of the degree of enrichment. The only remaining requirement on the radiation frequency is that it should be efficiently absorbed on a vibrational or electronic transition of the molecule from the ground state. This radically expands the range of objects which should exhibit the light-induced conversion effect even for existing sources of radiation.

The effect which we propose is physically completely analogous to light-induced drift (LID),[2] which, in particular, has been used previously to achieve the separation of

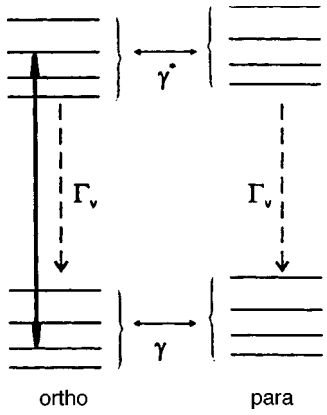

FIG. 1. Illustration of the light-induced conversion effect. The solid arrow symbolizes induced optical transitions.

nuclear spin modifications of heavy molecules,[3] and other light-induced gas-kinetic effects (see, for example, Ref. 4): If the radiation can excite particles selectively with respect to some physical parameter, then as a result of the difference of the relaxation rates of this parameter for excited and unexcited particles, its value in the radiation field will deviate from the thermodynamically equilibrium value.

In the present case this physical parameter is the concentration of one of the spin modifications of molecules which is selectively excited by laser radiation and relaxation is the process of conversion of the spin modifications. The conversion rates for excited and unexcited molecules should differ, to one or another degree, for any mechanism of this process, but the greatest difference (orders of magnitude) can be expected for a mechanism based on intramolecular magnetic interaction. This mechanism, which has been unequivocally proved for CH_3F molecules,[5–12] and seems to be characteristic of most heavy and complex molecules, is of a resonance character: The conversion rate increases sharply when the quantum states of the mixed spin modifications are close in energy. Then, for a given modification only one level (the most ''resonant'' one) through which conversion predominantly occurs can stand out. The realization of identical ''resonance'' conditions for the rotational levels of different vibrational ''electronic'' states of molecules is essentially precluded, so that the conversion rates for these states can differ radically. In what follows, we shall consider the conversion mechanism associated with intramolecular interaction.

For simplicity, we assume that the molecules exhibit only two (para and ortho) nuclear spin modifications (see Fig. 1). For definiteness, we shall consider laser excitation on a vibrational transition of the ortho modification. We shall assume an equilibrium Boltzmann population distribution over the rotational levels in the vibrational states; this is valid when the vibrational relaxation rate is sufficiently less than the rotational relaxation rate. These conditions can almost always be satisfied by adding an appropriate buffer gas. Under the conditions stipulated, the temporal variation of the concentration of the ortho component is described by the equation

$$dN_o/dt = \gamma^*(N_p^* - N_o^*) + \gamma[(N_p - N_p^*) - (N_o - N_o^*)]$$
$$= (\gamma^* - \gamma)(N_p^* - N_o^*) + \gamma(N_p - N_o); \quad (1)$$

$$\gamma^* \equiv \sum_{J_o^*} \gamma_{op}^* W(J_o^*), \quad \gamma \equiv \sum_{J_o} \gamma_{op} W(J_o).$$

Here N_o and N_p are the concentrations of the ortho and para components, and γ and γ^* are the conversion rates. An asterisk marks the characteristics of vibrationally excited molecules. The quantity $\gamma_{op} W(J_o)$ characterizes the partial rate of conversion through a rotational level J_o of the ortho modification; $W(J_o)$ is the Boltzmann factor.

If there is no radiation ($N_p^* = N_o^* = 0$), then it follows from Eq. (1) that under stationary conditions $N_p = N_o$ (thermodynamic equilibrium). If $\gamma^* = \gamma$, then equilibrium also remains when radiation is present. In the opposite case ($\gamma^* \neq \gamma$), according to Eq. (1), a new dynamic equilibrium, in which

$$N_p - N_o = (1 - \gamma^*/\gamma)(N_p^* - N_o^*), \quad (2)$$

is established.

Laser radiation excites only the ortho modification, but to one degree or another excited para molecules will also be present ($N_p^* \neq 0$) as a result of the resonant transfer of excitation from the ortho molecules. Since the conversion process is the slowest of all other relaxation processes (rotational and vibrational relaxation, diffusion processes), the establishment of the populations of the molecular levels against this background is instantaneous and corresponds to the instantaneous values of the concentrations of the ortho and para components. Specifically, the balance relation

$$\alpha N_o^*(N_p - N_p^*) - \alpha N_p^*(N_o - N_o^*) = \Gamma_v N_p^*, \quad (3)$$

holds for excited para molecules. Here the first term on the left-hand side describes the ''arrival'' of excited para molecules as a result of the transfer of excitation from ortho molecules; the second term corresponds to the reverse process; the coefficient α characterizes the excitation exchange rate. The term on the right-hand side is due to quenching of the excited vibrational state. From the relation (3) follows

$$N_p^* = \frac{\alpha N_p}{\Gamma_v + \alpha N_o} N_o^*. \quad (4)$$

For a suitable buffer gas and its pressure, the condition

$$\Gamma_v \gg \alpha(N_o + N_p), \quad (5)$$

can be satisfied. Then $N_p^* \ll N_o^*$ and N_p^* in the relation (2) can be neglected. The deviation from thermodynamic equilibrium for the concentrations of the para and ortho modifications is especially large, and it is especially simply related with the fraction of vibrationally excited ortho molecules. It is known that under certain conditions (sufficiently high radiation intensity and the required ratio of the relaxation rates) this fraction can be 1/2, and in this case from Eq. (2) follows

$$\frac{N_p}{N_o} = \frac{1}{2}\left(1 + \frac{\gamma^*}{\gamma}\right). \quad (6)$$

The limiting cases of this formula can be easily interpreted. If $\gamma^* \ll \gamma$, then $N_o = 2N_p$, which is natural, since conversion through the excited state essentially does not occur, while conversion through the ground state equalizes the total concentration of para molecules and the concentration of ortho molecules in the ground state, which is half of their total concentration. In the opposite limiting case ($\gamma^* \gg \gamma$) we have $N_o \ll N_p$, i.e., virtually all molecules are in the para modification. This is also understandable: Transfer of molecules into the para state occurs through an excited state, and the reverse process is strongly inhibited, since para molecules are primarily in the ground state.

Let us now discuss the conditions under which the distribution of the rotational levels of the vibrational states can be regarded as close to a Boltzmann distribution. If the laser radiation is absorbed on a vibrational–rotational transition, then the relative excess of the population of the upper level J_L of the optical transition above the amplitude of the Boltzmann ''cushion'' is determined by the parameter (see, for example, Refs. 4 and 13)

$$a = \Gamma_v / \Gamma W(J_L), \tag{7}$$

where Γ is the collisional half-width of the line and is determined primarily by rotational relaxation (broadening is assumed to be homogeneous); $W(J_L)$ is the Boltzmann factor for the level J_L. The parameter a in molecules can in itself be small, but it can be decreased even more by adding a buffer gas for which the ratio of the cross section of quenching of the vibrational state to the broadening cross section is characteristically quite small. For $a \ll 1$ the populations of the rotational levels of the vibrational states are completely described by a Boltzmann distribution.

The total population of a vibrational state of ortho molecules is determined by the relation[4,13]

$$N_o^* = N_o \frac{\kappa/2}{1 + \kappa + \Omega^2/\Gamma^2}, \quad \kappa = \frac{4|G|^2}{\Gamma_v \Gamma} W(J_L), \quad G = \frac{Ed}{2\hbar}. \tag{8}$$

Here Ω is the detuning of the radiation frequency from resonance, E is the amplitude of the electric field of the radiation, d is the matrix element of the dipole moment of the resonance transition, and κ is the so-called saturation parameter. It is evident from this formula that for a sufficiently large saturation parameter $N_o^* = N_o/2$, which is used in Eq. (6).

Let us now estimate the possible magnitude of the effect for $^{13}CH_3F$ molecules, which absorb CO_2 laser radiation (the $P(32)$ line of the 9.6 μm band) on the transition $R(4,3)$ essentially resonantly ($\Omega \simeq 26$ MHz with Doppler half-width $\simeq 40$ MHz). Only molecules of the ortho modification absorb radiation. We shall consider a $\simeq 30$ cm long absorbing cell. Since the absorption coefficient $\sim 0.3\ \text{cm}^{-1}/\text{torr}$,[14] the probe laser radiation required for testing is strongly absorbed over this distance at approximately 0.1 torr $^{13}CH_3F$ pressure. We shall take it as the working value. Unless special measures are taken, relation (5) will not be satisfied, so that to increase the constant Γ_v we propose adding a buffer gas whose molecules have a close vibrational quantum so that the vibrational excitation of $^{13}CH_3F$ would be transferred to them. In order to guarantee that this process be irreversible it is desirable to use a buffer gas with a vibrational quantum of somewhat lower energy. Assuming the rate of transfer of excitation to the buffer molecules to be comparable to the rate of exchange of excitation between the $^{13}CH_3F$ mol-

ecules themselves and choosing the pressure of the buffer gas of this type to be 0.5 torr, we obtain $\Gamma_v = 5\alpha(N_o + N_p)$, i.e., the condition (5) essentially holds.

We now consider the parameter (7). Taking account of the data in Ref. 15 on the rate of exchange of excitation between $^{13}CH_3F$ and $^{12}CH_3F$ molecules (5×10^5 s^{-1}/torr) we obtain for Γ_v the concrete total value $\Gamma_v \cong 40$ kHz. For the total gas pressure obtained thus far and for broadening $\simeq 20$ MHz/torr[16] by a ''resonant'' gas we obtain $\Gamma \simeq 12$ MHz. Since $W(J_L) \sim 10^{-2}$, the parameter a from Eq. (7) becomes $a \simeq 1/3$, which is still not sufficiently small. However, if a ''nonresonant'' gas, for example, helium at 10 torr pressure, is added as a second buffer component, then taking account of the broadening due to it (3 MHz/torr[16]) the resulting value of Γ becomes $\Gamma \cong 40$ MHz. The value of Γ_v will remain essentially unchanged, since the quenching of the vibrational state by helium ($\sim 10^2$ Hz/torr)[17] is negligible. Under these conditions we obtain $a \simeq 1/10 \ll 1$, i.e., relation (7) holds. We note that the value obtained for Γ is approximately the same as the Doppler half-width, so that the estimates based on the homogeneous broadening approximation are completely justified.

Finally, we shall estimate the attainable saturation parameter from Eq. (8). For a radiation power density $\sim 10^3$ W/cm^2 (a 10-W laser beam 1 mm in diameter), according to the estimates made in Ref. 14 we obtain $\kappa \simeq 50$, which is more than sufficient to saturate the vibrational transition.

In summary, the experimental conditions proposed above are close to optimal for light-induced conversion, and the simple formula (6), the consequences of which have already been discussed above, is completely valid for estimating its magnitude under these conditions.

We note that, in reality, the condition (5) is not fundamental, in any case in the situation $\gamma^* \gg \gamma$, i.e., when the effect is expected to be strongest. Concrete calculations show that for virtually complete ''transfer'' from the ortho into the para state occurs for $\Gamma_v \simeq \alpha(N_o + N_p)$ provided that N_o^* is not too small compared with N_o.

We note one other important circumstance. An external electric field can also radically affect the rate of light-induced conversion as well as the degree of transformation of one modification into another: The energy levels through which conversion occurs in the ground state and in excited vibrational states can be put into (or taken out of) resonance as a result of the Stark shift. The effect of an external electric field on the conversion rate of nuclear spin modifications of CH_3F has been reliably proved and investigated in detail in Refs. 10 and 11. From the results of these investigations it can also be concluded that an electric field also provides a promising means for identifying the levels through which conversion occurs.

In summary, we have shown that if molecules possess nuclear spin modifications, one of which is capable of absorbing laser radiation, a deviation from the natural ratio of concentrations of these modifications right up to complete exhaustion of one modification can be obtained by simply adjusting the experimental conditions.

This work was supported by the Russian Fund for Fundamental Research (Grants Nos. 98-02-17924 and 98-03-33124a).

*)e-mail: shalagin@iae.nsk.su

[1] L. V. Il'ichov, L. J. F. Hermans, A. M. Shalagin, and P. L. Chapovsky, Chem. Phys. Lett. **297**, 439 (1998).
[2] F. Kh. Gel'mukhanov and A. N. Shalagin, JETP Lett. **29**, 711 (1979).
[3] L. N. Krasnoperov, V. N. Panfilov, V. P. Strunin, and P. L. Chapovskiĭ, JETP Lett. **39**, 143 (1984).
[4] S. G. Rautian and A. M. Shalagin, *Kinetic Problems of Nonlinear Spectroscopy*, North-Holland (1991).
[5] P. L. Chapovskiĭ, Zh. Éksp. Teor. Fiz. **97**, 1585 (1990) [Sov. Phys. JETP **70**, 895 (1990)].
[6] P. L. Chapovsky, Phys. Rev. A **43**, 3624 (1991).
[7] B. Nagels, M. Schuurman, P. L. Chapovsky, and L. J. F. Hermans, J. Chem. Phys. **103**, 5161 (1995).
[8] B. Nagels, M. Schuurman, P. L. Chapovsky, and L. J. F. Hermans, Phys. Rev. A **54**, 2050 (1996).
[9] P. L. Chapovsky, Physica A **233**, 441 (1996).
[10] B. Nagels, M. Schuurman, L. J. F. Hermans, and P. L. Chapovsky, Chem. Phys. Lett. **242**, 48 (1995).
[11] B. Nagels, N. Calas, D. A. Roozemond *et al.*, Phys. Rev. Lett. **77**, 4732 (1996).
[12] E. Ilisca and K. Bahloul, Phys. Rev. A **57**, 4296 (1998).
[13] V. R. Mironenko and A. M. Shalagin, Izv. Akad. Nauk SSSR, Ser. Fiz. **45**, 995 (1981).
[14] V. N. Panfilov, V. P. Strunin, and P. L. Chapovskiĭ, Zh. Éksp. Teor. Fiz. **85**, (1983) [Sov. Phys. JETP **58**, 510 (1983)].
[15] E. N. Chesnokov and V. N. Panfilov, Zh. Éksp. Teor. Fiz. **73**, 2122 (1977) [Sov. Phys. JETP **46**, 1112 (1977)].
[16] W. K. Bihel, P. J. Kelly, and Ch. K. Rhodes, Phys. Rev. A **13**, 1817 (1976).
[17] E. Weitz and G. W. Flynn, J. Chem. Phys. **58**, 2678 (1973).

Translated by M. E. Alferieff

Charged mobile complexes in magnetic fields: a novel selection rule for magnetooptical transitions

A. B. Dzyubenko
Institut für Theoretische Physik, J. W. Goethe-Universität, 60054 Frankfurt, Germany; General Physics Institute Russian Academy of Sciences, 117942 Moscow, Russia

A. Yu. Sivachenko
The Weizmann Institute of Science, Rehovot 76100, Israel

(Submitted 10 September 1999)
Pis'ma Zh. Éksp. Teor. Fiz. **70**, No. 8, 504–509 (25 October 1999)

The implications of magnetic translations for internal optical transitions of charged mobile electron–hole ($e-h$) complexes and ions in a uniform magnetic field B are discussed. It is shown that transitions of such complexes are governed by a novel exact selection rule. Internal intraband transitions of two-dimensional (2D) charged excitons X^- in strong magnetic fields are considered as an illustrative example.
 [S0021-3640(99)00520-4]

PACS numbers: 71.35.Ee, 78.20.Ls

Recently, there has been considerable experimental and theoretical interest in the behavior of 2D semiconductor complexes — negatively X^- ($2e-h$) and positively X^+ ($e-2h$) charged excitons in magnetic fields (see, e.g., Refs. 1–5 and references therein). These three-particle bound states can be considered as analogs of the hydrogen atomic H^- and molecular H_2^+ ions, respectively. The application of a magnetic field B changes the hydrogenic spectra drastically (see, e.g., Refs. 6–8). As an example, whereas at $B=0$ the H^- ion supports in 3D only one bound singlet state, at any finite B there appear[7] bound triplet H^- states and an infinite number of quasi-bound states (resonances) associated with higher Landau levels (LLs). In 2D systems, it is the X^- triplet that becomes the ground state in high magnetic fields.[2,3] Singlet and triplet X^- and X^+ states are observed in 2D systems by means of interband optical magnetospectroscopy.[1] Intraband magnetospectroscopy, in which internal transitions from populated (ground) to excited states are induced by a photon, can provide additional information about binding of hydrogenlike complexes. In the σ^+ polarization internal transitions in high B are predominantly induced to the next electron LL. Such photoionizing bound-to-continuum X^- singlet and triplet transitions in the far-infrared (FIR) have been predicted theoretically and recently observed experimentally in GaAs quantum wells.[4] In this work we describe some general implications of the existing exact symmetry — magnetic translations — for internal transitions of charged mobile $e-h$ complexes in B. We also present theoretical predictions for internal transitions from the X^- ground triplet state in the σ^- polarization in high B. A preliminary account of some of these results and implications for interband magnetooptics of X^- have been reported in Ref. 5.

Consider the Hamiltonian of interacting particles of charges e_i in a magnetic field $\mathbf{B}$

$$H=\sum_i \frac{\hat{\pi}_i^2}{2m_i}+\frac{1}{2}\sum_{i\neq j} U_{ij}(\mathbf{r}_i-\mathbf{r}_j)\,, \tag{1}$$

here $\hat{\pi}_i=-i\hbar\nabla_i-\frac{e_i}{c}\mathbf{A}(\mathbf{r}_i)$, and the interparticle interaction potentials U_{ij} can be rather arbitrary. In the symmetric gauge $\mathbf{A}=\frac{1}{2}\mathbf{B}\times\mathbf{r}$ the total angular momentum projection M_z, an eigenvalue of $\hat{L}_z=\Sigma_i(\mathbf{r}_i\times-i\hbar\nabla_i)_z$, is an exact quantum number. In a uniform $\mathbf{B}=(0,0,B)$ the Hamiltonian (1) is also invariant under a group of magnetic translations whose generators are the components of the operator $\hat{\mathbf{K}}=\Sigma_j\hat{\mathbf{K}}_j$, $\hat{\mathbf{K}}_j=\hat{\pi}_j-(e_j/c)\mathbf{r}_j\times\mathbf{B}$ (see, e.g., Refs. 6,7). The operator $\hat{\mathbf{K}}$ is an exact integral of the motion, $[H,\hat{\mathbf{K}}]=0$, whose components commute in B as

$$[\hat{K}_x,\hat{K}_y]=-i\frac{\hbar B}{c}Q,\quad Q\equiv\sum_j e_j\,, \tag{2}$$

while $[\hat{K}_{ip},\hat{\pi}_{jq}]=0$, $p,q=x,y$. For neutral complexes (atoms, excitons, biexcitons) $Q=0$, and the states in $\mathbf{B}$ are classified according to the two-component continuous vector — the 2D magnetic momentum $\mathbf{K}=(K_x,K_y)$ (Refs. 6,7). For charged systems $Q\neq 0$, and the components of $\hat{\mathbf{K}}$ do not commute; this determines the macroscopic Landau degeneracy of the exact eigenstates of (1). Using the dimensionless operator $\hat{\mathbf{k}}=\sqrt{c/\hbar B|Q|}\,\hat{\mathbf{K}}$ whose components are canonically conjugate, one obtains the raising and lowering Bose ladder operators $\hat{k}_\pm=(\hat{k}_x\pm i\hat{k}_y)/\sqrt{2}$: $[\hat{k}_-,\hat{k}_+]=Q/|Q|$ (see (5) below). Therefore $\hat{\mathbf{k}}^2=\hat{k}_+\hat{k}_-+\hat{k}_-\hat{k}_+$ has the oscillator eigenvalues $2k+1$, $k=0,1,\ldots$. Since $[\hat{\mathbf{k}}^2,H]=0$ and $[\hat{\mathbf{k}}^2,\hat{L}_z]=0$, the exact charged eigenstates of (1) can be simultaneously labeled by the discrete quantum numbers k and M_z (Ref. 7).

The usual optical selection rules for the dipole-allowed transitions in the Faraday geometry (the light propagates along $\mathbf{B}$) are conservation of spin and $\Delta M_z=\pm 1$ for left- and right-circularly polarized light $\sigma^\pm$. There is an additional selection rule: the quantum number k is conserved. Indeed, the Hamiltonian $\hat{V}^\pm=\Sigma_i(e_i\mathcal{F}_0\hat{\pi}_i^\pm/m_i\omega)e^{-i\omega t}$ describing the interaction with the light of polarization $\sigma^\pm$ ($\mathcal{F}_0$ is the radiation electric field, $\hat{\pi}_i^\pm=\hat{\pi}_{ix}\pm i\hat{\pi}_{iy}$) commutes with $\hat{\mathbf{K}}_i$ and, therefore

$$[\hat{V}^\pm,\hat{\mathbf{k}}^2]=0\Rightarrow k \text{ is conserved.} \tag{3}$$

In fact the perturbation $\hat{V}=F(\hat{\pi}_i,t)$ can be an arbitrary function of the kinematic momentum operators $\hat{\pi}_i$ and time t. In some limiting cases (e.g., at low fields B) k can be associated[7] with the center of the cyclotron motion of a charged system as a whole. This gives some physical insight into its conservation. This selection rule is applicable to any charged $e-h$ system in B. In particular, it applies to mobile complexes — charged excitons X^-, X^+, multiply charged excitons X^{-n} (i.e., bound complexes $(n+1)e-h$ with $n>1$, which can exist in special quasi-2D geometries),[9] and to charged multiple-excitons X_N^- (X_N-e), which exist in 2D systems in high B.[2] In deriving (3) we only used translational invariance in the plane perpendicular to $\mathbf{B}$. Therefore, relation (3) holds in arbitrary magnetic fields and for systems of different dimensionality, including semicon-

ductors with a complex valence band described by the Luttinger Hamiltonian.[10] The selection rule (3) is also valid for internal transitions in electron systems. Note that for a translationally invariant one-component (e.g., electron) system with constant charge-to-mass ratio $e_i/m_i=\text{const}$, the well-known Kohn theorem[11] states that internal transitions can occur only at the bare electron cyclotron (e-CR) energy $\hbar\omega_{\text{ce}}=\hbar eB/m_e c$. This is a consequence of the operator algebra $[H,\hat{V}^{\pm}]=\pm\hbar\omega_{\text{ce}}\hat{V}^{\pm}$ involving the center-of-mass *inter*-LL ladder operators. On the other hand, relation (3) is based on the algebra of *intra*-LL ladder operators. However, for one-component systems the center-of-mass motion decouples from the internal degrees of freedom in B, and the theorems — though based on different operator algebras — give equivalent predictions in this case.

To make our further discussion concrete, let us consider transitions in the σ^- polarization in a 2D three-particle $2e-h$ system with Coulomb interactions, for a simple valence band, and in the limit of high magnetic fields:

$$\hbar\omega_{\text{ce}},\hbar\omega_{\text{ch}},|\hbar\omega_{\text{ce}}-\hbar\omega_{\text{ch}}|\gg E_0=\sqrt{\frac{\pi}{2}}\frac{e^2}{\epsilon l_B},\quad l_B=\left(\frac{\hbar c}{eB}\right)^{1/2}. \tag{4}$$

Then mixing between different LLs can be neglected and the X^- states can be classified according to the total electron and hole LL numbers, (N_eN_h). The corresponding basis for X^- is of the form[12] $\phi^{(e)}_{n_1m_1}(\mathbf{r})\,\phi^{(e)}_{n_2m_2}(\mathbf{R})\,\phi^{(h)}_{N_hM_h}(\mathbf{r}_h)$, and includes different three-particle $2e-h$ states such that the total angular momentum projection $M_z=N_e-N_h-m_1-m_2+M_h$ and LLs $N_e=n_1+n_2$, N_h are fixed. Here $\phi^{(e,h)}_{nm}$ are the e- and h- single-particle factored wave functions in B; n is the LL quantum number and m is the oscillator quantum number $[m_{ze(h)}=\overset{+}{(-)}(n-m)]$. We use the electron relative and center-of-mass coordinates: $\mathbf{r}=(\mathbf{r}_{e1}-\mathbf{r}_{e2})/\sqrt{2}$ and $\mathbf{R}=(\mathbf{r}_{e1}+\mathbf{r}_{e2})/\sqrt{2}$. Permutational symmetry requires that for electrons in the spin-singlet s (triplet t) state the relative motion angular momentum n_1-m_1 should be even (odd). To make this basis compatible with magnetic translations, i.e., to fix k, an additional Bogoliubov canonical transformation should be performed.[5]

The calculated eigenspectra of the three-particle $2e-h$ states with two electrons in the spin-triplet state t ($S_e=1$) are shown for two lowest $(N_eN_h)=(00)$, (01) LLs in Fig. 1. The spectra consist of continua, which correspond to the motion of a neutral magnetoexciton (MX).[4,8] In addition, there are discrete bound X^- states lying outside the continua in which the internal motions of all the particles are finite. The continuum in the $(N_eN_h)=(00)$ LL consists of a MX band of width E_0 extending down in energy from the free (00) LL and corresponding to the $1s$ MX ($N_e=N_h=0$)[8] plus a scattered electron in the zeroth LL, labeled $X_{00}+e_0$. In the next hole LL $(N_eN_h)=(01)$, the MX band is of width $0.574E_0$ (Ref. 8) and corresponds to the $2p^-$ MX ($N_e=0$, $N_h=1$) plus a scattered electron in the $N_e=0$ LL, labeled $X_{01}+e_0$. Moreover, there is a band above each free LL originating from the bound internal motion of two 2D electrons in B (labeled $2e+h_{N_h}$).[4] The spectra of the discrete bound X^- states are the following. In the lowest $(N_eN_h)=(00)$ LL there exists only one bound X^-_{t00} triplet state, lying below the lower edge of the $1s$ MX band, the binding energy of which is $0.043E_0$ (Refs. 2,3). In the next hole LL $(N_eN_h)=(01)$ the $2p^-$ MX band is narrow, and there appear *many* bound X^-_{t01} states lying below the continuum edge (Fig. 1). This should be contrasted with the

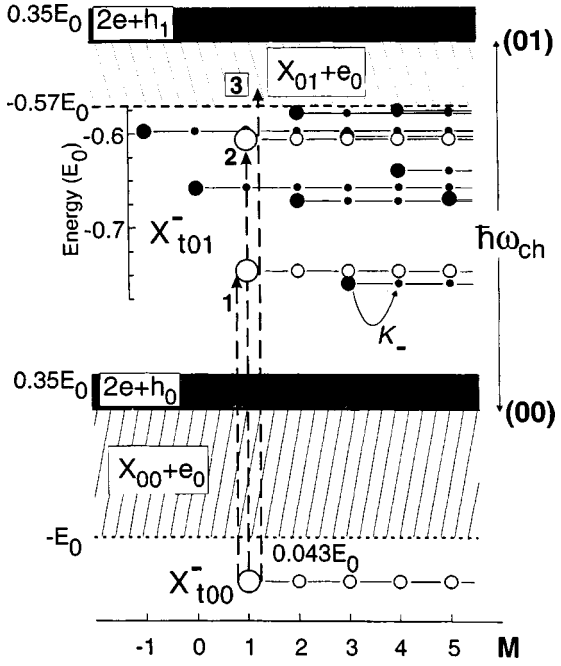

FIG. 1. Schematic drawing of bound and scattering electron triplet $2e-h$ states in the lowest LLs $(N_eN_h)=(00)$, (01). The quantum number $M=-M_z$ for the $(N_eN_h)=(00)$ states and $M=-M_z-1$ for the $(N_eN_h)=(01)$ states. Large (small) dots correspond to the bound parent $k=0$ (daughter $k=1,2,\ldots$) X^- states. Allowed strong transitions in the σ^- polarization must satisfy $\Delta N_h=1$, $\Delta M_z=-1$, and $\Delta k=0$. Filled dots in the (01) LL correspond to families of dark X^-_{t01} states (see text).

situation in the next electron LL $(N_eN_h)=(10)$, where only one bound triplet state X^-_{t10} exists.[4]

In the σ^- polarization, the h–CR-like inter-LL $\Delta N_h=1$ transitions are strong and gain strength in B. These are allowed by the usual selection rules: spin conserved, $\Delta M_z=-1$. Consider first the photoionizing X^- transitions in which the final three-particle states belong to the $X_{01}+e_0$ continuum. There is an onset at the edge indicated in Fig. 1 by transition *3*. It occurs at an energy $\hbar\omega_{\rm ch}+0.469E_0$, i.e., above the h–CR at an energy that equals the difference in the $1s$ and $2p^-$ MX binding energies, plus the X^-_{t00} binding energy. This transition may be thought of as the $1s\rightarrow 2p^-$ internal transition of the MX,[13] which is shifted and broadened by the presence of the second electron. Photoionizing transitions to the $2e+h_1$ band have extremely small oscillator strengths and can be neglected.

In order to understand bound-to-bound transitions $X^-_{t00}\rightarrow X^-_{t01}$, let us describe the structure of the X^- states in more detail. Generally, there exist *families* of macroscopically degenerate X^- states in B. Each ith family starts with its *parent state* (PS) $|\Psi^{(P_i)}_{M_z}\rangle$, for which $k=0$ and M_z has its maximum possible value for that family (cf. with translationally invariant states in 2D electron systems in strong B).[14] The normalized daughter

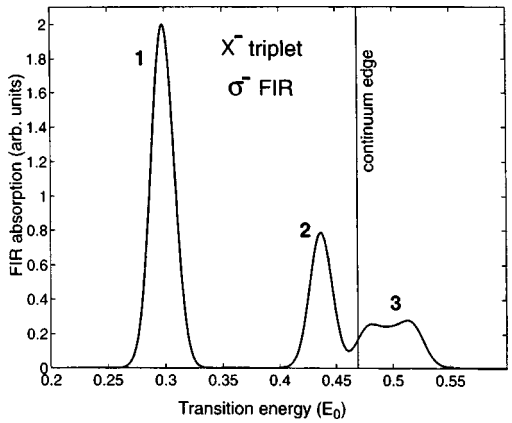

FIG. 2. Energies (counted from $\hbar\omega_{\rm ch}$, in units of $E_0=\sqrt{\pi/2}\,e^2/\epsilon l_B$) and dipole matrix elements of the inter-LL $\Delta N_h=1$ transitions (Fig. 1) from the ground triplet X^-_{t00} state in the high-field limit. The spectra have been convoluted with a Gaussian of width $0.02E_0$.

states with $k=1,2,\ldots$ in the ith family, $|\Psi^{(D_i)}_{M'_z}\rangle$, are constructed from the PS with the help of the ladder operators:

$$|\Psi^{(D_i)}_{M_z-l}\rangle=\frac{1}{\sqrt{l!}}\,\hat{k}_-^l|\Psi^{(P_i)}_{M_z}\rangle\,, \tag{5}$$

where we have used the relation $[\hat{L}_z,\hat{k}_-]=-\hat{k}_-$. Conservation of k implies therefore that internal transitions in the $\sigma^\pm$ polarization, satisfying the usual selection rule $\Delta M_z=\pm1$, spin conserved, are allowed only between states from families such that their PSs are connected by a dipole transition $|\Psi^{(P_j)}_{M_z}\rangle\to|\Psi^{(P_i)}_{M'_z}\rangle$, i.e., have $M'_z=M_z\pm1$. Indeed, for the transition dipole matrix element between the daughter states in the mth and nth generations we have from (5):

$$\mathcal{D}_{ij}=\langle\Psi^{(D_i)}_{M'_z-m}|\hat{V}^\pm|\Psi^{(D_j)}_{M_z-n}\rangle=\frac{1}{\sqrt{n!m!}}\langle\Psi^{(P_i)}_{M'_z}|\hat{k}_+^m\hat{V}^\pm\hat{k}_-^n|\Psi^{(P_j)}_{M_z}\rangle\,. \tag{6}$$

From the commutativity $[\hat{V}^\pm,\hat{k}_-]=[\hat{V}^\pm,\hat{k}_+]=0$ we see that either $\hat{k}_-$ annihilates the left PS ($n>m$) or $\hat{k}_+$ annihilates the right PS ($n<m$) in (6). Therefore $\mathcal{D}_{ij}=0$ unless $n=m$ and $M'_z-M_z=\pm1$. From the operator algebra it is clear that $\mathcal{D}_{ij}$ is the same in all generations, and thus it characterizes the two families of states.

This selection rule, due to the rich structure of the continuum, is easily satisfied for bound-to-continuum transitions. However, considering many families of the bound X^-_{t01} states in the next hole LL $(N_eN_h)=(01)$, we see that there are only two PSs that are connected by a FIR transition (Figs. 1 and 2). Therefore all families except these two are *dark*, i.e., are not accessible by internal transitions from the ground X^-_{t00} bound states: There exist only two strong bound-to-bound $X^-_{t00}\to X^-_{t01}$ transitions in the σ^- polarization, both lying above the h–CR (cf. Ref. 4). Breaking of translational invariance (e.g., by impurities) would make transitions to many dark states possible and lead to drastic

changes in the absorption spectra. We note also that in 2D systems the X^- states belonging to higher LLs are genuinely discrete only in a sufficiently strong B [cf. (4)]. With decreasing B, the discrete states merge with the MX continuum of lower LLs and become resonances. Such a situation is also typical for bulk 3D systems, where X^- (and H^-) states in higher LLs always merge with the continuum of the unbound internal z-motion in lower LLs.[7] Since the quantum number k is still rigorously conserved, the selection rule predicts which of the resonances are dark and which are not. The absorption spectra in such situation can have an asymmetric form typical for Fano resonances.

In conclusion, we have demonstrated that internal optical transitions of charged mobile complexes and ions in magnetic fields are governed by a novel exact selection rule, a manifestation of magnetic translational invariance. Internal bound-to-bound transitions of charged excitons X^- in 2D systems in B should be very sensitive to breaking of translational invariance (by impurities, disorder etc.). This can be used for studying the extent of X^- localization in quantum wells.

We thank S. M. Apenko, B. D. McCombe, D. M. Whittaker, and D. R. Yakovlev for helpful discussions. This work was supported by RBRF Grant # 97-2-17600 and the ''Nanostructures'' Grant # 97-1072. A.B.D. is grateful to the Humboldt Foundation for research support.

[1] G. Finkelstein, H. Shtrikman, and I. Bar-Joseph, Phys. Rev. Lett. **74**, 976 (1995); A. J. Shields, M. Pepper, M. Y. Simmons, and D. A. Ritchie, Phys. Rev. B **52**, 7841 (1995); D. R. Yakovlev, V. P. Kochereshko, R. Suris *et al.*, Phys. Rev. Lett. **79**, 3974 (1997); O. V. Volkov, V. E. Zhitomirskii, I. V. Kukushkin *et al.*, JETP Lett. **67**, 744 (1998).
[2] J. J. Palacios, D. Yoshioka, and A. H. MacDonald, Phys. Rev. B **54**, R2296 (1996).
[3] D. M. Whittaker and A. J. Shields, Phys. Rev. B **56**, 15 185 (1997).
[4] A. B. Dzyubenko, A. Yu. Sivachenko, H. A. Nickel *et al.*, http://xxx.lanl.gov/abs/cond-mat/9907124; Proceedings EP2DS-13, Ottawa, 1999, to be published in Physica E.
[5] A. B. Dzyubenko and A. Yu. Sivachenko, http://xxx.lanl.gov/abs/cond-mat/9908406; Proceedings EP2DS-13.
[6] L. P. Gor'kov and I. E. Dzyaloshinskii, Zh. Éksp. Teor. Fiz. **53**, 717 (1967) [Sov. Phys. JETP **26**, 449 (1968)].
[7] J. E. Avron, I. W. Herbst, and B. Simon, Ann. Phys. (N.Y.) **114**, 431 (1978).
[8] I. V. Lerner and Yu. E. Lozovik, Zh. Éksp. Teor. Fiz. **78**, 1167 (1980) [Sov. Phys. JETP **51**, 588 (1980)].
[9] V. I. Yudson, Phys. Rev. Lett. **77**, 1564 (1996).
[10] J. M. Luttinger, Phys. Rev. **102**, 1030 (1956).
[11] W. Kohn, Phys. Rev. **123**, 1242 (1961).
[12] A. B. Dzyubenko, Phys. Lett. A **165**, 357 (1992); **173**, 311 (1993).
[13] A. B. Dzyubenko, JETP Lett. **66**, 617 (1997).
[14] S. A. Trugman and S. Kivelson, Phys. Rev. B **31**, 5280 (1985).

Published in English in the original Russian journal. Edited by Steve Torstveit.

Equilibrium charge of small metal particles and hopping transport in a metal–insulator composite

É. M. Baskin and M. V. Éntin

Institute of Semiconductor Physics, Siberian Branch of the Russian Academy of Sciences, 630090 Novosibirsk, Russia

(Submitted 13 September 1999)
Pis'ma Zh. Éksp. Teor. Fiz. **70**, No. 8, 510–515 (25 October 1999)

It is shown that the thermodynamically equilibrium state of a system of small metal particles placed in a dielectric matrix are unavoidably charged. The charge of spherical metal particles with different radii is calculated at low temperatures. Hopping transport in a system of metal particles is studied. It is shown that it is limited by the charging energy, which serves as a typical hopping energy and can be gapless. © *1999 American Institute of Physics*. [S0021-3640(99)00620-9]

PACS numbers: 72.20.Ee, 72.80.Tm

Metal–insulator composites consisting of a dielectric matrix with embedded metal granules, ranging in size from several to hundreds of angstroms, are often used in practical applications. The question of the conductivity of composites is closely related with the charge state of the granules. Specifically, the proposed mechanism of hopping conduction near the Coulomb gap rests on the existence of an equilibrium charge on the metal granules,[1] which is due to the difference in the work function of different granules. This is a reasonable assumption for metal granules consisting of different materials.

However, identical metals whose work functions are implicitly assumed to be the same are often used in experiments (see the reviews in Refs. 2 and 3). For example, in a recent work,[4] just as in all previous works,[2,3] metal granules are assumed to uncharged at zero temperature. At the same time, in a system of doped multielectron quantum dots fluctuations of the number of impurities induce a redistribution of electrons between the impurities in the thermodynamically equilibrium state at zero temperature.[5] In the present letter we show that equilibrium charging of metal particles is also possible at low temperature but because of the variance of their sizes or shape.

Let us consider a system of metal spheres, which can exchange electrons, with radii R_i. The presence of the surface of a sphere leads to the additional, with respect to an infinite volume, electron energy αS, which is proportional to the surface area S. The surface tension α of the electron gas can be calculated for an ideal Fermi gas. For this, we consider the Ω potential of a Fermi gas in a quantum film of thickness d:

$$\Omega = -2TS \sum_{n=1}^{\infty} \int \frac{d^2p}{(2\pi\hbar)^2} \log\left(1+\exp\left(\frac{\mu-\epsilon}{T}\right)\right), \quad \epsilon = \frac{p^2}{2m} + \frac{(\pi\hbar n)^2}{2md^2} \tag{1}$$

Here m is the electron effective mass, T is temperature, μ is the chemical potential, and S is the surface area of the film. At low temperatures we obtain in the limit of a large film thickness

$$\Omega = -\frac{m^{3/2}(2\mu)^{5/2}}{15\pi^2\hbar^3}V + \frac{m\mu^2}{8\pi\hbar^2}2S \tag{2}$$

The first term corresponds to the contribution due to the volume of the system $V=dS$ and the second term is the contribution due to the surface tension energy $2\alpha S$, where $\alpha = m\mu^2/8\pi\hbar^2$, of the two surfaces of the electron gas.

Let us now consider a metal granule. It is obvious that in the limit of a large size of the system the volume and surface contributions to the energy are independent of the shape of the system, and they depend only on the volume and surface area, so that Eq. (2) is universal. The surface energy is less than the volume energy to the extent that the Fermi wavelength λ_F is small compared to the characteristic geometric size V/S of the system.

Surface tension produces an additional pressure $\delta P = 2\alpha/R_i$ on the surface of the electron gas and changes the chemical potential from that of an infinite system with the same electron density n: $\delta\mu_i = n^{-1}\delta P = 2\alpha/nR_i$. This change is responsible for the redistribution of the electrons between granules.

Let us consider a metal–dielectric composite consisting of metal granules embedded in a dielectric with permittivity κ. For simplicity we shall assume the granule number density N to be small, $NR^3 \ll 1$.

Let us assume that the ith granule contains z_i ions and Z_i electrons and its potential is

$$\phi_i = e(\delta Z_i/\kappa R_i), \tag{3}$$

To find the equilibrium charge of the granules $e\delta Z_i = e(z_i - Zi)$, an electrostatic correction $-e\phi_i$ must be included in the chemical potential. From the condition $Z_i = (-\partial\Omega/\partial\mu)_{T,\phi_i}$, we obtain in the limit $R_i \to \infty$

$$\frac{e^2\delta Z_i}{\kappa R_i} + \frac{2\alpha}{nR_i} = \delta\mu, \tag{4}$$

where $\delta\mu$ is the change in the chemical potential of the system compared with the macroscopic sample, and $n = z_i/V_i$ is the concentration of ions in a granule, and is equal to the electron density in an infinite sample.

In equilibrium the electrochemical potentials $\mu_i - e\phi_i$ of the granules must be the same. Using the condition of electrical neutrality, $\Sigma\,\delta Z_i = 0$, we find

$$\delta Z_i = \frac{2\alpha\kappa}{ne^2}\frac{R_i - \langle R\rangle}{\langle R\rangle}, \quad \delta\mu = \frac{2\alpha}{n\langle R\rangle}. \tag{5}$$

The brackets denote an average over granules. According to Eq. (5), the typical charge of a granule is determined by the ratio of the Fermi energy E_F of the metal to the interaction energy of the electrons in the metal, multiplied by the factor κ. In a typical case with $R_i - \langle R\rangle \sim \langle R\rangle$ the charge δZ_i can be less than or greater than 1. If $\alpha\kappa \ll ne^2$, then the

typical charge $\delta Z_i \ll 1$, and it is incorrect to neglect implicitly, as done earlier, the discreteness of the charge. In reality, the granules remain neutral in this case. An energy equal to the sum $e^2/2\kappa(1/R_i+1/R_j)$ of the charging energies of the two granules must be expended to transfer an electron from one granule to another. In consequence the system of granules is a Hubbard insulator, where Fermi excitations are separated from the ground state by a finite energy gap due to Coulomb repulsion.

If $\alpha\kappa \gg ne^2$, on the other hand, then the discreteness of the charge is immaterial, to a first approximation. The typical potential of a granule is of the order of $E_F\lambda_F/\langle R\rangle$, which can be much greater than the temperature. We note that the spacing $E_F(\lambda_F/\langle R\rangle)^3$ between the energy levels of a granule is much smaller than the typical potential. This justifies our quasiclassical approach.

According to Eq. (5), the charge of a granule should be fractional. This means that the local electrochemical potential is equalized to within the charging energy $U_c = e^2/2\kappa\langle R\rangle$ of a granule due to one electron. Redistribution of the electrons occurs as long as it is energetically favorable. For this reason, the first unfilled state of an electron on a granule lies above the total electrochemical potential by an amount ϵ_i less than the charging energy U_c. The last filled state $\epsilon_i - U_c$ lies in the range $(0,-U_c)$. Therefore the energy required to transfer an electron to infinity or to return an electron from infinity to a granule should be uniformly distributed in the range from 0 to U_c. Such a state of the system possesses a zero energy gap as a whole, which makes it possible to classify the system as a gapless Hubbard insulator.

Let us now consider nonspherical granules. In this case the potential of a granule is determined by its capacitance C_i, and the surface-tension shift of the chemical potential is determined by the ratio V_i/S_i: $2\alpha S_i/3nV_i$. We obtain instead of Eqs. (3)–(5)

$$\phi_i = \frac{e\,\delta Z_i}{\kappa C_i}, \quad \delta\mu = \frac{e^2\delta Z_i}{\kappa C_i} + \frac{2\alpha S_i}{3nV_i} = \frac{2\alpha}{3n}\frac{\langle C_i S_i/V_i\rangle}{\langle C_i\rangle}, \tag{6}$$

$$\delta Z_i = \frac{2\alpha\kappa}{3ne^2}\frac{C_i}{\langle C_i\rangle}(\langle C_i S_i/V_i\rangle - \langle C_i\rangle S_i/V_i). \tag{7}$$

The preceding calculations were performed neglecting the interaction of the charged granules with one another. The potential produced by a neighboring granule is less than the potential of the characteristic charge to the extent that the size R of the granules is small compared with the distance between the granules $N^{-1/3}$. If the granules are charged in an uncorrelated manner, then the fluctuations of the potential will diverge at large distances, similarly to the divergence of the potential in a completely compensated semiconductor.[1] Therefore long-range fluctuations of the potential lead to an additional correlated redistribution of charges screening these fluctuations. Let us estimate their magnitude. A fluctuation $\delta\phi$ is screened as a result of the redistribution of the charge on the granules with charging energy less than $\delta\phi$. Let r be the screening length. It is determined from the condition that the charge fluctuation δQ in a region of size r is compensated by a redistribution of one electron from each granule with energy ϵ_i less than $\delta\phi$:

$$\delta Q/e = \left(\frac{4\pi}{3}\delta Z N r^3\right)^{1/2} = \frac{4\pi}{3}\frac{\delta\phi}{U_c}Nr^3. \tag{8}$$

The fluctuation δQ produces a potential $\delta\phi \sim \delta Q/r$. Hence we obtain

$$r \sim \left(\frac{\kappa U_c}{e^2 N \delta Z} \right)^{1/2}, \quad \delta\phi \sim U_c \delta Z^{5/4} (NR^3)^{1/4}. \tag{9}$$

The condition that a small fraction of the electrons per granule is redistributed is equivalent to the requirement that $\delta\phi$ be small compared with U_c. This is valid if $\delta Z^5 NR^3 \ll 1$. The long-range potential fluctuations that are obtained are obviously less than the characteristic intrinsic potential of the granules $\phi \sim U_c \delta Z$.

Let us consider the conductivity of a composite consisting of spherical particles at low temperature. For $\alpha\kappa \ll ne^2$ conduction is due to electrons excited into the upper Hubbard band. Therefore conduction is purely activational with activation energy min $(|\pm U_c - \mu|)$, where μ lies in the Hubbard gap.[1)] Generally speaking, the activation energy is of the order of U_c. Since the density of states in the gap is extremely low, the chemical potential is determined by atypical fluctuations. For spherical particles such fluctuations seem to be particle-size fluctuations. Let us assume that small particles give up electrons and large particles accept electrons. However, since the surface energy per electron depends on the radius just as the Coulomb energy, the energy loss due to charging does not compensate the gain due to the surface, and the particles remain neutral irrespective of the radius. The situation changes when the asphericity of the particles is taken into account. Conduction this case will be examined elsewhere.

Let us now consider the gapless-insulator limit. In this case the basic transport characteristics resemble hopping transport along an impurity band with the exception of two features: in contrast to the impurity problem, hops between granules do not require the participation of phonons in the transport, and the characteristic hopping energy is determined not by the density of states but rather by the charging energy. Formally, the problem is described by the Miller–Abrahams model[1] with the position of the atomic levels replaced by the position of the bottoms ϵ_i of the corresponding granules. The system of equations for the current j_i between the granules and the potentials φ_i induced on the granules by an external field has the standard form, $j_{ij} = eW_{ij}(\varphi_i - \varphi_j)$, where

$$\ln W_{ij} = r_{ij}/a + 1/2T(|\epsilon_i - \epsilon_j| + |\epsilon_i - \mu| + |\epsilon_j - \mu|) = \zeta_{ij},$$

r_{ij} is the distance between the granules, and a is the localization length. An electron hops to the sites where ζ_{ij} satisfies the connectedness criterion $\zeta_{ij} < \zeta_c$.

For sufficiently high temperature, evidently, the tunneling factor will limit tunneling to distant granules. Therefore hops along nearest neighbors, corresponding to a conduction mechanism with a constant hopping length, will predominate. The characteristic activation energy is determined by a fraction of U_c. Specifically, we must single out the nearest neighbors whose bottoms fall within a band ξ. Gradually increasing the band width we add newer and newer sites into the network. The critical values ξ_c at which a connected network first arises determines the activation energy $\epsilon_c \sim U_c$. If the granules are assumed to be arranged in a periodic square or cubic lattice, then $\epsilon_c^{(2)} = 0.59U_c$ and $\epsilon_c^{(3)} = 0.31U_c$.

As the temperature decreases, electrons prefer to hop to distant granules, optimizing the activation factor. As a result, the conductivity of the system is determined by a variable hopping length mechanism. Hops will occur to the granules for which the loga-

rithm of the tunneling probability is of the same order of magnitude as the logarithm of the activation probability, satisfying the connectedness criterion. Analogously to Ref. 1, we obtain for the conductivity

$$\sigma = A \exp - \left(\frac{T_1}{T} \right)^{1/4}, \quad T_1 \sim U_c N^{-1} a^{-3}. \tag{10}$$

The pre-exponential in Eq. (10) is given by the characteristic frequency $A = v_F/R$ in a granule. Formula (10) is valid in the temperature range $(E_F/Z)^{4/3} T_1^{-1/3} \ll T \ll U_c (Na^3)^{1/3}$. The upper limit is determined by the requirement that the typical hopping energy not exceed U_c (otherwise the constant hopping length model is valid). The lower limit is due to the fact that the hopping energy must exceed the spacing between single-electron energy levels that is required in order for the assumption of a continuous spectrum of states in a granule to be valid.

At the lowest temperatures $T \ll (E_F/Z)^{4/3} T_1^{-1/3}$ the hopping energy is less than the spacing E_F/Z between the single-electron levels in a granule. In this limit, for an electron in the initial state with a definite energy there will be no granules with such a level. Threfore energy must be absorbed or released in a hop, i.e., phonons must be emitted or absorbed or other electrons must be excited in a hop. We shall consider the phonon mechanism. Since the temperature is low, an electron can use only the energy levels in a given granule that are closest to μ. Excited energy states with the same number of electrons as the ground state as well as states with a larger or smaller number of electrons can serve as such states. They must lie within the working band Δ determined by the typical hopping energy. The working band is chosen from the condition that a region of size r contain at least one state on a single granule in an infinite cluster. The number of states per unit volume is determined by the number of states in a single granule $Z\Delta/E_F \ll 1$ in the energy range Δ multiplied by the density of granules accessible to an electron with such an energy, $N\Delta/U_c$. The connectedness criterion has the form $\Delta^2 (4\pi/3) ZNr^3/E_F U_c = B_c$. As a result, we obtain for the conductivity

$$\sigma = B \exp - \left(\frac{T_2}{T} \right)^{2/5}, \quad T_2 \sim \left(\frac{E_F U_c}{ZNa^3} \right)^{1/2}. \tag{11}$$

Equation (11) gives a law that is close to the 1/2 law observed in a number of experiments (see reviews[2,3]). The transition between the 1/4 and 2/5 laws occurs at temperature $(E_F/Z)^{4/3} (Na^3/U_c)^{1/3}$.

We underscore that in contrast to the theory of a Coulomb gap,[1] due to the long-range interaction of charges on different granules, our approach takes account of only the stronger interaction of charges on the same granule. It is only near the percolation transition $NR^3 \sim 1$ that Coulomb gap effects become comparable to the effects considered here. The long-range Coulomb potential can influence the conductivity at such low temperatures, $T \lesssim U_c (NR^3)^{4/9} (Na^3)^{1/3}$, that the hopping energy becomes comparable to the Coulomb interaction of the charges on neighboring grains.

We also note that we have neglected the collectivization of the states of different granules, making the assumption that the charging energy U_c is much greater than the tunneling amplitude.

In summary, we have shown that the granules in a system of small metal granules can be charged even at zero temperature. Depending on the surface tension and Coulomb energy, the system can be a Hubbard insulator with or without a gap. For the gapless state low-temperature conduction is a hopping conduction with a variable activation energy determined by the charging energies of the granules.

We thank B. I. Shklovskiĭ for a discussion of the questions considered in this paper, and the Russian Fund for Fundamental Research for financial support within the framework of Grant No. 97-02-18397.

[1)] We note that the conductivity of a composite consisting of neutral granules has been studied in a recent work.[4] Unfortunately, the conclusion that $\ln \sigma \sim T^{-1/2}$ drawn there can be valid only in a limited temperature range. The point is that the approximation of the dependence of the hopping length on the grain size by a linear function is invalid in the limit of large hopping lengths. As a result, because of the presence of a rigid Hubbard gap, the conductivity has a finite activation energy in the low-temperature limit.

[1] B. I. Shklovskii and A. L. Efros, *Electronic Properties of Doped Semiconductors* (Springer-Verlag, New York, 1984).
[2] Ping Sheng, Philos. Mag. B **65**, 357 (1992).
[3] C. J. Adkins, in *Metal-Insulator Transitions Revisited*, edited by P. P. Edvards and C. N. R. Rao (Taylor & Francis, 1995).
[4] E. Z. Meĭlikhov, Zh. Éksp. Teor. Fiz. **115**, 1484 (1999) [JETP **88**, 819 (1999)].
[5] E. M. Baskin and M. V. Entin, *The 24th International Conference on the Physics of Semiconductors*, Jerusalem, Israel (1998), Abstracts, Vol. 2, Th-P126.

Translated by M. E. Alferieff

On the mechanism of dissipation in the internal Josephson effect in layered superconductors at low temperatures

S. N. Artemenko*)
Institute of Radio Engineering and Electronics, Russian Academy of Sciences, 103907 Moscow, Russia

(Submitted 16 September 1999)
Pis'ma Zh. Éksp. Teor. Fiz. **70**, No. 8, 516–521 (25 October 1999)

The current–voltage characteristics (IVCs) of a layered superconductor with singlet *d* pairing at low temperatures are calculated in the internal Josephson effect (IJE) regime. Coherent electron tunneling between layers is assumed. A finite resistance of the superconductor in the resistive state arises because of quasiparticle transitions through the superconducting gap near nodes. Because of charge effects the interaction of the Josephson junctions formed by the layers does not lead to substantial differences in the shapes of different branches of the IVCs. The model describes the basic qualitative features of the effect in high-temperature superconductors for voltages which are low compared with the amplitude of the superconducting gap. © *1999 American Institute of Physics.* [S0021-3640(99)00720-3]

PACS numbers: 74.50.+r, 74.72.Hs

The theoretical description of the internal Josephson effect in layered high-temperature superconductors is complicated by the fact that the electronic structure of both the superconducting and normal states is not adequately understood. Investigations of the electronic structure[1,2] show that in the $(0,\pi)$ directions the electronic spectral density is smeared by strong scattering of electrons by spin fluctuations.[3] In the (π, π) directions, corresponding to the nodes of the order parameter Δ in the superconducting state, the electronic structure of the material agrees with Fermi-liquid models. This gives hope of describing the internal Josephson effect (IJE) using ordinary Fermi-liquid approaches at low temperatures and voltages, where the contribution to the current should be determined primarily by electrons with low energy near nodes of the gap Δ.

The Josephson properties of a layered superconductor should depend strongly on the symmetry of the order parameter and should differ qualitatively in cases of coherent and incoherent tunneling between the superconducting layers. Incoherent scattering describes a system of Josephson tunnel junctions in which the parallel component of the momentum is not conserved in tunneling between layers, resulting in a finite resistance along the *c* axis perpendicular to the layers. If such junctions were formed by superconductors with an isotropic (*s*-type) order parameter, the product $V_c = I_c R_N$ of the critical current and the normal resistance would be of the order of the gap width. However, for *d* pairing inco-

herent tunneling leads to a zero or very small critical current along the c axis, so that to explain the high observed values of I_c it would be necessary to assume an unrealistic special form of the angular dependence of the probability of tunneling between layers. According to recent investigations of BSCCO/Pb tunnel junctions,[4] the fraction of the s component in the BSCCO order parameter does not exceed 10^{-3}. For incoherent tunneling between layers, this would lead to values of V_c approximately three orders of magnitude smaller than the observed values, which are close in order of magnitude to the amplitude Δ_0 of the gap.[5] Moreover, for such small values of I_c the regime in which some interlayer junctions are in a resistive state and others are in a superconducting state would be impossible for voltages across one junction of $V \sim \Delta_0$. Such a regime, characterized by the presence of different branches on the IVCs, is one of the most striking manifestations of the IJE in layered superconductors.

Coherent tunneling describes a three-dimensional, strongly anisotropic crystal. In this case, there is no need to assume artificially a special angular dependence of the tunneling probability in order to explain the large experimental value of I_c. However, the question of the character of the IJE in the presence of coherent tunneling likewise is not entirely clear. The finite resistance of a crystal in the normal state in this case is due to scattering. For Born scattering $\rho_c \propto 1/\tau$, where $1/\tau \ll \Delta_0$; in the opposite case the scattering would suppress d-pairing superconductivity ($\hbar = e = 1$). The typical voltages on one junction in Josephson experiments is of the order of $\Delta_0 \gg 1/\tau$. For such voltages (and frequencies of Josephson oscillations) the conductivity should decrease with increasing voltage,[6] which is not observed in experiments. If impurity scattering in superconducting layers is resonant scattering, then the resistance in the limit of low voltages does not depend on $1/\tau$ and agrees with the experimental data.[7] However, this mechanism can work only for $V < \gamma \sim \sqrt{\Delta_0/\tau}$. To explain the finite conductivity at voltages $V > \gamma$ requires a dissipation mechanism that is not associated with scattering by impurities. Transitions of quasiparticles through the superconducting gap can serve as such a mechanism. As was shown in Ref. 8, such a mechanism determines the natural width of the Josephson plasma resonance line at low temperatures. This mechanism becomes inefficient for $V > \Delta_0$, where scattering mechanisms associated with spin fluctuations and pseudogap effects must be taken into consideration, and our approach, which is based on Fermi-liquid ideas, no longer work.

We shall investigate a layered superconductor with d pairing and with coherent tunneling between layers, neglecting scattering, i.e., we consider a pure crystal or sufficiently high voltages, $V > 1/\tau$ for Born scattering and $V > \gamma$ for resonance scattering. Expressions for the current and charge densities are derived using the collisionless kinetic equations derived for the Green's functions by Volkov and Kogan[9] using the Keldysh technique. These equations are extended to the case of layered superconductors in the tight-binding approximation for the electron spectrum in a direction perpendicular to the layers and for d-pairing inside the superconducting layers. Our approach, describing a layered single crystal, is opposite to the model of random hops between layers, used in Ref. 10.

Let us consider the case of a uniform current along the c axis, which can be realized in narrow samples whose width in the ab plane is less than the Josephson length. We shall solve the equations for the diagonal and off-diagonal (with respect to the spin indices) components of the Keldysh propagator $g_{nm}(t)$ and $f_{nm}(t)$:

$$i\frac{\partial}{\partial t}g_{n\,m}+\Delta_n f^*_{n\,m}+f_{n\,m}\Delta_m+(\mu_n-\mu_m)g_{n\,m}$$

$$=t_\perp\sum_{i=\pm 1}(A_{n,\,n+i}g_{n+i\,m}-g_{n,\,m+i}A_{m+i\,m});\tag{1}$$

$$i\frac{\partial}{\partial t}f_{n\,m}-2\xi f_{n\,m}-\Delta_n g^*_{n\,m}+g_{n\,m}\Delta_m+(\mu_n+\mu_m)f_{n\,m}$$

$$=t_\perp\sum_{i=\pm 1}(A_{n,\,n+i}f_{n+i\,m}-f_{n,\,m+i}A^*_{m+i\,m}),$$

where $g_{nm}(\xi,\phi,t)$ and $f_{nm}(\xi,\phi,t)$ are matrices with respect to the spin indices. Here $\xi_p=\epsilon(\mathbf{p})-\epsilon_F$, $\epsilon(\mathbf{p})$ is the electron energy in the normal state, ϵ_F is the Fermi energy, $\mathbf{p}$ is the electron momentum in the ab plane, ϕ is the angle in momentum space, $t_\perp$ is the transfer integral, $\Delta_n=\Delta_n(\phi)$ and χ_n are, respectively, the superconducting order parameter and its phase in the nth layer, $\mu_n=\Phi_n+(1/2)(d\chi_n/dt)$ is the gradient-invariant scalar potential, Φ_n is the electric potential, and $A_{n,n+1}=\exp\varphi_n$, where $\varphi_n=\chi_{n+1}-\chi_n-2\pi sA_z/\Phi_0$ is the gradient-invariant phase difference between the layers and A_z is the vector potential in the direction of the c axis. The electric field can be expressed as

$$E_n s=\mu_n-\mu_{n+1}+\frac{1}{2}\frac{d\varphi_n}{dt}.\tag{2}$$

The scalar potential μ describes the imbalance of the populations of the electron- and hole-like quasiparticle branches and charge effects in Josephson plasma oscillations[11] and IJE.[6,12]

The current density between the layers $n+1$ and n and the charge density in layer n are calculated as

$$j_{n,n+1}=\frac{t_\perp}{2s}\int\frac{d\mathbf{p}}{(2\pi)^2}(A_{n+1,n}g_{n,n+1}-g_{n+1,n}A_{n,n+1}),\tag{3}$$

$$\rho_n=-\frac{1}{4is}\int\frac{d\mathbf{p}}{(2\pi)^2}(g_{nn}+g^*_{nn}),\tag{4}$$

where s is the crystal period in the c direction.

We solve Eqs. (1) using perturbation theory with respect to $t_\perp$. The contribution from transitions between the layers to the charge density is quadratic in $t_\perp$, so that in the leading approximation such transitions can be neglected. In the Fourier representation we obtain

$$g_{nn}+g^*_{nn}=\left[\frac{2\xi}{\varepsilon}-\frac{8\Delta^2\mu_\omega}{\varepsilon(4\varepsilon^2-\omega^2)}\right]\tanh\frac{\varepsilon}{2T},\tag{5}$$

where $\varepsilon=\sqrt{\xi^2+\Delta^2}$. Substituting this expression into Eq. (4), we obtain in the time domain

$$\rho_n = -\frac{\kappa^2}{8\pi}\int_0^\infty dt_1 F(t_1)\mu_n(t-t_1), \tag{6}$$

where κ is the reciprocal of the Thomas–Fermi screening radius,

$$F(t) = \int \frac{d\phi}{2\pi}\int_{-\infty}^{\infty} d\xi \frac{2\Delta^2(\phi)\sin 2\varepsilon t \tanh \varepsilon/2T}{\varepsilon^2}. \tag{7}$$

The function F describes the nonexponential relaxation of μ with a characteristic time of the order of $1/\Delta_0$. We shall require Eq. (6) in the case of slow variations of μ, where $F(t)\to 2\delta(t)$ and the integral in Eq. (6) reduces to $2\mu(t)$. Substituting now the expression for the charge density into Poisson's equation, we express the difference $\delta\mu_n = \mu_{n+1} - \mu_n$ of the scalar potentials between the layers in terms of the time derivative $\dot{\varphi}_n$ of the phase differences:

$$\delta\mu_n = \frac{a}{16\sqrt{1+a}}\sum_m (\dot{\varphi}_{n+m+1} + \dot{\varphi}_{n+m-1} - 2\dot{\varphi}_{n+m})\left(\frac{\sqrt{1+a}-1}{\sqrt{1+a}+1}\right)^{|m|}, \tag{8}$$

where $a = 4\epsilon_\perp/(\kappa s)^2$ and $\epsilon_\perp$ is the dielectric constant in a direction perpendicular to the layers. An estimate for $s = 15$ A, $1/\kappa = 2$ A, and $\epsilon_\perp = 12$ gives $a \approx 0.85$, and the factor in front of the sum in Eq. (8) is about 0.04. Therefore $\delta\mu_n$ is small compared with $\dot{\varphi}_n$, and it follows that the change effects and the contribution $\delta\mu_n$ in the electric field between the layers are small [see Eq. (2)].

To calculate the current we shall have to solve Eqs. (1) in a linear approximation in $t_\perp$. However, the equations are still difficult to solve for arbitrary $\mu_n(t)$ and $\varphi_n(t)$, so that we introduce equations for the current density in two limiting cases. First, we find the solution for $g_{n,n+i}$ in a linear approximation in the potential μ, describing charge effects which, according to the estimate made above, are small. In this limit the current between the layers n and $n+1$ can be represented in the form of a component that depends only on the phase difference φ_n and a component that also depends on the potential difference $\delta\mu_n(t)$,

$$j_{n,n+1}(t) \equiv j^\varphi(t) + j^\mu(t).$$

Assuming $t_\perp$ to be independent of the momentum, we obtain

$$j^\varphi(t) = j_c\int_0^\infty dt_1 F(t_1)\cos\frac{\varphi_n(t-t_1)}{2}\sin\frac{\varphi_n(t)}{2}; \tag{9}$$

$$\begin{aligned} j^\mu(t) = j_c\int_0^\infty dt_1\int_0^\infty dt_2 F(t_2)\Bigg\{\Bigg[\cos\frac{\varphi_n(t-t_1)}{2}\delta\mu_n(t-t_1-t_2) \\ -\cos\frac{\varphi_n(t-t_1-t_2)}{2}\delta\mu_n(t-t_1)\Bigg]\cos\frac{\varphi_n(t)}{2} + \sin\frac{\varphi_n(t-t_1)}{2} \\ \times\delta\mu_n(t-t_1-t_2) + \sin\frac{\varphi_n(t)}{2}\Bigg\}. \end{aligned} \tag{10}$$

Since according to (8) $\delta\mu_n(t)$ depends on the phase difference between different pairs of layers, the current component (10) describes the interaction of ''Josephson junctions''

because of charge effects. Such an interaction has been investigated on the basis of a phenomenological approach in Ref. 13, where other results were obtained.

Equations (9) and (10) simplify in several limiting cases. For $T \ll \omega$ and $V \ll \Delta_0$ the current can be represented as a sum of superconducting, normal, and interference components, and the quasiparticle current contains a contribution that depends on the difference of the scalar potentials:

$$j^{\varphi}(t) = j_c \sin \varphi_n + j_c \frac{\pi}{2\Delta_0} \frac{d\varphi_n}{dt}(1 - \cos \varphi_n); \tag{11}$$

$$j^{\mu}(t) = 2 j_c \int_0^{\infty} dt_1 \sin \frac{\varphi_n(t - t_1)}{2} \delta\mu_n(t - t_1) \sin \frac{\varphi_n(t)}{2}. \tag{12}$$

The explicit form of the angular dependence $\Delta(\phi)$ was used to calculate these expressions. The dissipative current components appear as a result of quasiparticle transitions through the superconducting gap. In addition, the finite conductivity at low voltages, i.e., Ohm's law, arises because of the nodes in $\Delta(\phi)$, since in this case, as voltage increases, the range of angles ϕ at which transitions through the gap are possible increases. In an approximation linear in φ the dissipative contribution to the current vanishes, since in the spatially uniform case transitions through the gap are forbidden in the absence of a third body. This forbiddenness is lifted in the nonlinear regime, since in the presence of a current along the c axis the phase depends on the layer number and the system becomes inhomogeneous.[8] In the linear approximation the forbiddenness is lifted by scattering. In this case, using the computational method of Ref. 8, we obtain

$$j(t)/j_c = \varphi_n + \frac{2\nu}{6\Delta_0^2} \frac{d\varphi_n}{dt} - \frac{\pi}{2\Delta_0} \delta\mu_n. \tag{13}$$

The expression for the current density also simplifies in the limit of frequencies which are high compared with the Josephson plasma resonance frequency ω_p (in strongly anisotropic Bi- and Tl-based cuprates $\omega_p \ll \Delta_0$), where the ac electron current is shunted by the displacement current,

$$\nu_{AC} \sim \nu_{DC} \left(\frac{\omega_p^2}{\omega^2} \right) \ll \nu_{DC},$$

and the time dependence of the phase differences has the simple form $\varphi_n \approx 2\omega_n t + \varphi_\omega$, where $\varphi_\omega \ll 1$.

When all layers are in the resistive state or in the limit $a \to 0$, we have $\delta\mu = 0$, and the IVC at $T = 0$ has the form

$$j = j_c \left\{ \theta(2\Delta_0 - V) \left[\frac{2\Delta_0}{V} \mathbf{K}\left(\frac{V}{2\Delta_0} \right) - \mathbf{E}\left(\frac{V}{2\Delta_0} \right) \right] + \theta(V - 2\Delta_0) \left[\mathbf{K}\left(\frac{2\Delta_0}{V} \right) - \mathbf{E}\left(\frac{2\Delta_0}{V} \right) \right] \right\}. \tag{14}$$

At low voltages the slope of the IVC (14) is described by the conductivity $\sigma_q = \pi e s j_c / \Delta_0 = e^2/8\pi\lambda^2\Delta_0$. This value agrees with the experimental data of Ref. 7 and differs by a factor of $8/\pi^2$ from the conductivity at zero bias in the presence of resonance scattering. The expression (14) contains a logarithmic peak at $V = 2\Delta_0$ and a descending

branch at higher voltages, which is not observed in the experimental IVCs. This shows that our approach is inapplicable at high voltages V, where electrons with energy differing from the Fermi energy by an amount of the order of Δ_0 come into the picture. Such electrons are strongly scattered by spin fluctuations, and interactions with spin fluctuations will broaden the logarithmic peak and lead to a finite resistance at high voltage.

Let us now consider the situation where some junctions formed by superconducting layers are in a resistive state and the others are in a superconducting state. An ac current is transported through the superconducting layers in the form of a displacement current. The total dc voltage is the sum of the voltages across the junctions in the resistive state, and the number of branches in the IVC is equal to the number of junctions. In addition, in the limit of small a, the branch n is described by the first term in Eq. (14) with V replaced by V/n. For $\omega \gg \omega_p$ the current density calculated with an arbitrary ratio between $\delta\mu_n$ and $\dot{\varphi}_n$ and $T=0$ has the form

$$j_{n,n+1}=\sqrt{\frac{\dot{\varphi}_n+\delta\mu_n}{(\dot{\varphi}_n-\delta\mu_n)^3}}\left[\mathbf{K}\left(\frac{\sqrt{\dot{\varphi}_n^2-\delta\mu_n^2}}{2\Delta_0}\right)-\mathbf{E}\left(\frac{\sqrt{\dot{\varphi}_n^2-\delta\mu_n^2}}{2\Delta_0}\right)\right]. \tag{15}$$

For finite a the form of the branches constructed as a function of the total voltage along the c axis divided by the number of junctions depends on whether the neighboring junctions are in a resistive or superconducting state. However, as follows from Eq. (8) and the estimates made below that formula, the contribution of the scalar potential is small. For values of the material parameters which were used above, different branches differ by not more than 3–4%, and these differences decrease as the parameter a decreases. We note the branches observed in the experiments on BSCCO have essentially the same form.[4,5]

In summary, the model with singlet d-type pairing and coherent pairing describes qualitatively the IVCs observed in the IJE regime with low voltages. Quasiparticle transitions through the superconducting gap in the region of its nodes give a dissipation mechanism leading to a quasiparticle conductivity that is close to the observed value. The interaction induced, as a result of charge effects, between the Josephson junctions formed by superconducting layers leads to negligible differences in the form of the branches of the IVCs with reasonable values of the parameters of the superconductor. For voltages of the order of Δ the model does not describe the experimental data. This is because electrons which interact strongly with spin fluctuations come into the picture.

I thank L. N. Bulaevskiĭ and R. Kleĭner for a helpful discussion. This work was supported by Grant 98-02-17221 of the Russian Fund for Fundamental Research and Grant 96053 of the Russian Government Program on Superconductivity.

*)e-mail: art@mail.cplire.ru

[1] M. R. Norman, P. Bourges, Y. Sidis *et al.*, Phys. Rev. Lett. **79**, 3506 (1997).
[2] M. R. Norman, M. Randeria, H. Ding *et al.*, Phys. Rev. B **60**, 7585 (1999).
[3] L. B. Ioffe and A. J. Millis, Phys. Rev. B **58**, 11631 (1998).
[4] M. Mößle and R. Kleiner, Phys. Rev. B **59**, 4486 (1999).
[5] R. Kleiner and P. Müller, Phys. Rev. B **49**, 1327 (1994).
[6] S. N. Artemenko and A. G. Kobelkov, Phys. Rev. Lett. **78**, 3551 (1997).
[7] Yu. I. Latyshev, T. Yamashita, L. N. Bulaevskii *et al.*, Phys. Rev. Lett. **83**, 2336 (1999).

[8] S. N. Artemenko, L. N. Bulaevskii, M. P. Maley, and V. M. Vinokur, Phys. Rev. B **59**, 11587 (1999).
[9] A. F. Volkov and Sh. M. Kogan, Zh. Éksp. Teor. Fiz. **65**, 2038 (1973) [Sov. Phys. JETP **38**, 1018 (1974)].
[10] M. J. Graf, M. Palumbo, D. Rainer, and J. A. Sauls, Phys. Rev. B **52**, 10588 (1995).
[11] S. N. Artemenko and A. G. Kobel'kov, JETP Lett. **58**, 445 (1993); Physica C **253**, 373 (1995).
[12] D. Ryndyk, Phys. Rev. Lett. **80**, 3376 (1998).
[13] S. Koyama and M. Tachiki, Phys. Rev. B **45**, 16183 (1996).

Translated by M. E. Alferieff

NMR on ^{55}Mn in the ferromagnetic Ni-substituted manganite $La_{0.6}Pb_{0.4}Mn_{0.86}Ni_{0.14}O_3$

M. M. Savosta*) and E. E. Solov'ev

A. A. Galkin Donetsk Physicotechnical Institute, Ukrainian National Academy of Sciences, 340114 Donetsk, Ukraine

(Submitted 1 September 1999; resubmitted 16 September 1999)
Pis'ma Zh. Éksp. Teor. Fiz. **70**, No. 8, 522–527 (25 October 1999)

NMR on ^{55}Mn in the single-crystal manganite $La_{0.6}Pb_{0.4}Mn_{0.86}Ni_{0.14}O_3$ ($T_C = 242$ K), which exhibits metallic conductivity below T_C, is investigated in the temperature range 61–215 K. At low temperatures, together with a line corresponding to the averaged hyperfine field at the ^{55}Mn nuclei (the averaging is due to the motion of electronic holes along Mn sites), the NMR spectrum also contains two lines corresponding to localized states Mn^{4+} and Mn^{3+}. In the temperature range 100–200 K it is found that the complicated NMR spectrum is transformed into a single line on account of a delocalization of the holes in the e_g orbitals of manganese. A comparison of the NMR data with the temperature dependence of the resistivity suggsets that a wide distribution of charge-carrier mobilities exists in the crystal. © *1999 American Institute of Physics.* [S0021-3640(99)00820-8]

PACS numbers: 76.60.Es, 75.50.Dd, 72.60.+g

Ferromagnetic manganites based on $LaMnO_3$ belong to a class of materials in which there is a close relationship between the electric and magnetic properties. These compounds have been attracting intense attention in the last few years in connection with the anomalously large negative magnetoresistive effect near the magnetic ordering temperature of the Mn spins (see, for example, the reviews in Refs. 1–3). To explain the simultaneous appearance of ferromagnetism and metallic conductivity when antiferromagnetic $LaMnO_3$ is doped with divalent ions, Zener[4] proposed a double-exchange model in which taking account of the strong intraatomic exchange interaction between localized t_{2g} electrons and delocalized e_g electron holes results in parallel orientation of the spins of neighboring Mn ions. The double-exchange mechanism is based on the idea that doping induces holes in the e_g orbitals of manganese and results in a mixed Mn^{3+}/Mn^{4+} valence. We note that recent experimental investigations of the electronic structure of lanthanum manganites have cast doubt on this hypothesis.[5]

Nuclear magnetic resonance (NMR) on ^{55}Mn nuclei is very sensitive to the state of the electronic shell of manganese ions, since the hyperfine interaction with the intrinsic $3d$ electrons makes the main contribution to the local field on the nuclei. NMR on ^{55}Mn nuclei in the system $La_{1-x}Ca_xMnO_3$ ($0.125 \leqslant x \leqslant 0.3$) at low temperatures has been investigated in Ref. 6. For compositions with metallic conductivity ($x = 0.2, 0.3$), a single

line at $\simeq 375$ MHz was observed. Such an NMR spectrum can be explained by the averaging of hyperfine fields at the ^{55}Mn nuclei as a result of the rapid motion of electronic holes ($f_{\rm hop} \gg f_{\rm NMR}$) along manganese sites. For compositions with $x \leqslant 0.175$ additional lines at frequencies $\simeq 320$ and $\simeq 410$ MHz, corresponding to quasilocalized ($f_{\rm hop} \ll f_{\rm NMR}$) Mn^{4+} and Mn^{3+} states, were observed in the NMR spectrum; this correlates with the semiconductor character of the conductivity. Similar results have recently been obtained[7] for NMR on ^{55}Mn nuclei in the system $La_{1-x}Sr_xMnO_3$.

The substitution of other 3*d* elements for Mn ions has a large effect on the magnetic and electric properties of manganites. As the concentration of the Fe, Ni, and Co substituent ions increases, the Curie temperature and the spontaneous magnetization decrease rapidly, while the semiconductor properties become more pronounced.[8–12] NMR on ^{55}Mn nuclei in Fe-substituted manganites $La_{0.7}Pb_{0.3}Mn_{1-y}Fe_yO_3$ ($0.0 \leqslant y \geqslant 0.17$) was investigated in Ref. 13. When the Mn ions were replaced by iron, together with a line corresponding to the average hyperfine field on the ^{55}Mn nuclei, two additional lines corresponding to localized Mn^{4+} and Mn^{3+} ions were observed in the NMR spectrum at $T = 1.6-4.2$ K. However, the temperature dependence of the NMR spectra was not studied.

In the present letter, we report the results of an investigation of the temperature dependence of NMR on ^{55}Mn nuclei in the single-crystal manganite $La_{0.6}Pb_{0.4}Mn_{0.86}Ni_{0.14}O_3$. Substitution of nickel for Mn ions likewise results in the localization of holes in the e_g orbitals of manganese and, correspondingly, a complicated NMR spectrum is observed at low temperatures. As the temperature increases, the spectrum transforms into a single line associated with an increase in the velocity of electronic holes along manganese sites. The NMR data are compared with the temperature dependence of the resistivity.

EXPERIMENTAL PROCEDURE AND SAMPLES

The measurements were performed on an incoherent NMR spectrometer with slow frequency scanning and analog accumulation of the signal. In the range 200–450 MHz an oscillatory loop with an Ω-shaped inductor was used for the resonance circuit in the high-frequency oscillator, which was at the same time the NMR sensor. This arrangement made for a substantially higher sensitivity compared to the long-line oscillator that is conventionally used in this frequency range, on account of the better filling of the sensor by the sample. A double-pulse spin echo method was used to detect the NMR spectra. At temperatures below 100 K the form of the spectrum depends on the time interval τ between the exciting and refocusing pulses (Fig. 1). This is due to the difference in the spin–spin relaxation time T_2 for different points of the spectrum. To obtain the true form of the NMR spectrum, in this case the data were extrapolated to $\tau = 0$ assuming an exponential τ dependence of the spin-echo signal amplitude:

$$A_\tau = A_0 e^{-2\tau/T_2}. \quad (1)$$

It should be noted that for the lowest values $\tau \sim 2-5$ μs a deviation was observed from a monotonic variation of the form (1) of the spectrum as a function of τ. This deviation is evidently due to a large contribution of a signal from more rapidly relaxing nuclei in the domain walls. For this reason, the corresponding spectra were not taken into account in the extrapolation.

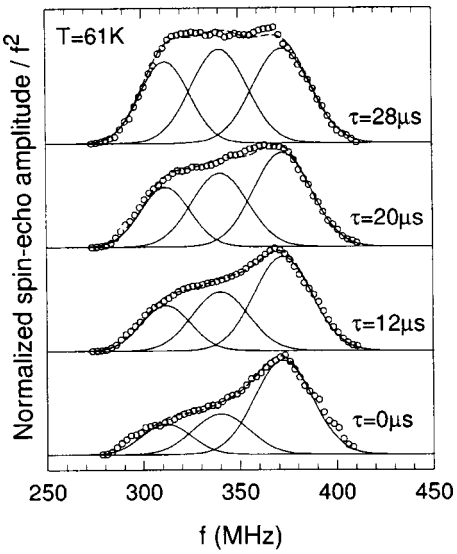

FIG. 1. ^{55}Mn NMR spectra of $La_{0.6}Pb_{0.4}Mn_{0.86}Ni_{0.14}O_3$ at $T=61$ K for three values of the time interval τ between the exciting and refocusing pulses, and the spectrum extrapolated to zero delay (○). The amplitude of the spectra for $\tau=12$, 20, and 28 μs is magnified by a factor of 3.5, 8, and 19, respectively. The solid curves represent the decomposition of the spectra into three lines with spin–spin relaxation rates $T_2=29$, 26, and 19 μs for the bottom, middle, and top lines, respectively. The dashed curves are the result of a fitting procedure.

Single-crystal $La_{0.6}Pb_{0.4}Mn_{0.86}Ni_{0.14}O_3$ samples were grown at M. V. Lomonosov Moscow State University by spontaneous crystallization from a flux. The results of the investigations of the magnetic and electric properties of the samples are presented in Ref. 8.

EXPERIMENTAL RESULTS

The ^{55}Mn NMR spectra with the standard correction for an f^2 frequency dependence of the spin-echo signal amplitude and with a correction for the spin–spin relaxation are presented in Fig. 2. At low temperatures a complicated spectrum is observed in the frequency range 280–410 MHz. The decomposition of the spectrum at $T=61$ K into three Gaussian lines shows the contribution of the localized Mn^{4+} ions ($f_{\mathrm{NMR}}\simeq 310$ MHz), Mn^{3+} ions ($f_{\mathrm{NMR}}\simeq 375$ MHz), and delocalized holes ($f_{\mathrm{NMR}}\simeq 340$ MHz), as discussed above. It should be noted that such a decomposition makes it possible to describe adequately the change in the form of the spectrum as a function of τ (Fig. 1), assigning to each of the three lines its own time T_2, which varies from 29 μs for the line corresponding to Mn^{4+} up to 19 μs for the line corresponding to Mn^{3+}. The more rapid relaxation for Mn^{3+} ions compared with Mn^{4+} ions agrees with the results obtained in Ref. 6. The form of the NMR spectrum does not change much in the temperature range 61–98 K (Fig. 2). As the temperature increases above 98 K, the amplitude of the central line, corresponding to delocalized holes, starts to increase compared with the amplitude of the peripheral lines. It is significant that at $T=116$ K, where the amplitudes of all lines are comparable, the presence of three peaks in the NMR spectrum is clearly visible. Finally, at $T\sim 195$ K the NMR spectrum transforms into a single line, whose width does

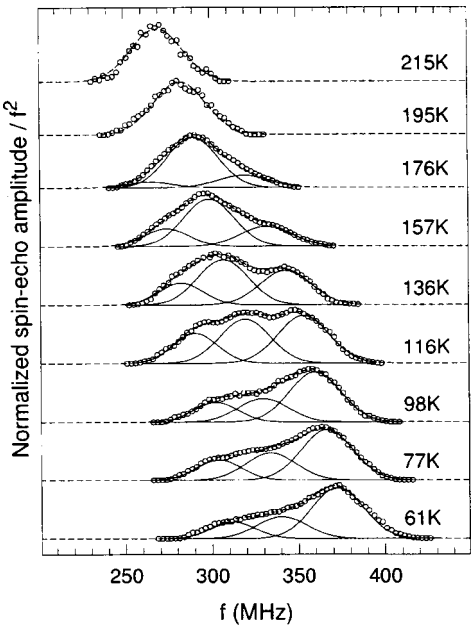

FIG. 2. Temperature dependence of the ^{55}Mn NMR spectra of $La_{0.6}Pb_{0.4}Mn_{0.86}Ni_{0.14}O_3$ (○). The solid curves represent the decomposition of the spectra into three lines with fixed width 30, 35, and 34 MHz for the bottom, middle, and top lines, respectively. The dashed curves are the result of a fitting procedure.

not change with a further increase in temperature. The relative fraction of delocalized electronic holes at Mn sites ($f_{\text{hop}} \gg f_{\text{NMR}}$) as a function of temperature is presented in Fig. 3a, and the temperature dependences of the frequencies of the lines corresponding to Mn^{4+}, Mn^{3+}, and delocalized holes is shown in Fig. 3b for the case when the NMR spectra are decomposed into three lines of fixed width. Extrapolation of the temperature dependences of the frequencies to $T=0$ K gives $f \sim 315$ MHz for Mn^{4+} and f

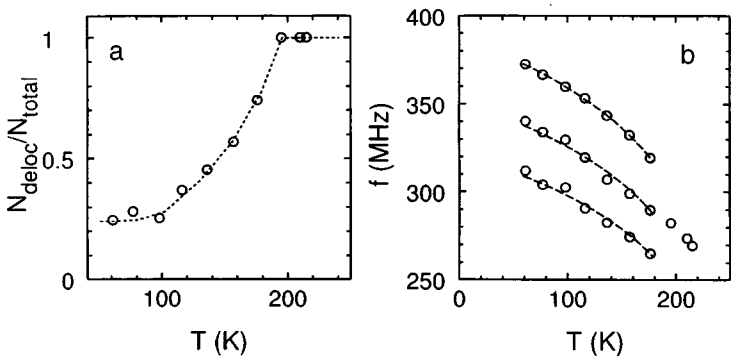

FIG. 3. a) Relative fraction of delocalized electronic holes at Mn sites as a function of temperature. b) Temperature dependence of the NMR frequencies for delocalized Mn^{4+} and Mn^{3+} ions and delocalized holes. The dashed curves were obtained by fitting a smooth curve to the data for the high-frequency line and normalizing to the frequency of the remaining lines.

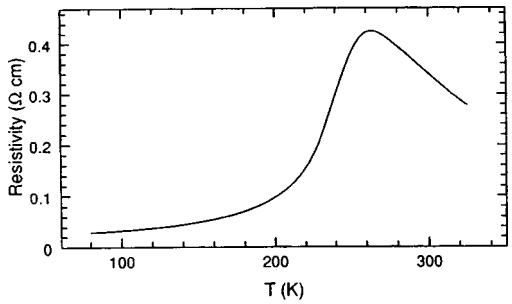

FIG. 4. Temperature dependence of the resistivity for single-crystal $La_{0.6}Pb_{0.4}Mn_{0.86}Ni_{0.14}O_3$.

$\sim$385 MHz for Mn^{3+}. These values are somewhat lower than the frequencies of the corresponding lines which were observed at liquid-helium temperatures in $La_{0.85}Ca_{0.15}MnO_3$ (320 and 410 MHz)[6] and in $La_{0.7}Pb_{0.3}Mn_{1-y}Fe_yO_3$ (330 and 420 MHz).[13] The difference could be due to a different degree of covalence of the Mn–O bonds in the three systems.

DISCUSSION AND CONCLUSIONS

In Ref. 9 the decrease in the Curie temperature due to the substitution Ni (Co)→Mn in $La_{2/3}Ca_{1/3}MnO_3$ is due to the nonequivalence of the ground-state energy of neighboring Mn and Ni (or Mn and Co) ions, which makes motion of electronic holes along the corresponding bonds impossible and, in consequence, makes the double-exchange mechanism less effective. The complicated ^{55}Mn NMR spectrum of $La_{0.6}Pb_{0.4}Mn_{0.86}Ni_{0.14}O_3$ at low temperatures attests to the appearance of quasilocalized Mn^{4+} and Mn^{3+} states as a result of the substitution Ni→Mn in accordance with this model. It should be noted that all three lines in the NMR spectrum have a large NMR gain $\eta \simeq 2000$, characteristic for a weakly anisotropic ferromagnet, and the same temperature dependence (dashed lines in Fig. 3b) as well as close relaxation times T_2 for $T \geqslant 100$ K. All this indicates a close relation between localized and delocalized holes at the microscopic level, i.e., we are dealing with a nonuniformity within the ferromagnetic domains.

The transformation of a complicated NMR spectrum into a single line as the temperature increases (Fig. 2) attests to an increase in the velocity of holes along Mn sites. At the same time, as one can see from Fig. 4, this effect does not result in a decrease of resistivity. On the contrary, an increase of the resistivity, characteristic for ferromagnetic manganites with metallic conductivity, is observed in the temperature range 100–200 K. This behavior can be explained by assuming that the substitution Ni→Fe results in a wide charge-carrier mobility distribution — from mobile itinerant carriers, which are responsible for the observed conductivity, to quasilocalized states, which result in the appearance of additional lines in the NMR spectrum at low temperatures. The number of mobile itinerant carriers can be very small, since the resistance of an Ni-substituted crystal at $T = 77$ K is 60 times greater than for unsubstituted $La_{0.6}Pb_{0.4}MnO_3$ (Ref. 8). In this situation, the transformation of the NMR spectrum could be due to thermal activation of

low-mobility charge carriers, which at low temperatures are localized because the double-exchange mechanism is ''switched off'' and which have a negligible effect on the resistivity despite their large number.

This narrowing of the ^{55}Mn NMR spectra with increasing temperature as a result of the change in the velocity of electronic holes along Mn sites has been observed in polycrystalline $Pr_{0.7}Ba_{0.3}MnO_3$ (Ref. 14). The existence of quasilocalized Mn^{4+} and Mn^{3+} states in this crystal at low temperatures is of a different nature then in $La_{0.6}Pb_{0.4}Mn_{0.86}Ni_{0.14}O_3$. Specifically, it is a result of the disorder in the lattice due to the large difference of the ionic radii of Pr^{3+} and Ba^{2+}. It should be noted that since the substitution Mn→Ni results in weaker disorder in the lattice, the NMR lines for $La_{0.6}Pb_{0.4}Mn_{0.86}Ni_{0.14}O_3$ are much narrower than for $Pr_{0.7}Ba_{0.3}MnO_3$, which made it possible to observe directly the intensity redistribution of the lines corresponding to localized and delocalized holes with increasing temperature.

In summary, using ^{55}Mn NMR we investigated in detail the temperature-induced delocalization of electronic holes in e_g orbitals of manganese in the Ni-substituted ferromagnetic manganite $La_{0.6}Pb_{0.4}Mn_{0.86}Ni_{0.14}O_3$. Comparing the NMR data with the temperature dependence of the resistivity indicates the existence of a wide charge-carrier mobility distribution in this crystal.

We are sincerely grateful to M. M. Lukina for providing the single-crystal samples and S. I. Khartsev for measuring the resistivity.

*)e-mail: savosta@host.dipt.donetsk.ua

[1] É. L. Nagaev, Usp. Fiz. Nauk **166**, 833 (1996).
[2] A. P. Ramirez, J. Phys.: Condens. Matter **9**, 8171 (1997).
[3] C. N. R. Rao, R. Manesh, A. K. Raychaudhuri, and R. Mahendiran, J. Phys. Chem. Solids **59**, 487 (1998).
[4] C. Zener, Phys. Rev. **82**, 403 (1951).
[5] T. Saitoh, A. E. Bocquet, T. Mizokawa *et al.*, Phys. Rev. B **51**, 13942 (1995).
[6] G. Matsumoto, J. Phys. Soc. Jpn. **29**, 615 (1970).
[7] A. Anane, C. Dupas, K Le Dang *et al.*, J. Phys.: Condens. Matter **7**, 7015 (1995).
[8] E. P. Svirina and L. P. Shlyakhina, Vestn. Mosk. Univ., Ser. 3, Fiz. Astron. **34**, 97 (1993).
[9] M. Rubinstein, D. J. Gillespie, and J. E. Snyder, Phys. Rev. B **56**, 5412 (1997).
[10] S. B. Ogale, R. Shreekala, R. Bathe *et al.*, Phys. Rev. B **57**, 7841 (1998).
[11] R. Ganguly, I. K. Gopalakrishnan, and J. V. Yakhmi, Physica B **266**, 332 (1999).
[12] G. H. Rao, J. R. Sun, A. Kattwinkel *et al.*, Physica B **269**, 379 (1999).
[13] L. K. Leung and A. H. Morrish, Phys. Rev. B **15**, 2485 (1977).
[14] M. M. Savosta, P. Novák, Z. Jirák *et al.*, Phys. Rev. Lett. **79**, 4278 (1997).

Translated by M. E. Alferieff

Giant domain walls in a ferromagnet

V. E. Zubov and A. D. Kudakov*)
M. V. Lomonosov Moscow State University, 119899 Moscow, Russia

V. S. Tsepelev
Urals State Technical University, 620002 Ekaterinburg, Russia

(Submitted 12 August 1999; resubmitted 17 September 1999)
Pis'ma Zh. Éksp. Teor. Fiz. **70**, No. 8, 528–530 (25 October 1999)

Giant domain walls with a width of ~ 7 μm are observed on the surface of a ferromagnet — an amorphous magnetically soft alloy. A magnetooptic investigation shows that the walls have a Néel structure in the subsurface region. The subsurface structure of these walls differs substantially from that of the narrower walls previously observed in iron, Permalloy, and amorphous materials. According to the theoretical model of Scheinfein and co-workers, which relates the width of an asymmetric Bloch wall in the bulk with the width at the surface, the width of the wall in the bulk is estimated to be 3–4 μm. © *1999 American Institute of Physics*. [S0021-3640(99)00920-2]

PACS numbers: 75.60.Ch, 75.50.Bb

The subsurface structure of domain walls (DWs) in bulk ferromagnets has been successfully investigated for iron and hematite single crystals by Krinchik and Benidze[1] using a magnetooptic micromagnetometer. It was found that a 180° DW on the surface of iron single crystals has a Néel structure, and its effective width is $\Delta_s = 0.6 - 0.8$ μm. The experimentally observed structure corresponds to the model of an asymmetric Bloch DW for bulk ferromagnets, in which a transition from a Bloch structure in the bulk of the crystal to a Néel structure in the subsurface region occurs by an asymmetric bending of the wall.[2] In Ref. 3 the fine structure of a 180° DW on the surface was inferred from magnetooptic measurements, and it was shown that the fine structure of the wall is uniquely related with the direction of its asymmetric bending. Using spin-polarized electronic microscopy, Scheinfein *et al.*[4] have confirmed the existence of an asymmetric Bloch wall in iron and other ferromagnets and they have shown by numerical simulation that the width of a 180° DW at the surface is approximately two times greater than the width in the bulk. Another important result obtained in Ref. 4 is that the width of the DW on the surface is determined only by the magnetocrystalline anisotropy constant (K) and the exchange coupling constant (A) in the bulk of the ferromagnet and does not depend on the surface anisotropy, surface magnetostriction, or other surface parameters. As the magnetic anisotropy decreases, the width Δ_v of the DW in the bulk, determined by the parameter $\sqrt{A/K}$, increases. According to the results of Ref. 4, Δ_s should also increase with Δ_v. Indeed, 180° DWs wider than in iron have been observed at the surface of ferromagnets with effective anisotropy less than in iron: $\Delta_s = 0.8$ μm in Permalloy[5] and

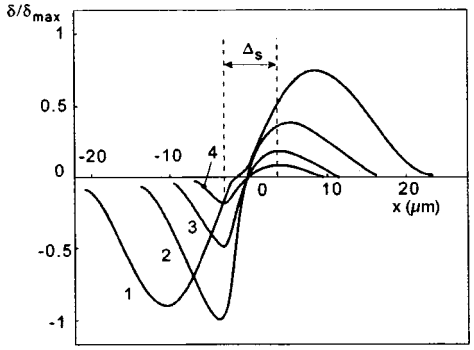

FIG. 1. EKE due to the magnetization component I_x in a DW for various values of H_y: curve *1* — 0.16 Oe; *2* — 0.08 Oe; *3* — 0.04; *4* — 0.02 Oe.

$\Delta_s = 0.9$ and 1.7 μm in amorphous ribbons.[6] Ryan and Mitchell[7] have observed very wide walls ($\Delta_s = 2.7$ μm) in Permalloy plates obtained by electrochemical deposition. In the present letter we report the observation and investigation of a giant asymmetric Bloch wall with effective width $\Delta_s = 7$ μm in an amorphous ferromagnet.

The samples consisted of ribbons of magnetically soft amorphous alloy with the composition $Fe_{76.1}Cu_1Nb_3Si_{13.8}B_{6.1}$. The ribbons were prepared using a new technology developed at the Urals State Technical University. Prior to pouring, the melt was subjected to time-and-temperature heat treatment regime in order to obtain a uniform, homogeneous, and equilibrium distribution of dopants at the macro- and microlevels and thereby to improve the magnetically soft properties of the alloy. The time and temperature parameters of the heat treatment of the liquid metal were determined from the results of investigations of a complex of physical properties of the liquid metal.[8] The ribbons investigated were 28 μm thick and 0.55 mm. Each sample contained one 180° DW, perpendicular to the ribbon plane, lying at the center parallel to the long side and dividing the sample into two domains, each approximately 0.3 mm wide.

The subsurface magnetic properties of the ribbons were investigated using a magnetooptic micromagnetometer.[3] Magnetization reversal of the samples was performed with an 80 Hz ac magnetic field using Helmholtz coils. The amplitude of the field was varied from 0 to 3 Oe. The coercive force of the DW, determined by a magnetooptic method, was 0.01 Oe. The wall penetrates completely through the sample. This was determined by observing the wall on the free and contact sides of the ribbons.

Figure 1 shows curves of $\delta(x)$ — the equatorial Kerr effect (EKE). These curves are due to the magnetization component I_x at the surface of the sample inside the DW with periodic rocking of the DW in the direction of the x axis. In the chosen coordinate system the y axis is directed along the ribbon, and the z axis is perpendicular to the plane of the ribbon. The curves were obtained for various values of the field amplitude H_y with the entrance window of the photodetector moving in the focal plane of the microscope along the x axis perpendicular to the image of the DW. The displacement x of the entrance window of the photodetector is scaled, taking account of the magnification of the microscope, in the sample plane (see Refs. 1 and 3 for a more accurate description of the method used to investigate the DW). The sign-alternating EKE curves presented in Fig. 1

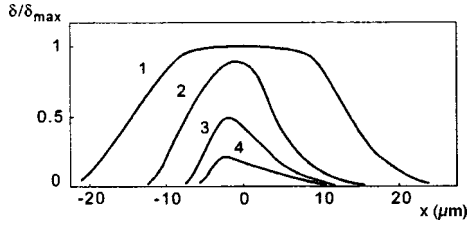

FIG. 2. EKE due to the magnetization component I_y in the region of oscillations of the DW for different values of H_y: *1* — 0.16 Oe; *2* — 0.08 Oe; *3* — 0.04; *4* — 0.02 Oe.

show that a 180° DW at the surface has a Néel magnetization component I_x (see Refs. 1 and 3 for a more detailed discussion). The absence of a normal magnetization component I_z in the DW at the surface, as established by measuring the polar Kerr effect, shows that the wall at the surface has a Néel structure. We determine the effective width Δ_s of the wall, following Ref. 1, as the minimum distance between the positive and negative extrema in the EKE curves, due to the component I_x, and realized as the amplitude of the oscillations of the DW decreases. The position of the positive and negative extrema corresponds to points inside the wall, where the component I_x changes most rapidly. It is evident from Fig. 1 that $\Delta_s \cong 7$ μm. The difference in the magnitude of the positive and negative extrema in the dependence $\delta(x)$ and the different extent of the sections with positive and negative values of the EKE are interesting. Such a difference has not been previously observed in iron[1,3] or Permalloy[5] or amorphous alloys.[6] Figure 2 shows the EKE due to the component I_y in the sample as a function of the coordinate x. In weak fields, where the amplitude of the oscillations of the DW is much smaller than the width of the wall, the EKE is due to the component I_y inside the wall itself (curve *4*). It is evident from the figure that curve *4* is asymmetric relative to its maximum: The effect drops off rapidly to the left of the maximum, and it has a very flat form to the right of the maximum. This agrees with the behavior of curve *4* (Fig. 1) due to the component I_x in the DW, which shows a distinct positive maximum and drops off very slowly with increasing x to the right of this maximum.

Using the result of Ref. 4 that the structure of an asymmetric Bloch DW at the surface is determined only by the bulk magnetic parameters, it is possible to estimate the width of the DW in the bulk of the experimental ribbons and the effective uniaxial anisotropy in the bulk. Setting $\Delta_v = \Delta_s/2 = 3.5$ μm and using $A = 1 \times 10^{-6}$ erg/cm from Ref. 9 for an amorphous alloy with composition close to the composition studied here, we obtain using the formula $\Delta_v = \pi\sqrt{A/K}$ the uniaxial anisotropy constant in the bulk $K \cong 80$ erg/cm^3. If it is assumed that a cubic magnetic anisotropy characterized by a constant K_1 exists in the material, then Lilley's formula $\Delta_v = 10.87\sqrt{A/K_1}$ for the width of a 180° DW in a cubic crystal can be used to estimate K_1 (Ref. 10). Hence we obtain $K_1 = 960$ erg/cm^3. This is two orders of magnitude less than the magnetocrystalline anisotropy constant in iron silicide $K_1 = 8 \times 10^4$ erg/cm^3 (Ref. 9).

This work was supported by the Russian Fund for Fundamental Research (Grant No. 99-0216595).

*)e-mail: kudakov@adk.phys.msu.su

[1]G. S. Krinchik and O. M. Benidze, Zh. Éksp. Teor. Fiz. **67**, 2180 (1974) [Sov. Phys. JETP **40**, 1081 (1975)].
[2]A. Hubert, Z. Angew. Phys. **32**, 58 (1971).
[3]V. E. Zubov, G. S. Krinchik, and A. D. Kudakov, Zh. Éksp. Teor. Fiz. **94**, 248 (1988) [Sov. Phys. JETP **67**, 2527 (1988)].
[4]M. R. Scheinfein, J. Unguris, J. L. Blue *et al.*, Phys. Rev. B **43**, 3395 (1991).
[5]A. Blyushke, V. E. Zubov, G. S. Krinchik *et al.*, Pis'ma Zh. Tekh. Fiz. **16**, 16 (1990) [Sov. Tech. Phys. Lett. **16**, 290 (1990)].
[6]R. Schafer, W. K. Ho, J. Yamasaki *et al.*, IEEE Trans. Magn. **MAG-27**, 3678 (1991).
[7]P. J. Ryan and T. B. Mitchell, J. Appl. Phys. **63**, 3162, (1988).
[8]Yu. N. Starodubtsev, L. D. Son, V. S. Tsepelev *et al.*, Rasplavy **4**, 76 (1992).
[9]G. Herzer, IEEE Trans. Magn. **MAG-26**, 1397 (1990); J. Magn. Magn. Mater. **112**, 258 (1992).
[10]B. A. Lilley, Philos. Mag. **41**, 792 (1950).

Translated by M. E. Alferieff

Contribution to the theory of spin relaxation at finite temperatures in the odd-filling quantum Hall effect regime

S. M. Dikman*)
Institute of Solid State Physics, Russian Academy of Sciences, 142432 Chernogolovka, Moscow Region, Russia

S. V. Iordanskiĭ
L. D. Landau Institute of Theoretical Physics, Russian Academy of Sciences, 117940 Moscow, Russia

(Submitted 20 September 1999)
Pis'ma Zh. Éksp. Teor. Fiz. **70**, No. 8, 531–536 (25 October 1999)

Spin relaxation in a two-dimensional electron gas (2D EG) is treated as the establishment of equilibrium in a gas of spin excitons as a result of processes that change the number of spin excitons. Coalescence is the dominant channel above a temperature of the order of 1 K. The coalescence of excitons can occurr as a result of spin–orbit and Coulomb interactions in the 2D EG. The rate of coalescence falls exponentially at low temperatures. The relaxation time is calculated, and the critical temperature below which the main annihilation process becomes that due to the exciton–phonon interaction is determined. © *1999 American Institute of Physics.* [S0021-3640(99)01020-8]

PACS numbers: 73.40.Hm, 71.10.Ca

1. Investigations of spin relaxation are one way to determine the fundamental properties of a two-dimensional electron gas (2D EG).[1–8] On the one hand, the two-dimensionality strongly intensifies the spin–orbit interaction for conduction electrons in GaAs/AlGaAs heterostructures, but, on the other hand, Coulomb correlations in the quantum Hall effect regime radically restructure the energy spectrum in a 2D EG, which can slow down, rather than speed up, relaxation (compare the experimental results of Refs. 1–3 and Ref. 4).

The deviation of a 2D EG spin system from equilibrium can be described as the appearance of spin waves or, equivalently, spin excitons consisting of an effective hole in the distribution of electrons polarized in the direction of the field and an electron with opposite spin, which are bound by the Coulomb interaction.[9,10] The appearance of a single spin exciton with nonzero 2D momentum changes by 1 the spin projection of all electrons, $S_z \rightarrow S_z - 1$ (the z axis is directed along the magnetic field). The total spin S also decreases by 1: $S \rightarrow S - 1$. The appearance of a spin exciton with zero momentum (a so-called ''zero'' exciton; see Refs. 7 and 8) changes similarly the component S_z by 1 but leaves S unchanged, which corresponds to a deviation of the total spin **S** from the direction of the field **B** without a change in the value of S itself. In both cases the spin relaxation process can be described in terms of the annihilation or creation of spin

excitons, if the density of excitons with nonzero momentum is assumed to be small.

The experimental realization of an initial state as a state in which the spin of the entire system is rotated as a whole relative to its equilibrium direction encounters methodological difficulties. In the experiment of Ref. 4, with odd filling ($\nu=2n+1$), the total spin of the electrons always remained polarized in the direction of the field, but in the relaxation process S differed from the equilibrium value. Therefore, in this experiment the number of zero excitons was negligibly small compared with the total number of excitons with nonzero momentum. In a previous work we studied the relaxation of the density of such ''nonzero'' excitons.[8] The annihilation (or, conversely, creation) of a spin exciton accompanied by the emission (absorption) of an acoustic phonon was studied. The process was determined by the spin–orbit or electron–phonon interactions. As a result, the exciton lifetime turns out to be essentially independent of temperature[1)] and, according to the calculations, more than an order of magnitude greater than the value measured in Ref. 4.

In addition to this, there exists another spin relaxation channel due to interexciton collisions which lead to coalescence of excitons. This is the subject of the present letter. We shall estimate in this case the character of the temperature dependence for the spin equilibration time. The annihilation of excitons in this case is due to the spin–orbit interaction and occurs without the participation of phonons. Energy conservation in an elementary event requires that

$$\epsilon(q_1)+\epsilon(q_2)=\epsilon(|\mathbf{q}_1+\mathbf{q}_2|)\,, \tag{1}$$

where $\epsilon(q)$ is the energy of a spin exciton, which depends on the two-dimensional wave vector $\mathbf{q}$ of the exciton. In our problem only values $ql_B\ll 1$ (l_B is the magnetic length) are important, so that

$$\epsilon(q)\approx|g\mu_b B|+(ql_B)^2/M\,, \tag{2}$$

where M is the spin-exciton mass (in real heterostructures $M^{-1}\approx 40-80$ K, and the Zeeman gap is such that $|g\mu_b B|\approx 3$ K at $B=10$ T). As a result, the relation (1) reduces to $\mathbf{q}_1\cdot\mathbf{q}_2 l_B^2=M|g\mu_b B|$, which in any case gives a lower limit for the total kinetic energy of the interacting excitons: $(q_1^2+q_2^2)l_B^2/2M\geqslant|g\mu_b B|$. In calculating the total annihilation flux, the phase volumes of the wave vectors for which coalescence occurs will enter with the weight $\exp[-(q_1^2+q_2^2)l_B^2/2MT]$, which will give a factor $\exp(-|g\mu_b B|/T)$. The inverse exciton lifetime for the process under study should be proportional to the exciton density, which at low temperatures near equilibrium will also behave as $\exp(-|g\mu_b B|/T)$ (see Refs. 8 and 11). Ultimately, for low values of T the effective relaxation time is determined by the exponential law $\exp(2|g\mu_b B|/T)$. We shall see that for $T\approx 1.5$ K (this temperature corresponds to the experiment of Ref. 4) the ''coalescence'' relaxation channel is the dominant channel, and our calculation is in complete agreement with the measurements performed in Ref. 4.

2. We write the single-particle Hamiltonian for the 2D electrons in a GaAs/AlGaAs heterostructure:

$$H_1=-|g\mu_b B|\sigma_z/2+\hbar\omega_c[l_B^2\mathbf{k}^2/2-\nu l_B(\mathbf{k}\times\boldsymbol{\sigma})_z/\sqrt{2}-u l_B(\mathbf{k}\cdot\boldsymbol{\sigma})/\sqrt{2}]\,. \tag{3}$$

Here $\omega_c=eB/m_e^* c$ is the cyclotron frequency, l_B is the magnetic length, $\boldsymbol{\sigma}$ are the Pauli matrices, and $\mathbf{k}$ is the 2D operator $k_i=-i\nabla_i+eA_i/c\hbar$ ($i=x,y$). The term with the

coefficient v appears because of the absence of mirror symmetry in the $\hat{z}$ direction and is proportional to the normal component of the electric field in the 2D layer.[12] The term containing the parameter u appears because of the lifting of spin degeneracy in the conduction band of a crystal without a center of inversion.[13] In writing the representation (3) we assumed that the direction $\hat{z}$ normal to the layer of the 2D EG is parallel to one of the principal axes of the GaAs crystal. The final answers depend only on the combination u^2+v^2. For $B=10$ T and an effective layer thickness $d=5$ nm (see, for example, its definition in Ref. 8), one has $u^2+v^2\sim 10^{-4}-10^{-5}$. This combination is inversely proportional to B, and in the asymptotic limit $d\to 0$ it is inversely proportional to d^4 (see Ref. 8).

The Hamiltonian (3), up to terms first order in u and v inclusively, is diagonal in the spinor basis:

$$\Psi_{npa}=\begin{pmatrix} \psi_{np} \\ v\sqrt{n+1}\,\psi_{n+1\,p}+iu\sqrt{n}\,\psi_{n-1\,p} \end{pmatrix},$$

$$\Psi_{npb}=\begin{pmatrix} -v\sqrt{n}\,\psi_{n-1\,p}+iu\sqrt{n+1}\,\psi_{n+1\,p} \\ \psi_{np} \end{pmatrix}, \tag{4}$$

where $\psi_{np}(\mathbf{r})=L^{-1/2}e^{ipy}\phi_n(pl_B^2+x)$ is the wave function of an electron in the Landau gauge ($L\times L$ is the size of the 2D system, ϕ_n is the oscillator function of the nth harmonic). The corresponding expansion of the single-electron creation $\Psi^+(\mathbf{r})$ and annihilation $\Psi(\mathbf{r})$ operators with respect to the basis of states a and b (4) can be substituted into the formula

$$\mathcal{H}_{\text{int}}=\frac{1}{2}\int d\mathbf{r}_1 d\mathbf{r}_2 \Psi^+(\mathbf{r}_1)\Psi^+(\mathbf{r}_2)\tilde{V}(\mathbf{r}_1-\mathbf{r}_2)\Psi(\mathbf{r}_2)\Psi(\mathbf{r}_1) \tag{5}$$

to obtain the effect of Coulomb Hamiltonian of the 2D EG. We shall solve the problem in the strong magnetic field approximation (see Refs. 9, 10, and 14 as well as Refs. 7, 8, and 15). This makes it possible to find for integer filling factors, to a first approximation in the parameter $E_C/\hbar\omega_c$ ($E_C=e^2/\varepsilon l_B$ is the characteristic Coulomb energy), exact answers for the eigenstates of the lower part of the spectrum.[9,10,14] It is convenient to use the so-called excitonic representation,[7,8,15,16] switching from Fermi creation and annihilation operators in the states (4) in the operators

$$\mathcal{Q}^+_{\mathbf{q}}=\frac{1}{\sqrt{\mathcal{N}}}\sum_p e^{-iq_xp}b^+_{p+\frac{q_y}{2}}a_{p-\frac{q_y}{2}},$$

$$\begin{pmatrix} \mathcal{A}^+_{\mathbf{q}} \\ \mathcal{B}^+_{\mathbf{q}} \end{pmatrix}=\begin{pmatrix} \mathcal{A}_{-\mathbf{q}} \\ \mathcal{B}_{-\mathbf{q}} \end{pmatrix}=\frac{1}{\mathcal{N}}\sum_p e^{-iq_xp}\begin{pmatrix} a^+_{p+\frac{q_y}{2}}a_{p-\frac{q_y}{2}} \\ b^+_{p+\frac{q_y}{2}}b_{p-\frac{q_y}{2}} \end{pmatrix} \tag{6}$$

(see also Refs. 17 and 18). Here $\mathcal{N}$ is the number of magnetic-flux quanta, equal in the case of an odd filling factor to the number of electrons in the highest nonempty, nth Landau level. In formulas (6) the orbital index n is dropped. It is assumed to be the same for all states a and b, since spin excitations are studied within one level. The generator of the spin-excitonic states is the operator $\mathcal{Q}^+_{\mathbf{q}}$, which acts on the ground state $|0\rangle$. We shall

consider only odd filling factors, so that in the state $|0\rangle$ the spins of all the electrons in the nth Landau level are aligned along the magnetic field. The complete Hamiltonian of the electrons in the excitonic representation can be expressed in terms of the operator (6), and only the terms which do not commute with $\mathcal{Q}_{\mathbf{q}}^{+}$ are ''important.'' Moreover, in the first-order approximation with respect to $E_C/\hbar\omega_c$ it is sufficient to consider only terms which do not ''mix'' different Landau levels.

We therefore write $\mathcal{H}=\mathcal{H}_1+\mathcal{H}_2+\mathcal{H}_2'$. Here $\mathcal{H}_1$ is the part of the single-electron Hamiltonian $\int d\mathbf{r}\Psi^{+}H_1\Psi$ that does not commute with $\mathcal{Q}_{\mathbf{q}}^{+}$, specifically, $\mathcal{H}_1=|g\mu_b B|\mathcal{B}_0$. The corresponding part $\mathcal{H}_2$ of the operator (5) in the zeroth approximation in the spin–orbit parameters u and v can also be expressed in terms of excitonic operators (6); ultimately, it determines the spin-wave spectrum $\epsilon(q)$ (see Refs. 9, 10, and 14). We shall be interested in only small values of q. Then formula (2) with

$$\frac{1}{M}=l_B^2\int_0^\infty\frac{q^3dq}{4\pi}V(q)e^{-q^2l_B^2/2}[L_n(q^2l_B^2/2)]^2 \tag{7}$$

is valid. Finally, $\mathcal{H}_2'$ represents the terms of the operator (5) which are of first order in the parameters u and v:

$$\mathcal{H}_2'=\mathcal{N}^{1/2}\sum_{\mathbf{q}}(iuq_+-vq_-)U(q)(\mathcal{A}_{\mathbf{q}}^{+}+\mathcal{B}_{\mathbf{q}}^{+})\mathcal{Q}_{\mathbf{q}}+\text{h.c.}, \tag{8}$$

where the function $U(q)$ can be expressed in terms of the Fourier component $V(q)$ of the Coulomb potential $\tilde{V}(\mathbf{r})$ averaged in the layer, and the Laguerre polynomial $U(q)=V(q)e^{-q^2l_B^2/2}[L_n(q^2l_B^2/2)]^2/2\pi l_B^2$ (we used in Eq. (8) the conventional notation $q_{\pm}=\mp i(q_x\pm iq_y)/\sqrt{2}$).

3. An elementary event corresponds to a transition from the state $|\mathbf{q}_1,\mathbf{q}_2\rangle=\mathcal{Q}_{\mathbf{q}_1}^{+}\mathcal{Q}_{\mathbf{q}_2}^{+}|0\rangle$ into the state $|\mathbf{q}_1+\mathbf{q}_2\rangle=\mathcal{Q}_{\mathbf{q}_1+\mathbf{q}_2}^{+}|0\rangle$ or vice versa. The two-exciton state $|\mathbf{q}_1,\mathbf{q}_2\rangle$ is ''almost'' an eigenstate with energy $\epsilon(q_1)+\epsilon(q_2)$, since $[\mathcal{H}_1+\mathcal{H}_2,\mathcal{Q}_{\mathbf{q}_1}^{+}\mathcal{Q}_{\mathbf{q}_2}^{+}]|0\rangle=[\epsilon(q_1)+\epsilon(q_2)]|\mathbf{q}_1,\mathbf{q}_2\rangle+\ldots$, where the dots denote negligibly small terms with a norm of the order of $E_C/\mathcal{N}^{1/2}$. The operator (8) does not conserve the number of excitons and determines the transition matrix element

$$\mathcal{M}(\mathbf{q}_1,\mathbf{q}_2)=\langle\mathbf{q}_1+\mathbf{q}_2|\mathcal{H}_2'|\mathbf{q}_1,\mathbf{q}_2\rangle. \tag{9}$$

The latter quantity can be found quite easily using the commutation relations presented in Ref. 8 for the operators (6). For small q_1 and q_2 a calculation gives

$$\mathcal{M}(\mathbf{q}_1,\mathbf{q}_2)=\frac{2l_B}{M\mathcal{N}^{1/2}}[iu(q_{1-}+q_{2-})-v(q_{1+}+q_{2+})],\quad q_1l_B\ll1,\quad q_2l_B\ll1, \tag{10}$$

where M is determined by formula (7).

The relaxation rate or, equivalently, the total flux of annihilating excitons is determined by the standard perturbation theory formula

$$R=\frac{1}{2}\sum_{\mathbf{q}_1,\mathbf{q}_2}\frac{2\pi}{\hbar}|\mathcal{M}(\mathbf{q}_1,\mathbf{q}_2)|^2\delta(\epsilon_1+\epsilon_2-\epsilon_{12})[n_1n_2(1+n_{12})-n_{12}(1+n_1)(1+n_2)]. \tag{11}$$

For compactness, here we have introduced the notation $\epsilon_i=\epsilon(q_i)$, $n_i=n(\epsilon_i)$ $(i=1,2)$, $\epsilon_{12}=\epsilon(|\mathbf{q}_1+\mathbf{q}_2|)$, and $n_{12}=n(\epsilon_{12})$, where $n(\epsilon)$ is the Bose distribution function of the excitons

$$n(\epsilon)=\frac{1}{\exp[(\epsilon-\mu)/T]-1} \quad (\mu<|g\mu_b B|)\,. \tag{12}$$

It is assumed that thermal equilibrium is established between excitons much more rapidly then the excitons are annihilated (i.e., much more rapidly than the spin relaxes).

Equations (1), (2), (9), and (12) completely determine the flux R. It is a function of B,T, and the number N of excitons in the system. The chemical potential is given by the relation between the number of excitons with the total spin of the 2D EG: $N(\mu)=\mathcal{N}-S$ (see Refs. 8 and 11); in addition, $N|_{\mu=0}=N_0$, where N_0 is the equilibrium number of excitons. We shall calculate the relaxation rate in its final stage, where $|\Delta S|\equiv N-N_0 \ll N_0$. In this case, the inequality $\mu\ll T$ should hold. Switching in Eq. (11) from summation to integration, we find $R=(N-N_0)/\tau_{\mathrm{II}}$, where the inverse spin relaxation time depends only on T and B:

$$1/\tau_{\mathrm{II}}(B,T)=\frac{2\pi}{\hbar}(u^2+v^2)|g\mu_b B|\exp(-2|g\mu_b B|/T)F(|g\mu_b B|/T)\,. \tag{13}$$

The function $F(\beta)$ is given by the expression

$$F(\beta)=\frac{1}{\pi\beta}\int\limits_{\xi\eta>\beta^2/4}\int \frac{d\xi d\eta\,(\xi+\eta)e^{\beta-\xi-\eta}}{(\xi\eta-\beta^2/4)^{1/2}(1-e^{-\beta-\xi})(1-e^{-\beta-\eta})(1-e^{-2\beta-\xi-\eta})}, \tag{14}$$

and it decreases smoothly, assuming the values $F(\beta\ll 1)\approx 1.86/\beta^2$, $F(1)\approx 2.92$, and $F(\beta\gg 1)\approx 1$. We note that T appearing in Eq. (13) is the temperature of the 2D EG at the moment the equilibrium spin is established.

Formula (13) confirms the exponential temperature dependence of the relaxation rate. We note that the mass of the spin exciton does not enter in the final answer. However, the implicit dependence on the number n of the Landau level is determined by the magnetic field B, giving an integer filling factor $\nu=2n+1$ with a fixed surface electron density.

4. Comparing the answer (13) with the experimentally measured relaxation time we can estimate the value of u^2+v^2. Following Ref. 4, setting $B=4.9$ T, $T=1.5$ K, and $\tau_{\mathrm{II}}\approx 10$ ns, we find $u^2+v^2\approx 2\times 10^{-4}$. This agrees completely with the theoretical estimates and the experimentally measured spin–orbit interaction parameters.

The inverse relaxation time (13) can be compared with the corresponding value of τ_{I}^{-1} determined by the electron–phonon interaction[8] (in this case the answer depends on the mass M). It is evident that the total inverse spin relaxation time is the sum

$$1/\tau_{\mathrm{SR}}=1/\tau_{\mathrm{I}}+1/\tau_{\mathrm{II}}\,, \tag{15}$$

where $\tau_{\mathrm{I}}(B,T)$ is given by Eq. (6.30) in Ref. 8. We shall perform the calculation for $1/M=19B^{1/2}$ K and $u^2+v^2=10^3/B$ (B in teslas). The result is[2)]

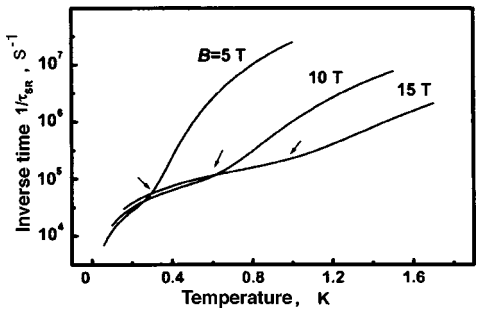

FIG. 1. Total inverse spin relaxation time (15) versus the temperature for three different values of the magnetic field: 5, 10, and 15 T. The arrows indicate the region of the transition from the low- to the high-temperature relaxation regime.

$$\frac{1}{\tau_{\mathrm{I}}} = 4.8\times 10^4 [\, TB^{1/2}\gamma_1(\beta) + 190T^2B^{-3}\gamma_2(\beta)] \ \mathrm{s}^{-1},$$

$$\frac{1}{\tau_{\mathrm{II}}} = 2.48\times 10^8 e^{-2\beta}F(\beta) \ \ \mathrm{s}^{-1}. \tag{16}$$

Here $\beta = |g\mu_b B|/T \approx 0.3B/T$ (the field was measured in teslas and the temperature in kelvins), while the functions γ_κ are determined in Ref. 8 ($\gamma_\kappa(\beta \gg 1) \approx \kappa$, $\gamma_\kappa(\beta \ll 1) \propto \beta$). The temperature dependence of the total inverse relaxation time (15) is shown in Fig. 1. For different values of the field the transition from the low-temperature regime, determined by the time τ_I, to the high-temperature regime, with characteristic time τ_{II}, occurs at different values of T. The transition region is clearly seen in the figure presented, since the sign of the second derivative $d^2\tau_{\mathrm{SR}}^{-1}/dT^2$ changes in the process.

The temperature of the transition from one relaxation regime to another can be determined from the equation $\tau_{\mathrm{I}}(B,T^*) = \tau_{\mathrm{II}}(B,T^*)$. The result shown in Fig. 2 does not depend on the magnitude of the spin–orbit interaction. The range of values of B and T under the curve $T^*(B)$ corresponds to the spin relaxation channel with $\tau_{\mathrm{SR}} \simeq \tau_{\mathrm{I}}$, and correspondingly the region above the curve corresponds to the channel $\tau_{\mathrm{SR}} \simeq \tau_{\mathrm{II}}$. Evi-

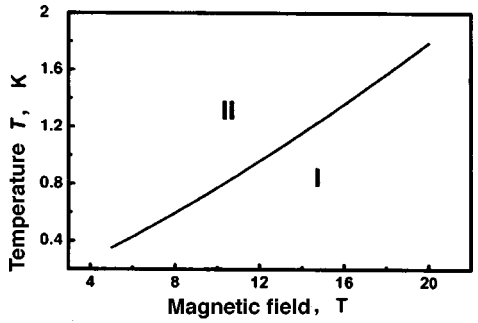

FIG. 2. Transition temperature T^* as a function of the magnetic field. The region I corresponds to the first spin relaxation channel (the corresponding time τ_{I} is calculated in Ref. 8). In the range II of fields and temperatures the relaxation is determined by the time τ_{II} (see expressions (15) and (16) in the text).

dently, the experimental conditions of Ref. 4 are characterized by the parameters B and T corresponding to values deep in the region II. We hope that this work will serve as a stimulus for experiments in a wider range of magnetic fields and temperatures (with a fixed odd filling factor), so that it would be possible to observe a transition between two different relaxation regimes.

This work was supported by the Russian Fund for Fundamental Research.

*)e-mail: dickmann@issp.ac.ru

1)The temperature dependence for this relaxation channel is due to the fact that the spin–orbit interaction, being proportional to the 2D wave vector q of the excitons, effectively becomes weaker with increasing temperature, since $\langle q^2 \rangle \propto T$.

2)The remaining parameters required to calculate τ_I are presented in Ref. 8. We note that the numerical estimate given there for the excitonic mass was obtained for the ultra-two-dimensional case (i.e., $d \ll l_B$). Moreover, in Ref. 8 we did not distinguish between the longitudinal and transverse sound velocities. Now we have taken into account the fact that longitudinal phonons contribute to the deformation interaction, and the ''piezoelectric'' part in our specific case is determined only by the transverse phonons.

[1] S. Bar-Ad and I. Bar-Joseph, Phys. Rev. Lett. **68**, 349 (1992).
[2] G. Müller, L. Weiss, A. V. Khaetskii *et al.*, Phys. Rev. B **45**, 3932 (1992).
[3] V. Srinivas, Y. J. Chen, and C. E. Wood, Phys. Rev. B **47**, 10907 (1993).
[4] V. E. Zhitomirskiĭ, V. E. Kirpichev, A. I. Filin *et al.*, JETP Lett. **58**, 439 (1993).
[5] G. Bastard, Phys. Rev. B **46**, 4253 (1992).
[6] A. V. Khaetskii, Phys. Rev. B **45**, 13777 (1992).
[7] S. M. Dikman and S. V. Iordanskiĭ, JETP Lett. **63**, 50 (1996).
[8] S. M. Dikman and S. V. Iordanskiĭ, Zh. Éksp. Teor. Fiz. **110**, 238 (1996) [JETP **83**, 128 (1996)].
[9] Yu. A. Bychkov, S. V. Iordanskiĭ, and G. M. Éliashberg, JETP Lett. **33**, 143 (1981).
[10] C. Kallin and B. I. Halperin, Phys. Rev. B **30**, 5655 (1984).
[11] I. V. Lerner and Yu. E. Lozovik, Zh. Éksp. Teor. Fiz. **80**, 1488 (1981) [Sov. Phys. JETP **53**, 763 (1981)].
[12] Yu. A. Bychkov and É. I. Rashba, JETP Lett. **39**, 66 (1984).
[13] M. I. D'yakonov and V. Yu. Kachorovskiĭ, Fiz. Tekh. Poluprovodn. **20**, 178 (1986) [Sov. Phys. Semicond. **20**, 110 (1986)].
[14] I. V. Lerner and Yu. E. Lozovik, Zh. Éksp. Teor. Fiz. **78**, 1167 (1980) [Sov. Phys. JETP **51**, 588 (1980)].
[15] S. Dickmann, Physica B **263–264**, 202 (1999).
[16] A. B. Dzyubenko and Yu. E. Lozovik, J. Phys. A: Math. Gen. **24**, 415 (1991).
[17] M. Rasolt, B. I. Halperin, and D. Vanderbilt, Phys. Rev. Lett. **57**, 126 (1986).
[18] Yu. A. Bychkov and S. V. Iordanskiĭ, Fiz. Tverd. Tela (Leningrad) **29**, 2442 (1987) [Sov. Phys. Solid State **29**, 1405 (1987)].

Translated by M. E. Alferieff

Cs/GaAs(100) surface: two-dimensional metal or Hubbard insulator?

O. E. Tereshchenko, V. L. Al'perovich,*) and A. S. Terekhov
Institute of Semiconductor Physics, Siberian Branch of the Russian Academy of Sciences, 630090 Novosibirsk, Russia; Novosibirsk State University, 630090 Novosibirsk, Russia

A. N. Litvinov
Novosibirsk State University, 630090 Novosibirsk, Russia

(Submitted 21 September 1999)
Pis'ma Zh. Éksp. Teor. Fiz. **70**, No. 8, 537–542 (25 October 1999)

The evolution of the characteristic electron energy loss spectra accompanying the deposition of cesium on GaAs(100) surfaces with various superstructural reconstructions is studied experimentally. It is shown that the appearance of loss peaks in the GaAs band gap for Cs coverages $\theta_{Cs}>0.5$ monolayers is due to resonances in the longitudinal and transverse polarizability of two-dimensional metallic clusters of adatoms. © *1999 American Institute of Physics.*
[S0021-3640(99)01120-2]

PACS numbers: 81.15.Ef, 73.40.−c, 68.35.Bs

A gallium arsenide surface with adsorbed layers of alkali metals is of great interest for investigating the interaction of adatoms with semiconductors. Thus far the most complete data on the structure and electronic properties of such systems have been obtained for the nonpolar GaAs(110) face.[1] Specifically, it has been shown by scanning tunneling microscopy (STM) that ordered one-dimensional rows form on the Cs/GaAs(110) surface at low coverages $\theta_{Cs}<0.5$ monolayers (ML), while for $\theta_{Cs}>0.5$ ML two-dimensional clusters of cesium adatoms form.[2] In Ref. 3 intense peaks with energies $E\approx 0.4$ eV (L1 peak) and 1 eV (L2 peak) in the band gap of the semiconductor were observed in the characteristic electron energy loss spectra for a Cs/GaAs(110) surface with $\theta_{Cs}\geqslant 0.5$ ML. These peaks were attributed to the formation of a Mott–Hubbard insulator state, arising as a result of Coulomb correlations in a system of two-dimensional electrons. For the GaAs(110) surface this idea was substantiated theoretically in Ref. 4. Later, comparison of the loss spectra measured with various alkali metals deposited on a GaAs(110) surface made it possible to suggest an alternative picture for the formation and the electronic properties of such a surface: the formation of two-dimensional clusters of adatoms with a metallic electronic spectrum.[5] To determine the generality of the phenomenon observed and the validity of the models proposed in Refs. 3–5, in the present work we studied experimentally the evolution of the characteristic electron energy loss spectra as Cs was deposited on the polar face GaAs(100) with various superstructural reconstructions.

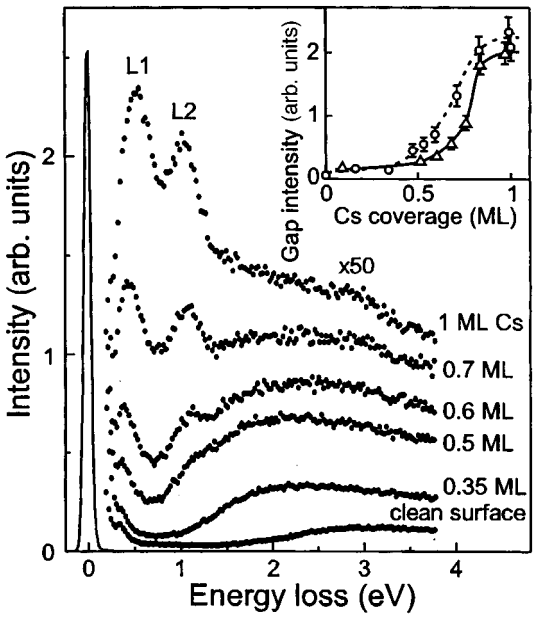

FIG. 1. Evolution of electron energy loss spectra with cesium adsorption on an As-stabilized (100)GaAs(2×4) surface. The solid line shows a peak due to elastically reflected electrons. $T=300$ K, $\vartheta_i=\vartheta_s=60°$. Inset: Integrated intensity of the losses in the GaAs band gap versus θ_{Cs}. The circles show the dependence obtained with Cs deposited on an As-stabilized (100)GaAs(2×4) surface; the triangles are for a Ga-stabilized (100)GaAs(4×2) surface. The lines are drawn as an aid to the eye.

The experiment was performed on *p*-(100)GaAs epitaxial layers with hole density $p\approx 10^{18}$ cm^{-3}. A pure GaAs(100) surface with various superstructural reconstructions was prepared using the method described in Ref. 6 by removing the oxides in a solution of HCl in isopropyl alcohol in a dry nitrogen atmosphere, transferring the sample in a hermetically sealed container without contact with air into an ADES-500 ultrahigh-vacuum electron spectrometer, and subsequent heating in vacuum. The base pressures in the analytic and preparatory chambers were 3×10^{-11} and 8×10^{-11} torr, respectively. The surface structure and composition were determined by low-energy electron diffraction (LEED) and x-ray photoelectron spectroscopy (XPES). Cesium deposition and all measurements were performed at room temperature. The effective thickness θ_{Cs} of the cesium coating was determined from the dependence of the area of the photoemission peak $Cs3d_{5/2}$ on the cesium deposition time (dose). As the dose increases, the area of the peak, which is proportional to the amount of Cs on the surface, increased and then saturated. The thickness of the coating corresponding to the saturated value of the area of the peak was taken as one monolayer $\theta_{Cs}=1$ ML.[7] The characteristic loss spectra were measured with incident electron energy 15 eV, with total energy resolution not worse than 90 meV, and angular resolution 1.5°.

Figure 1 shows the characteristic electron energy loss spectra measured with Cs deposition on a pure As-stabilized surface with (2×4) reconstruction. It is seen that on

the clean surface there are no energy losses to transitions involving the participation of surface states in the GaAs band gap $E_g \approx 1.42$ eV.[8] The weak peak at $E \approx 0.36$ eV is due to the excitation of vibrations of the C–H bonds of the residual methane radicals, with a density $\leqslant 0.01$ ML.[6] When up to half a monolayer of cesium is deposited, the threshold of the transitions shifts to lower energies, and the intensity of the losses increases substantially (severalfold) in the entire energy range. For $\theta_{Cs} \approx 0.5$ ML coverage two loss peaks L1 and L2 with $E \approx 0.52$ eV and 1.05 eV, respectively, appear in the spectrum, and they increase rapidly as θ_{Cs} increases further. Similar changes occurred in the loss spectra with Cs deposited on a Ga-stabilized (100)GaAs(4×2) surface and on a surface with intermediate composition and $(3\times1)/(3\times6)$ reconstruction. The inset in Fig. 1 shows the curves of the integrated intensity of the electron energy losses in the band gap versus the coverage for cases where cesium is deposited on As- and Ga-stabilized GaAs(100) surfaces. It is seen that both dependences have a threshold character and are due mainly to an increase in the intensity of the L1 and L2 peaks for $\theta_{Cs} > 0.5$ ML.

The qualitative similarity of the loss spectra measured in this work with Cs deposited on GaAs(100) surfaces with various superstructures and the similarity with spectra obtained previously on the nonpolar Cs/GaAs(110) face[3] attest to the universality of the mechanisms leading to the formation of the structure and electronic properties of the interface of gallium arsenide with adsorbed cesium layers. It can be inferred that the appearance of the loss peaks L1 and L2 on a Cs/GaAs(100) surface, just as on a Cs/GaAs(110) surface,[2,3,5] is due to a phase transition, in which individual Cs atoms combined into close-packed two-dimensional clusters. The reason for the transition is that as the coverage increases, the dipole–dipole repulsion arising between polarized cesium adatoms as a result of the depolarization effect is replaced by attraction as a result of the formation of a lateral bond between the adatoms.

In Ref. 3 the peaks L1 and L2 were explained by the formation of a Mott–Hubbard insulator state in the Cs/GaAs(110) system with coverage $0.5 \leqslant \theta_{Cs} \leqslant 1$ ML. Specifically, the peak L1 was attributed to a transition through the gap in a Hubbard insulator. At the same time, in a recent work[5] comparison of the loss spectra measured on (110)GaAs interfaces with various alkali metals revealed a correlation between the positions of the L1 and L2 peaks with the energy of surface plasmons in metals. Moreover, as the thickness of the coating increased above 1 ML (at low temperature), the L2 peak shifted toward the energy of surface plasmons of the metal. Together with the results of scanning tunneling microscopy,[2] these data attest to the formation of two-dimensional clusters of adatoms with a metallic electronic spectrum. The L2 peak was interpreted as excitation of plasmons in two-dimensional clusters, and the L1 peak was interpreted as excitation of coupled plasma oscillations in a system of clusters.[5] In this picture the increase in the intensity and the constancy of the energy positions of the peaks were explained by the fact that as θ_{Cs} increases, the area occupied by clusters increases, while the density of adatoms in the clusters remains unchanged.

To further clarify the nature of the peaks L1 and L2, we measured the loss spectra on a Cs/GaAs(100) surface for various angles of incidence ϑ_i and scattering ϑ_s of electrons (Fig. 2). As the angles vary, the energy position of the peaks L1 and L2 remains constant near 50 meV and 100 meV, respectively, in agreement with the results for the (110)GaAs surface.[3,5] At the same time, the ratio of the amplitudes of the peaks depends strongly on the angles: it is seen from Fig. 2 that the amplitude of the L2 peak increases

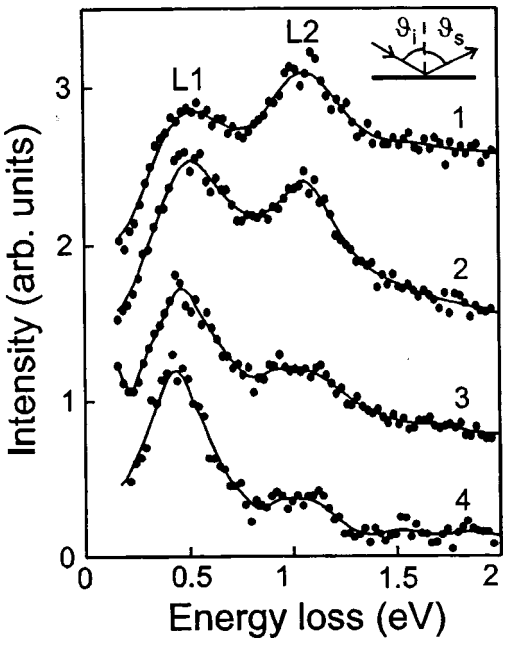

FIG. 2. Loss spectra measured on a Cs/(100)GaAs surface with $\theta_{Cs}=1$ ML for different angles of incidence ϑ_i and scattering ϑ_s of electrons. The spectra *1–3* correspond to fixed $\vartheta_i=60°$ and different $\vartheta_s=85°$ (curve *1*), 60° (*2*), and 10° (*3*). Spectrum *4* corresponds to $\vartheta_i=\vartheta_s=30°$. The spectra *1, 2,* and *4* are shifted along the ordinate by 1, 0.5, and 0.2 units, respectively. The lines are drawn as an aid to the eye. Inset: Schematic diagram of the geometry of the experiment.

with ϑ_i and ϑ_s. An increase in the inelastic loss efficiency with decreasing angle between the momentum vectors of the incident and scattered electrons (for scattering by the surface — for the lowest-angle trajectories) is characteristic for the excitation of longitudinal plasma oscillations.[9] Thus the measured angular dependences allow us to conclude that the peak L2 corresponds to longitudinal plasmons in two-dimensional cesium clusters. We note that to describe such plasmons correctly, the partial transfer of charge from electropositive cesium atoms to the orbitals of surface atoms of the semiconductor must be taken into account.[1]

The amplitude of the peak L1 as a function of the angles varies much more slowly than the amplitude of the peak L2. Therefore the peak L1 is of a different nature and is not associated with the excitation of longitudinal plasmons. Judging from its energy position, the peak L1 could be due to single-particle transitions of electrons from the GaAs valence band into empty metal-induced states above the Fermi level.[10] The similarity of the dose dependences of the intensities of the L1 and L2 peaks can be explained by the influence of the two-dimensional plasma on the single-particle transitions. It is well-known that the interaction of plasma oscillations and single-particle transitions results in combined excitations — so-called interband (transverse) plasmons.[11–13] Therefore the peak L1 can be interpreted as a transverse excitation in two-dimensional cesium clusters.

Longitudinal two-dimensional plasmons are gapless and possess strong dispersion:

For small wave vectors **q** the plasmon frequency $\omega_{2D} \propto \sqrt{q}$ (Ref. 11). However, a strong dependence of the position of the L2 peak (and also the L1 peak) on the angle of emergence of the scattered electrons is not observed, either for the Cs/GaAs(110) surface studied in Refs. 3 and 5 or for the Cs/GaAs(100) surface studied in the present work. The reason seems to be that plasma oscillations are localized in clusters, so that the observed frequency corresponds to a finite value of the wave vector of the order of the reciprocal of the cluster size.[14] It should be underscored that in contrast to Cs/GaAs(110),[2] the Cs/GaAs(100) surface with $\theta_{Cs} \approx 1$ ML is disordered, so that the description of elementary surface excitations using a dispersion law is, strictly speaking, inapplicable. In Ref. 15 disordering was observed using an STM with Cs deposited on an As-stabilized (100)GaAs(2×4) surface. We determined the degree of disorder of the Cs/GaAs(100) interface by the LEED method and by measuring the width $\Delta\vartheta_s$ of the angular distribution of elastically scattered electrons. For all initial reconstructions, $\Delta\vartheta_s$ increased from $\Delta\vartheta_s \approx 5°$ on the clean surface to $\Delta\vartheta_s \sim \pi$ for $\theta_{Cs} \approx 1$ ML. On a (100)GaAs(2×4) surface an increase in the background, due to diffusely scattered electrons, and broadening of the reflections in the LEED pattern were observed starting at $\theta_{Cs} \sim 0.1$ ML, and at $\theta_{Cs} \sim 0.5$ ML the (2×4) superstructure completely vanished. The Ga-stabilized surface was found to be more resistant to disordering. For $\theta_{Cs} < 0.3$ ML no degradation of the LEED pattern was observed, in agreement with the results of Ref. 16 on the observation of diffusion and ordering of Cs on a Cs/GaAs(100) surface at low coverage; the (4×2) superstructure remained right up to 0.75 ML and transformed into (1×1) only for $\theta_{Cs} \approx 1$ ML. Thus, essentially identical behavior of the loss spectra is observed on a well-ordered Cs/GaAs(110) surface,[2,3,5] on a disordered Cs/GaAs(100) interface with initial As-stabilized (2×4) reconstruction, and on an interface with an intermediate order, obtained by depositing cesium on a Ga-stabilized surface with (4×2) reconstruction.

In conclusion, we note that the results obtained show that a Cs/GaAs surface is not a Hubbard insulator but rather a two-dimensional metal. For explaining the electronic spectrum it is important that the cesium layer is a ''granular metal,'' i.e., it consists of two-dimensional clusters. A characteristic feature of a polar GaAs face with (100) orientation is the disordering of the Cs/GaAs(100) interface with ~ 1 ML Cs deposited on surfaces with various reconstructions. The electronic spectrum of the Cs/GaAs(100) interface at sufficiently large coverages $\theta_{Cs} > 0.5$ ML is universal and is due to longitudinal and transverse excitations in two-dimensional metallic clusters. One of the characteristic electron energy loss peaks (the one at $E \approx 1$ eV) is due to the excitation of localized longitudinal plasmons in cesium clusters, and the other (at $E \approx 0.5$ eV) is tentatively attributed to transitions from the valence band into metal-induced states. These results also appear to be valid for GaAs interfaces with other alkali metals.

We thank N. S. Ruda for growing the epitaxial GaAs layers and A. O. Govorov, A. V. Chaplik, and M. V. Éntín for helpful discussions and remarks. This work was supported by the program ''Surface Atomic Structures'' of the Ministry of Science (Grant 4.4.99) and by the program ''Integration'' of the Ministry of Education of the Russian Federation through Novosibirsk State University (Project 274).

*)e-mail: alper@thermo.isp.nsc.ru

[1] F. Bechstedt and M. Scheffler, Surf. Sci. Rep. **18**, 145 (1993).
[2] L. J. Whitman, J. A. Stroscio, R. A. Dragoset, and R. J. Celotta, Phys. Rev. Lett. **66**, 1338 (1991).
[3] E. W. Plummer, T. M. Wong, and N. J. DiNardo, Phys. Rev. Lett. **65**, 2177 (1990).
[4] O. Pankratov and M. Scheffler, Phys. Rev. Lett. **70**, 351 (1993).
[5] U. del Pennino, R. Compañò, B. Salvarani, and C. Mariani, Surf. Sci. **409**, 258 (1998).
[6] O. E. Tereshchenko, S. I. Chikichev, and A. S. Terekhov, J. Vac. Sci. Technol. A **17**, 2655 (1999).
[7] D. Rodway, Surf. Sci. **147**, 103 (1984).
[8] O. E. Tereshchenko, S. I. Chikichev, and A. S. Terekhov, Appl. Surf. Sci. **214**, 7580 (1998).
[9] V. F. Kuleshov, Yu. A. Kukharenko, S. A. Fridrikhov *et al.*, *Spectroscopy and Diffraction of Electrons in the Investigation of Solid Surfaces* [in Russian] (Nauka, Moscow, 1985).
[10] V. L. Alperovich, A. G. Paulish, and A. S. Terekhov, Phys. Rev. B **50**, 5480 (1994).
[11] A. V. Chaplik, Surf. Sci. Rep. **5**, 289 (1985).
[12] M. Nakayama, T. Kato, and K. Ohtomi, Solid State Commun. **50**, 409 (1984).
[13] T. Aruga, H. Tochihara, and Y. Murata, Phys. Rev. Lett. **53**, 372 (1984).
[14] A. V. Chaplik and A. O. Govorov, J. Phys.: Condens. Matter **8**, 4071 (1996).
[15] J. Kim, M. C. Gallagher, and R. F. Willis, Appl. Surf. Sci. **67**, 286 (1993).
[16] V. L. Alperovich and D. Paget, Phys. Rev. B **56**, R15565 (1997).

Translated by M. E. Alferieff

Characteristic features of the formation of the resistive state in a $Bi_2Sr_2CaCu_2O_y$ crystal

V. N. Zavaritskiĭ*)

P. L. Kapitsa Institute of Physics Problems, Russian Academy of Sciences, 117334 Moscow, Russia; Institute of General Physics, Russian Academy of Sciences, 117942 Moscow, Russia

(Submitted 28 October 1998; resubmitted 23 September 1999)
Pis'ma Zh. Éksp. Teor. Fiz. **70**, No. 8, 543–548 (25 October 1999)

The effect of a magnetic field $H\perp(ab)$ on the transverse current–voltage characteristics (IVCs) of the mixed state of a single crystal of the layered superconductor $Bi_2Sr_2CaCu_2O_y$ (BSCCO) is investigated. It is established that in a wide range of temperatures and fields above the irreversibility line the initial part of the IVC is described by the law $V\propto I^{\gamma}$ with $\gamma\simeq 1$. As the current increases further, this law is replaced by a section where $V\propto\exp(I)$. It is established that the multivalued, multibranch characteristics, interpreted as a manifestation of an internal Josephson effect, do not change appreciably when the crystal passes into a state with nonzero linear resistance. The character of the dependence of the characteristic switching current on the first resistive branch, $I_J(H,T)$, is determined. © *1999 American Institute of Physics.* [S0021-3640(99)01220-7]

PACS numbers: 74.72.Hs, 74.50.+r

The layered structure of a material is manifested in many macroscopic properties of high-T_c superconductors (HTSCs), specifically, in the characteristics of the mixed state, which are the subject of intense study.[1] Nonetheless, the physical picture is far from complete; in particular, there has been a need for more systematic investigations. For example, conclusions about the characteristic features of the dynamics of vortices in different regions of the $H-T$ diagram are largely based on the results of measurements of the resistance, while there are only a very few investigations of the current–voltage characteristics (IVCs) of HTSC crystals,[2–5] and those have been designed to investigate the ''internal'' Josephson effect (IJE) and have used relatively insensitive apparatus or have set out to measure the critical current, which was determined according to the moment at which a measurable voltage appeared. They have thus ignored the question of asymmetry of the IVC, to say nothing of hysteresis phenomena, which at best were only mentioned. Moreover, it has been asserted in a number of works that the transverse IVCs of $Bi_2Sr_2CaCu_2O_y$ (BSCCO) crystals are nonlinear in the normal state and in the mixed state;[4,5] this result requires rethinking the entire set of resistive measurements, which presumed the system response to be linear.

In the present work the transverse IVCs of a BSCCO crystal were used to study the effect of an external field $H\perp(ab)$ on the character of the destruction of the nondissipa-

tive state of a layered superconductor. The experiments were performed at a level of sensitivity more than four orders of magnitude higher than that used in Refs. 2, 4, and 5. Experimental evidence was obtained for the Ohmic nature of the system in a wide range of fields and temperatures above the irreversibility line, and it was established that the nonlinearities of IVC develop at higher electric field intensities. It was shown that the complicated form of the single-valued part of the IVC can be satisfactorily described by the flux-creep model modified for the case of low barriers. The character of the dependence of the characteristic switching current on the first resistive branch, $I_J(H,T)$, was determined and it was found that the multivalued, multibranch characteristics in the IJE regime do not change appreciably when the crystal passes into a state with a nonzero linear resistance.

The basic results were obtained on a ≈ 1.5 μm thick BSCCO crystal with basal plane dimensions $\approx 350\times 215$ μm. The critical temperature, $T_{c0}\simeq 91.2\pm 0.2$ K, was determined at the level $R=10^{-4}R(95\ \mathrm{K})$ according to the temperature dependence of the transverse resistance $R(T)$, which was measured in a laboratory field using an ac bridge (5–10 μA) at 25–77 Hz. A previously tested method was used to monitor the macroscopic uniformity of the composition of and the absence of blocks in the sample.[6] The measurements were performed using a four-contact scheme. Methods for preparing low-resistance electric contacts and securing the crystal were described previously.[7]

The quasistationary IVCs were measured in the constant-current-source regime. The noise of the level of circuit did not exceed 2 nV in a 15 T field. The experiments were performed in a short-circuited solenoid at constant (± 5 mK) temperature. A re-entrant method was used to monitor the reproducibility of the characteristics and to ''follow'' the quasiparticle branches, so that each IVC was measured at least three times. In measurements of the initial section of a characteristic, the current through the sample was increased from zero with constant step on a logarithmic scale (10–100 points per decade); the initial increment was 10^{-9} A. To determine the location of the jump on the first resistive branch, the steady voltage drop on the sample was compared with the value measured at the preceding step, and the current I_J corresponding to the measurement before the value of this difference reached the threshold value $0.2\delta V$, where δV is the characteristic magnitude of the first jump (see Fig. 1), was recorded. The value of I_J was refined in the course of the measurements with repeated passage over the resistive branches; the current scan step was fixed at a level of 0.1–0.2 times the last increment used in the first step. The measurements were performed in the range 20–100 K. The temperature of the sample was measured with a calibrated CGR-2000 thermometer placed in the experimental cell. Thermal contact was obtained with a heat-exchange gas. For active temperature monitoring[6] additional temperature sensors, resistive and capacitive, placed near the cell were used. The orientation of the sample relative to the external field was reproducibly set directly during in the experiment according to the maximum of the angular dependence of the resistance in the mixed state of the crystal. In a number of experiments, simultaneous measurements were performed of the characteristics of a large-area sample ($\approx 315\times 810$ μm), whose disorientation angle did not exceed 5°. Additional monitoring for the absence of superheating effects was performed by comparing the IVC of the main crystal with these characteristics.

It was established that in the entire experimental range of fields and temperatures the transverse IVC of a BSCCO crystal is symmetric with respect to a change in the sign of

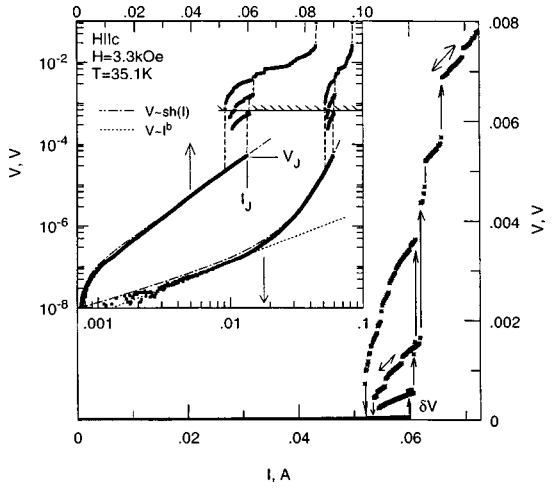

FIG. 1. Typical transverse IVC of a BSCCO crystal; the double-headed arrows in the main panel indicate the single-valued sections of the IVC, the arrows show jumps between the resistive branches. The results of the measurements with $H \simeq 3.3$ kOe and $T \simeq 35.1$ K are presented. Inset: The same data are presented in log–log and semilogarithmic scales: the arrows on the curves indicate the corresponding abscissa; the hatched line shows the sensitivity level characteristic for an IJE experiment;[2,5] the dotted lines show the fit by a power law, $V \sim I^{\gamma}$, and the dot-and-dash line shows the relation $V \propto \exp(U_0/T)\sinh(U_0 j/T j_0)$.

the current and is qualitatively similar to the typical characteristics of the IJE.[2,5] As one can see from the main panel in Fig. 1, a complicated characteristic forms when the current exceeds I_J: It is single-valued within each resistive branch and hysteretic in the region of transitions between branches.[1)]

In contrast to Refs. 2 and 5, which identified the initial section of the IVC of a layered HTSC with a nondissipative Josephson supercurrent I_J, we observed that in a wide range of fields and temperatures the multivalued, multibranched IVCs develop against the background consisting of a single-valued resistive ''pedestal,'' which seems to be due to the dynamics of the vortex system. As is evident from the inset in Fig. 1 and from Fig. 2a, the initial sections of the characteristics can be approximated by a power law $V \propto I^{\gamma}$ with $\gamma \simeq 1$.

This character of the IVC of a system of Josephson junctions could be due to the successive activation of an additional normal resistance, for example, accompanying the suppression of superconductivity of the subsurface layers of the crystal because of the breakdown of oxygen stoichiometry or as a result of diffusion of the conducting composite in the process of annealing the contacts.[5] However, the agreement of the (i) absolute values of the resistance, determined from the initial sections of the IVCs in the linear response region ($\gamma \simeq 1$) and measured for a weak current, (ii) the character of its field and temperature dependences, whose variation over more than four decades is satisfactorily described by the relation[7] $R(H,T) \propto H^{\beta}(T)\exp(-U/T)$, and (iii) the 20–30% agreement between estimates of the transverse resistivity for our samples, $\rho_c(100\ \mathrm{K}) \approx 10-20\ \Omega \cdot \mathrm{cm}$, and reference data[8] show that the contribution from the above-mentioned parasitic effects is not the major factor — on the contrary, the resistive ''pedestal'' reflects the physical properties of the experimental object.

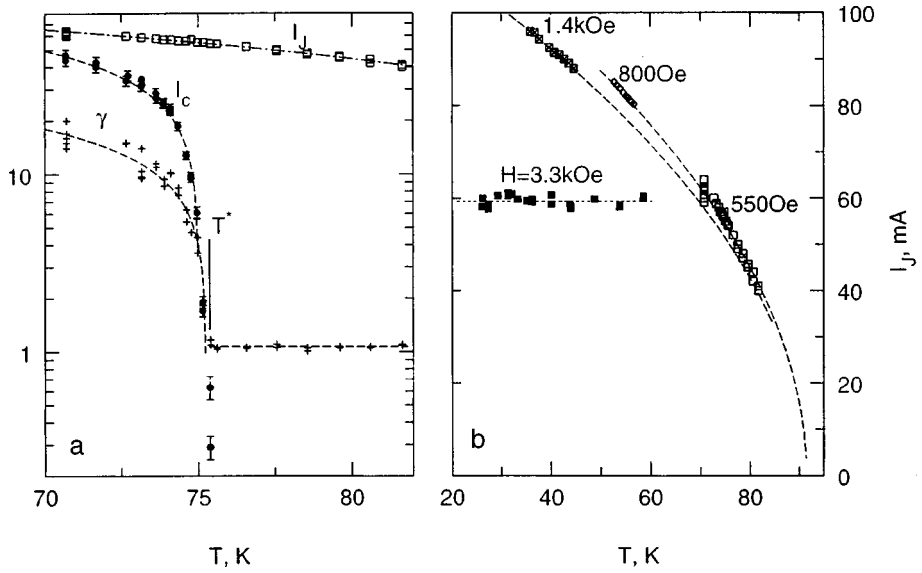

FIG. 2. a) Temperature dependences of the parameters of the IVC near the irreversibility line for $H=0.55$ kOe; γ, I_c, and I_J are shown by crosses, filled circles, and open squares, respectively. The dashed and dot-and-dash lines show fits of these dependences by $\gamma, I_c \propto (T^*-T)^{0.5}$ and $I_J \propto (100-T)$; the arrow shows the position of the irreversibility line, T^*. b) Temperature dependences $I_J(T)$ determined for a set of fields whose values are indicated on the curves; dashed curves — fit of the dependence $I_J \propto \sqrt{T_c-T}$ to the data.

As the current increases, the power law is replaced by a section of leading growth of the voltage, where the curve follows the empirical relation $V=A\exp(I/I_0)$, which is obvious from a semilogarithmic representation of the data, likewise presented in the inset in Fig. 1 (top curve and scale). Analysis of the entire array of characteristics investigated in the present work established that the characters of the temperature and field dependences $A(H,T)$ and $R(H,T)$ are identical, which indicates that the same physical mechanism is responsible for these diverse sections of the IVCs. This result is direct experimental evidence of the adequacy of the model of thermally activated flux creep, modified for the case of low barriers and high temperatures,[9] which predicts the following dependence of the vortex velocity f on the current density j: $f \sim \exp(-U_0/T)\sinh(U_0 j/Tj_c)$, which satisfactorily fits the entire single-valued part of the characteristic (see the dot-and-dash line in the inset in Fig. 1).

The typical character of the variation of the parameters of the transverse IVCs as the ''line of irreversibility'' $H^*(T^*)$ is crossed is illustrated in Fig. 2a, which shows the results of an analysis of a series of characteristics measured for a number of temperatures under the conditions of a fixed external field. As one can see, the exponent γ, which remains virtually constant at high temperatures, shows rapid growth as the temperature decreases below T^*. It is natural to attribute this growth to a transition of the vortex system from the liquid phase (with a quasi-Ohmic response) into an ordered phase (with a nonvanishing supercurrent). This result is supported by the character of the dependence of the critical current[2)] I_c, which vanishes at this temperature. We note that, besides the data presented, this transition is also probably manifested in the systematic deviation of

the dependences $A(T)$ away from the simple thermal activation law observed near T^*.

Comparing the characters of the dependences in Fig. 2a indicates that the mechanisms responsible for γ, I_c, and I_J are different. The initial sections of the IVCs and the corresponding parameters, γ and I_c, are evidently determined by the character of the depinning of the vortex system and demonstrate a strong temperature variation near T^*, satisfactorily approximated by a dependence of the form $\gamma, I_c \propto (T^* - T)^{\delta}$ with exponent $\delta \simeq 0.5 \pm 0.07$. At the same time, neither I_J nor the system of resistive branches changes much at a transition of the vortex system into a liquid state, which (in the IJE model[2]) attests to a nonvanishing phase correlation between neighboring planes in the crystal. This result can thereby be taken as experimental confirmation of the model of Ref. 10, where it is shown that a nonvanishing Josephson current can exist under the conditions of breakdown of macroscopic phase coherence in a system of Josephson junctions. In this model the single-valued part of the characteristic is due to phase-slip, while the resistive branches are due to quasiparticle tunneling complicated by flux trapping by a long junction, which are probably responsible for the fine structure of an individual branch. The great simplification of the picture observed in increasing fields (temperatures) is evidence of the latter.

As one can see from Fig. 2b, in weak fields (550–1400 Oe) a qualitative similarity is observed in the character of the temperature dependence of the characteristic current I_J. The finiteness of the experimental temperature range leaves a freedom in the choice between an approximation by the simplest dependence $\propto (T_0 - T)$ with $T_0 \simeq 100 - 110$ K, shown by the dot-and-dash line in Fig. 2a, and a more complicated dependence, for example, $I_J \sim (T_c - T)^{1/2}$, which likewise satisfactorily describes the results of these measurements, as one can see from Fig. 2b. As the field increases, the character of the temperature dependence $I_J(T)$ changes substantially, as follows from the results for $H = 3.3$ kOe presented in Fig. 2b and from the quantitative agreement between the field dependences $I_J(H)$ measured at different temperatures and the dependences presented in Fig. 3. This could be due to the characteristics features of the $H - T$ diagram of the vortex structure in BSCCO, which contains a set of phases differing in the character of the disorder. Then it is natural to ascribe the temperature-dependent characteristics to the vortex crystal, and the sharp weakening of the dependence to a transition to an ''entangled solid'' region (entangled vortex phase A/B).[1]

A strong magnetic field dependence of the characteristic current I_J was found. As is evident from the inset in Fig. 3, it can be fit by a power law $I_J \propto H^{-\alpha}$, $\alpha \simeq 0.6$, in a field range with an upper limit, outside of which strong deviations, possibly indicating a transition to a stronger law, are observed. In discussing this result, it is necessary to take account of the fact that the characteristic dimensions of the crystal satisfy $d \gg \lambda_c$, where $\lambda_c \approx 7000$ Å is the c component of the London penetration depth. The perpendicular field, which suppresses the Josephson coupling between the layers, increases λ_c by destroying the ordering of the point-like vortices in neighboring planes, so that for sufficiently strong fields λ_c can be expected to equal the dimensions of the sample, and a transition into a regime with a uniform current distribution should occur. Assuming that I_J characterizes a transition of the system of Josephson junctions into a quasiparticle tunneling regime, the data in Fig. 3 can be explained in the model mentioned,[10] which predicts a similar dependence with exponents α, equal to 1 and 1/2 for the cases $d \leqslant \lambda_c$ and $d \gg \lambda_c$, respectively. As one can see from the inset in Fig. 3, these laws can be

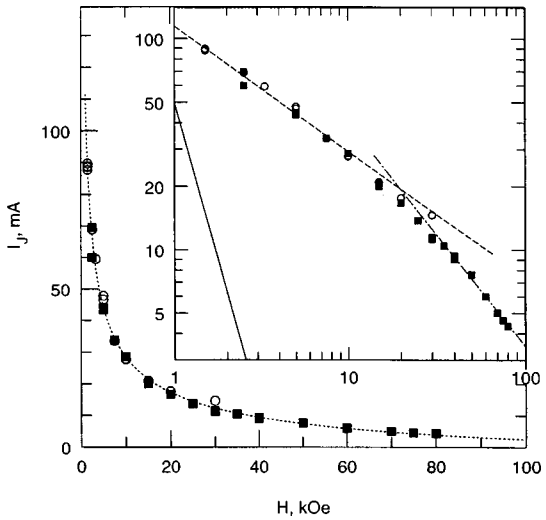

FIG. 3. Field dependence of the ''Josephson'' current I_J. The data are presented for 21 and 36 K — filled and open symbols, respectively. Inset: Same data replotted on a log–log scale and fits of the theoretical dependence, $I_J \propto H^{-\alpha}$, are presented for two values of α: 0.6 and 1.1. Solid line — approximation of the dependence $I_c(H) \propto H^{-3}$.

fit to the experimental data. Additional evidence in support of this scenario is lent by the fact that the estimates of the characteristic field ($\lambda_c = d$) for the investigated crystal, 30–40 kOe,[10] are in saatisfactory agreement with the value $H \simeq 15-20$ kOe at which the character of the dependence in the inset in Fig. 3 is observed to change.[10]

In summary, in the present work the dynamic characteristics of a vortex ensemble was studied under conditions of suppression of the Josephson coupling between layers in a BSCCO crystal by an external field $H \perp (ab)$. The likely mechanisms responsible for different sections of the transverse IVCs were determined, and direct experimental evidence was obtained which shows that the effective interlayer Josephson interaction is conserved at the transition of the vortex system into the liquid phase.

This work was performed as part of projects supported by EPSRC, the Russian Fund for Fundamental Research, and the Council on superconductivity. I am especially grateful to A. Koshelev, L. Bulaevskiĭ, and D. Geshkenbeĭn for helpful discussions.

*)e-mail: vlad@kapitza.ras.ru

1)A discussion of the evolution of the resistive branches falls outside the scope of the present letter, but it is pertinent to point out that as the voltage increases, an additional splitting into subbranches is observed. This splitting is clearly seen in the second branch in Fig. 1. The characteristic remains reversible with respect to a change in the sign of the current scan within a branch and exhibits hysteresis on switching between neighboring subbranches.

2)The critical transport current I_c was determined in two ways: as the current leading to an increase by 5–10 nV of the steady voltage drop between the contacts, and by a power-law extrapolation of the initial section of the IVC for $U < 1$ μV.

[1] G. Blatter, M. V. Feigel'man, V. B. Geshkenbein *et al.*, Rev. Mod. Phys. **66**(4), 1125 (1994).
[2] R. Kleiner, F. Steinmeyer, G. Kunkel *et al.*, Physica C **185-189**, 2617 (1991).

[3] J. H. Cho, M. P. Maley, S. Flesher *et al.*, Phys. Rev. B **50**, 6493 (1994); N. Morozov, M. P. Maley, L. N. Bulaevskii, and J. Sarrao, Phys. Rev. B **57**, R8146 (1998).
[4] S. Luo, G. Yang, and C. E. Gough, Phys. Rev. B **51**, 66551 (1995).
[5] A. Yurgens, D. Winkler, N. V. Zavaritsky *et al.*, Phys. Rev. Lett. **79**, 5122 (1997).
[6] V. N. Zavaritsky and W. Y. Liang, J. Low Temp. Phys. **105**, 1273 (1996).
[7] V. N. Zavaritskiĭ, JETP Lett. **65**, 663 (1997); *ibid*. **65**, 448 (1998).
[8] S. L. Cooper and K. E. Gray, in *Physical Properties of High Temperature Superconductors* edited by D. M. Ginsberg (World Scientific, Singapore, 1994) Vol. 4, p. 61.
[9] A. P. Malozemoff, in *Physical Properties of High Temperature Superconductors*, edited by D. M. Ginsburg [Russian translation, Mir, Moscow, 1990, p. 69].
[10] A. E. Koshelev, Phys. Rev. Lett. **77**, 3901 (1996); A. E. Koshelev, L. N. Bulaevskii, and M. P. Maley, Phys. Rev. Lett. **81**, 902 (1998); A. E. Koshelev, private communication.

Translated by M. E. Alferieff

ERRATA

Erratum: Predicted existence of H_3^{++} molecular ions in strong magnetic fields [JETP Lett. 69, No. 11, 844–850 (10 June 1999)]

A. Turbiner, J.-C. Lopez, and U. H. Solis
Instituto de Ciencias Nucleares, UNAM, 04510 México D. F., México
Pis'ma Zh. Eksp. Teor. Fiz. **70**, No. 8, 549 (25 October 1999)

[S0021-3640(99)01320-1]

PACS numbers: 99.10.+g, 31.15.Pf, 33.15.−e

Our article in the 10 June 1999 issue is dedicated to the memory of B. B. Kadomtsev.

